Solid State Lighting Technology and Application Series

Clemens J.M. Lasance
András Poppe *Editors*

# Thermal Management for LED Applications

For internal use by Mentor Graphics marketing only

# Solid State Lighting Technology and Application Series

**Series Editor**
G. Q. Zhang

For further volumes:
http://www.springer.com/series/8864

For internal use by Mentor Graphics marketing only

Clemens J. M. Lasance • András Poppe
Editors

# Thermal Management for LED Applications

For internal use by Mentor Graphics marketing only

Springer

*Editors*
Clemens J. M. Lasance
Philips Research Emeritus
Eindhoven, The Netherlands

SomelikeitCool
Eindhoven, The Netherlands

András Poppe
MicReD unit, Mentor Graphics
Mechanical Analysis Division
Budapest, Hungary

Budapest University of Technology
and Economics
Department of Electron Devices
Budapest, Hungary

For internal use by Mentor Graphics marketing only

ISSN 2196-4203
ISBN 978-1-4614-5090-0 ISBN 978-1-4614-5091-7 (eBook)
DOI 10.1007/978-1-4614-5091-7
Springer New York Heidelberg Dordrecht London

Library of Congress Control Number: 2013943845

© Springer Science+Business Media New York 2014
This work is subject to copyright. All rights are reserved by the Publisher, whether the whole or part of the material is concerned, specifically the rights of translation, reprinting, reuse of illustrations, recitation, broadcasting, reproduction on microfilms or in any other physical way, and transmission or information storage and retrieval, electronic adaptation, computer software, or by similar or dissimilar methodology now known or hereafter developed. Exempted from this legal reservation are brief excerpts in connection with reviews or scholarly analysis or material supplied specifically for the purpose of being entered and executed on a computer system, for exclusive use by the purchaser of the work. Duplication of this publication or parts thereof is permitted only under the provisions of the Copyright Law of the Publisher's location, in its current version, and permission for use must always be obtained from Springer. Permissions for use may be obtained through RightsLink at the Copyright Clearance Center. Violations are liable to prosecution under the respective Copyright Law.
The use of general descriptive names, registered names, trademarks, service marks, etc. in this publication does not imply, even in the absence of a specific statement, that such names are exempt from the relevant protective laws and regulations and therefore free for general use.
While the advice and information in this book are believed to be true and accurate at the date of publication, neither the authors nor the editors nor the publisher can accept any legal responsibility for any errors or omissions that may be made. The publisher makes no warranty, express or implied, with respect to the material contained herein.

Printed on acid-free paper

Springer is part of Springer Science+Business Media (www.springer.com)

# Preface

Light emitting diodes (LEDs) are a solid-state lighting source increasingly being used in display backlighting, communications, medical services, signage, and general illumination. LEDs offer design flexibility, have small exterior outline dimensions, higher energy efficiency, have longer life, provide higher performance, a wider range of controllable color temperatures, are eco-friendly products, and don't suffer from low-temperature startup problems, as compared to conventional lighting sources. Unfortunately, they produce heat, and contrary to conventional lighting sources this does cause serious problems (please keep in mind that if the bulb would have been invented today it would never have been legalized because of the excessive touch temperatures).

This book is about thermal management of LEDs and especially LED applications. The main question to be addressed is why we need thermal management in the first place. As Christian Belady put it eloquently in 2001:

> The ultimate goal of system thermal design is not the prediction of component temperatures, but rather the reduction of thermally associated risk to the product.

Hence, if your boss asks you: "Take care that the junction temperature does not exceed 125 °C", you may answer: "Why? Do we sell temperatures?" and then you may educate your boss: "The real objectives to realize are: we want to keep the Lifetime beyond x years, we want to keep the Color Point within margin y, and we want to raise the Efficiency to z %. And yes, these objectives that determine the quality of our LED-based products are linked to the junction temperature, but never as a goal in itself."

The book is divided in four parts: Part A: Basic Physics, Part B: Testing and Standardization, Part C: Advances in Cooling Technologies, and Part D: Applications.

*Part A: Basic Physics*

The evident link between temperature and various quality-related issues is the rationale behind Chap. 1, an Introduction to LED Thermal Management and Reliability, presenting a general overview of LED basics, LED manufacturing and LED failure mechanisms. Obviously, the first step in reaching the aforementioned goal of LED thermal design is to understand the basics of LED physics: what are the

For internal use by Mentor Graphics marketing only

reasons that the temperature is rising anyway? This subject is treated in Chap. 2 on the basics of solid-state physics of LEDs. To be able to perform back-of-the-envelope calculations to get a rough idea about the feasibility of your design from a thermal point of view is an important first step: this topic is treated in Chap. 3.

*Part B: Testing and Standardization*

This part starts with Chap. 4 dealing with basic thermal characterization and testing. How to test LEDs from a lighting point of view is the subject of Chap. 5. Chapter 6 discusses the increasing need for a more sophisticated thermal characterization of LEDs and LED-based products. Unfortunately, the progress in thermal characterization has not kept pace with the exponential growth of the LED-business. Due to the lack of worldwide-accepted standards a manufacturer can publish whatever thermal information she/he wants. Hence, it becomes a problem for the experienced user because the thermal data that are published are often rather useless in practice when accuracy is at stake.

*Part C: Advances in Cooling Technologies*

Air cooling is by far the most frequent cooling method and will be for a long time to come. Natural and forced convection cooling, including synthetic jet cooling, is discussed in Chap. 7. Another important thermal management control option is the thermal interface material (TIM). For high-performance LED-based products it may even be the limiting factor in the thermal resistance chain. Current and future thermal interface materials are dealt with in Chap. 8. An even more important thermal control option is area enlargement, either by heat sinks attached to the LED substrate or by first transferring the heat through heat pipes to a location where area enlargement is easier to handle. Chapter 9 deals with the fundamentals a designer should master to enable an optimal choice out of the thousands of heat sinks available on the market.

*Part D: Applications*

Chapter 10 is related to Chap. 9 but focuses on applications in practice. Problems inherent to LED manufacturing from a thermal point of view are the subject of Chap. 11. Thermal management of sophisticated LED solutions is treated in Chap. 12, while another important application field, namely LED-driven display technologies, is discussed in Chaps. 13 and 14, the first providing a historical overview, and the second the state-of-the-art. Many LED applications are designed for use in harsh environments, for example automotive, aircraft, outdoor lighting, and signage everywhere on earth. Chapter 15 provides insight in the challenges these applications are facing. The book closes with Chap. 16 showing an overview of future directions in LED applications.

In summary, the editors are convinced that this book covers (almost) all aspects of thermal management that are relevant to the design of LEDs and LED–based systems.

In closing this preface, the editors would like to express their sincere thanks to all authors who made this book possible.

Philips Research Emeritus, The Netherlands — Clemens J. M. Lasance
Budapest University of Technology and Economics and Mentor Graphics, Hungary — András Poppe

For internal use by Mentor Graphics marketing only

# Contents

**Part I Basic Physics**

1 **Introduction to LED Thermal Management and Reliability** ......... 3
Michael Pecht, Diganta Das and Moon-Hwan Chang

2 **Solid-State Physics Fundamentals of LED Thermal Behavior** ....... 15
Jinmin Li, JunxiWang, Zhe Liu and András Poppe

3 **Basics of Thermal Design for LEDs** ............................ 53
Cathy Biber

**Part II Testing and Standardization**

4 **Thermal Testing of LEDs** ...................................... 73
Gábor Farkas and András Poppe

5 **Laboratory Measurement of Optical Properties of LEDs** ........... 167
János Schanda, Péter Csuti and Ferenc Szabó

6 **Standardization of LED Thermal Characterization** ................ 197
András Poppe and Clemens J. M. Lasance

**Part III Advances in Cooling Technologies**

7 **Air Cooling for LED Lighting** .................................. 267
Raghav Mahalingam

8 **Advances in Thermal Interface Materials for Power LED Applications** ............................................. 299
David L. Saums

9 **Heat Sink Basics from an Industrial Point of View** ................ 347
Clemens J. M. Lasance

For internal use by Mentor Graphics marketing only

## Part IV Applications

**10 Considerations for an Optimal Choice of Heat Sinks for LED Applications** . . . . . 391
Norbert P. Engelberts

**11 Testing Issues in LED Manufacturing** . . . . . 419
Richard Young

**12 Thermal Management of Sophisticated LED Solutions** . . . . . 449
Theo Treurniet

**13 Thermal Challenges in LED-Driven Display Technologies: The Early Days** . . . . . 465
Kazuaki Yazawa

**14 Thermal Challenges in LED-Driven Display Technologies: State-of-the-Art** . . . . . 477
G. A. Luiten

**15 LEDs in Harsh Environments** . . . . . 499
Ross Wilcoxon and Jim Petroski

**16 Future Directions in LED Applications** . . . . . 519
Robert F. Karlicek

**Index** . . . . . 543

For internal use by Mentor Graphics marketing only

# Contributors

For internal use by Mentor Graphics marketing only

**Cathy Biber, PhD** Biber Thermal Design Ltd., Portland, OR, USA
e-mail: biberthermal@gmail.com

**Moon-Hwan Chang, PhD** Center for Advanced Life Cycle Engineering (CALCE), University of Maryland, Building 89, Room 1103, College Park, MD 20742, USA
e-mail: mhchang@calce.umd.edu

**Péter Csuti** Department of Electrical Engineering and Information Systems, University of Pannonia, Egyetem u. 10, 8200 Veszprém, Hungary
e-mail: csutip@vision.uni-pannon.hu; csuti.peter@virt.uni-pannon.hu

**Diganta Das, PhD** Center for Advanced Life Cycle Engineering (CALCE), University of Maryland, Building 89, Room 1103, College Park, MD 20742, USA
e-mail: digudas@calce.umd.edu

**Norbert P. Engelberts** Optimal Thermal Solutions BV, Bussum, The Netherlands
e-mail: nengelberts@ots-eu.com

**Gábor Farkas, PhD** Mentor Graphics MAD MicReD unit, Infopark D, Gábor Dénes utca 2, Budapest 1117, Hungary
e-mail: gabor_farkas@mentor.com

**Robert F. Karlicek, Jr., PhD** Smart Lighting Engineering Research Center, Rensselaer Polytechnic Institute, CII7015, 110 8th Street, Troy, NY 12180, USA
e-mail: karlir@rpi.edu

**Clemens J. M. Lasance, Ir** Philips Research Laboratories Emeritus, Consultant at SomelikeitCool, Nuenen, The Netherlands
e-mail: lasance@onsnet.nu

**Jinmin Li** Institute of Semiconductors, Chinese Academy of Science, A35, QingHua East Road, Haidian District, 912, 100083 Beijing, P. R. China
e-mail: jmli@semi.ac.cn

**Zhe Liu** Institute of Semiconductors, Chinese Academy of Science, A35, QingHua East Road, Haidian District, 912, 100083 Beijing, P. R. China

**G. A. Luiten, Ir** Philips Research, Eindhoven, Netherlands
e-mail: wendy.luiten@philips.com

**Raghav Mahalingam, PhD** Nuventix, 4635 Boston Lane, Austin, TX 78735 USA
e-mail: raghav@nuventix.com

**Michael Pecht, PhD** Center for Advanced Life Cycle Engineering (CALCE), University of Maryland, Building 89, Room 1103, College Park, MD 20742, USA
e-mail: pecht@calce.umd.edu

**Jim Petroski** Cedar Rapids, IA 52402, USA
e-mail: jpetroski@rambus.com

**András Poppe, PhD** Mentor Graphics Mechanical Analysis Division, MicReD unit, Budapest XI, Infopark D, Gábor Dénes utca 2, 1117, Budapest, Hungary
e-mail: andras_poppe@mentor.com

Department of Electron Devices, Budapest University of Technology and Economics, Budapest, Hungary
e-mail: poppe@eet.bme.hu

**David L. Saums** DS&A LLC, 100 High Street Amesbury MA 01913, USA
e-mail: dsaums@dsa-thermal.com

**János Schanda, Professor Emeritus** Department of Electrical Engineering and Information Systems, University of Pannonia, Egyetem u. 10, 8200 Veszprém, Hungary
e-mail: schanda@vision.vein.hu; schanda.janos@virt.uni-pannon.hu

**Ferenc Szabó, PhD** Department of Electrical Engineering and Information Systems, University of Pannonia, Egyetem u. 10, 8200 Veszprém, Hungary
e-mail: szabof@vision.uni-pannon.hu; szabo.ferenc@virt.uni-pannon.hu

**Theo Treurniet, PhD** LED Platform Development, Philips Lighting, 80020, 5600 JM, Eindhoven, The Netherlands
e-mail: theo.treurniet@philips.com

**Junxi Wang** Institute of Semiconductors, Chinese Academy of Science, A35, QingHua East Road, Haidian District, 912, 100083 Beijing, P. R. China

**Ross Wilcoxon, PhD** Cedar Rapids, IA 52402, USA
e-mail: ross.wilcoxon@gmail.com

**Kazuaka Yazawa, PhD** Birck Nanotechnology Center, Purdue University, 1205W. State Street, West Lafayette, IN 47907-2057, USA
e-mail: kyazawa@purdue.edu, kaz@soe.ucsc.edu

University of Santa Cruz, Santa Cruz County, CA, USA

**Richard Young, PhD** Instrument Systems GmbH, Munich, Germany
e-mail: young@instrumentsystems.com

For internal use by Mentor Graphics marketing only

# Part II
# Testing and Standardization

For internal use by Mentor Graphics marketing only

# Chapter 4
# Thermal Testing of LEDs

**Gábor Farkas and András Poppe**

**Abstract** In this chapter, after a generic discussion of thermal testing techniques used to characterize packaged semiconductor devices; the latest practical test methods widespread in thermal testing of LED components and SSL luminaires are discussed. Thus, the focus is on the latest, power semiconductor and LED-specific test procedures, environments and thermal metrics—all derived from the classical JEDEC JESD51 family of testing standards. Detailed discussion is devoted to the transient extension of the so-called static test method and the differential measurement principle in its practical realization.

Different representations of the thermal impedance are presented starting from the classical $Z_{th}(t)$ functions ending with the so-called *structure functions*. These are discussed in depth because they became the de facto standard in laboratory testing of thermal properties of LED components, in reliability analysis and in quality assurance at leading LED manufacturers. The basic concepts are introduced through practical examples.

## 4.1 Introduction

A common feature in present engineering tasks is struggling with growing *power level* in electronic systems. Solid-state lighting luminaires now operate at dozens of watts; the driving electronics has to produce many amperes. In other fields of electronics, processors now run at aggressive clock frequencies, electric cars have commutators working at kilowatts and hundred amperes. These are challenges not only for thermal management but also need clever solutions in thermal testing.

What is more important, the *power density* also increases. Video projectors, which were formerly of suitcase size, now resemble a pocketbook, mobile phones produce although a few watts only but in an extremely tight case with no ventilation at all.

Furthermore, many systems work in extremely *harsh environments*. Automotive electronics, for example, has to operate in the − 30 to + 80 °C external temperature range; this is similar for LED-based automotive lighting solutions or for street lighting

G. Farkas (✉) · A. Poppe
Mentor Graphics MAD MicReD unit, Infopark D, Gábor Dénes utca 2,
Budapest 1117, Hungary
e-mail: gabor_farkas@mentor.com; andras_poppe@mentor.com

C. J. M. Lasance, A. Poppe (eds.), *Thermal Management for LED Applications,*
Solid State Lighting Technology and Application Series 2,
DOI 10.1007/978-1-4614-5091-7_4, © Springer Science+Business Media New York 2014



For internal use by Mentor Graphics marketing only

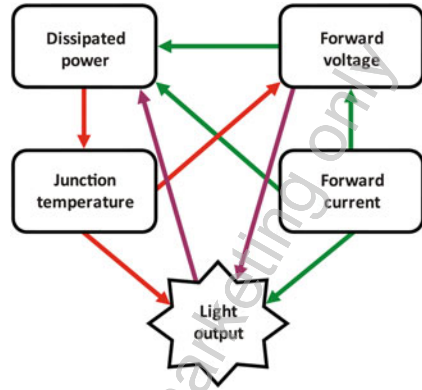


**Fig. 4.1** Light output depends on "everything"

luminaires. Of course, at the hottest points of such a system, semiconductor junctions can reach 150 °C or even more, near their operation limits.

In conventional electronics as well as in solid-state lighting, the junction temperature ($T_J$) is a primary quantity influencing system reliability and lifetime. The junction temperature of an LED is not just a performance indicator of the thermal design but also plays a major role in lighting design since many properties of the light output of an LED depend on the absolute junction temperature (Fig. 4.1). This means that thermal management should be an integral part of the system design of an LED-based lighting solution, resulting in changing roles of different engineering disciplines in the overall design process.

The spectacular technological development described above has been achieved by *thermally aware system design*.

As it is known, thermally aware design has two pillars, *measurement* and *simulation*. However, both of them implicitly rely on a third one, modeling the thermal behavior of the system.

This mandatory modeling step is very evident in case of simulations where you create a solid model first, then do some meshing, etc. However, many limitations and misunderstandings originate from improperly handling the inherent model creation in case of measurements.

At first sight, one could think that the precision of thermal testing depends on the *resolution*, *accuracy*, *repeatability*, and *reproducibility* of the measurement.[1] A simple example can prove that this is not generally true.

If we ask, for example, how much is the distance between London and Moscow, the correct answer is 2,500 km. This statement already contains a lot of implicit modeling factors such as: we measure the length of the arc on the globe and not the chord; we do not talk about driving distance, etc.

At present, we have length-measuring instruments with an accuracy of centimeters, resolution of millimeters, and we also have satellites. With these tools, we can

[1] Some of these topics will be discussed later in this chapter and many more in Chap. 11, but their detailed treatment is beyond the scope of this book.

For internal use by Mentor Graphics marketing only

give a much more precise number for the distance of two towers in the cities, for example, but this was not the question.[2] We cannot improve measuring the distance of the two cities, as they are not point-like objects, and modeling them as such is an obvious mistake. The achievable accuracy of this measurement is 20 km considering the real objects to be measured and the relevant models to be used for them. These factors manifest as inherent *uncertainty* of the measurement.

Even in special literature, we find papers where some quantities with limited relevance like chip temperature or package case temperature are measured at four-digit accuracy and then derived quantities are calculated at six-digit accuracy. In the following sections, we will clarify possibilities and limits of measurements.

Before the advent of new thermal design methods, the major cause of system breakdown was the overheating of critical components. Failure analysis (FA) shows that nowadays systems are correctly designed in this respect. The typical component breakdown is caused by repeated *thermal transients*. Heating and cooling induces shear stress at the material interfaces in the structure (die attach, solder joint) resulting in delamination, tear off, etc. The poorer heat removal through a diminished surface can then cause thermal runaway.

This is one of the reasons for introducing thermal transient measurements and simulation techniques. As we can see later, these methods also unfold internal structural details that cannot be identified by static measurements.

## 4.2 Modeling of Devices for Measurement and Simulation

When we measure parameters of semiconductor devices, we inherently have an underlying *model* in mind. The model parameters like single junction temperature, single lumped thermal resistance, or thermal capacitance are highly simplified.

In reality, there is always a given distribution of the temperature over the active area of a device; and thermal systems are infinite distributed RC systems. The question is how good our implicit models are reduced to single (average) temperature value or to a few thermal network elements.

For a long time, packaged electronic components were represented by a single thermal resistance in the data sheet. Power devices were usually encapsulated in packages with a dedicated cooling surface, called “case.”

At discrete semiconductors (diodes, transistors), the hottest portion of the device was the pn-junction. As first estimation, the engineer accepted that applying $P_H$ heating power at the junction of the packaged device mounted on a surface of $T_C$

[2] The mentioned cities span over a large surface while distance is defined between two points. The question is: are there some points in these cities which are characteristic for the real target of the distance measurement and where are they located? We face similar questions in the thermal testing of semiconductor devices. To which point of the active semiconductor we assign the “junction temperature”? Resistance (strictly speaking) is defined between two nodes of a graph. Which are the distinct points between which we define the thermal resistance? See Chap. 6 for further details on these issues.

For internal use by Mentor Graphics marketing only

temperature; the device will reach maximum junction temperature in a longer run.

$$T_J = P_H \cdot R_{thJC} + T_C \tag{4.1}$$

At present, the range of LED devices is very wide. There are small devices for which the usual approximations and assumptions of the classical thermal testing are still more or less valid, but nowadays we face a couple of challenges, which are not yet followed up by standards:

- Instead of LED packages containing a small chip, we have to characterize large modules with multiple devices, chip arrays, etc. causing various dissipation patterns on the chip surfaces.
- Packages have become large and very flat, the idea of a homogenous temperature on a case surface (and also on the chip surface) is no more acceptable.
- For many devices (LEDs and driving electronics), the heat flow through package pins became a major, often dominant factor.
- There are direct mounting (chip on board) solutions.
- With surface mount technologies the heat leaves in very complex and manifold ways through pins, exposed tabs, mould surface towards different layers of the printed board, to the air, sometimes to heat sinks, fans, etc.

Single thermal resistance values such as the junction-to-case $R_{thJC}$ are still part of a data sheet facilitating component selection at early design phases. However, the complex, three-dimensional reality can only be handled with sophisticated simulation tools along with thermal measurements.

Not only the conventional concept of a single thermal resistance is insufficient for adequate design in solid-state lighting, but we have also serious doubts about the nature of the innocent $P_H$ heating power in Eq. (4.1). This will be treated more in detail in Sect. 4.3.7.

The most exciting question is the temperature of the semiconductor in a specific environment. With more measurements at various boundaries, we can get relevant data about this. A simple and effective use of the measured values is if we order them into a consistent structure of a few model elements (compact model).

Most accurate results, such as temperature and heat flux at many points of the chip, package, and environment can be gained using *detailed models* consisting of many hundreds of thousand elements, e.g., with finite element (FEM) or finite difference (FDM) methods (see Fig. 4.2). If we want to see the effect of convection ("still" or moving air around the component), we can rely on computational fluid dynamics (CFD) methods.

This kind of simulation needs special expertise and this level of accuracy can be achieved at the manufacturer of the component only, where all geometrical and material details are known.

Building compact models of a few elements gives a much faster and simpler approach, describing the component with reasonable accuracy for the application engineer. Some compact models are behavioral ones while others also reveal essential structural information.

For internal use by Mentor Graphics marketing only!

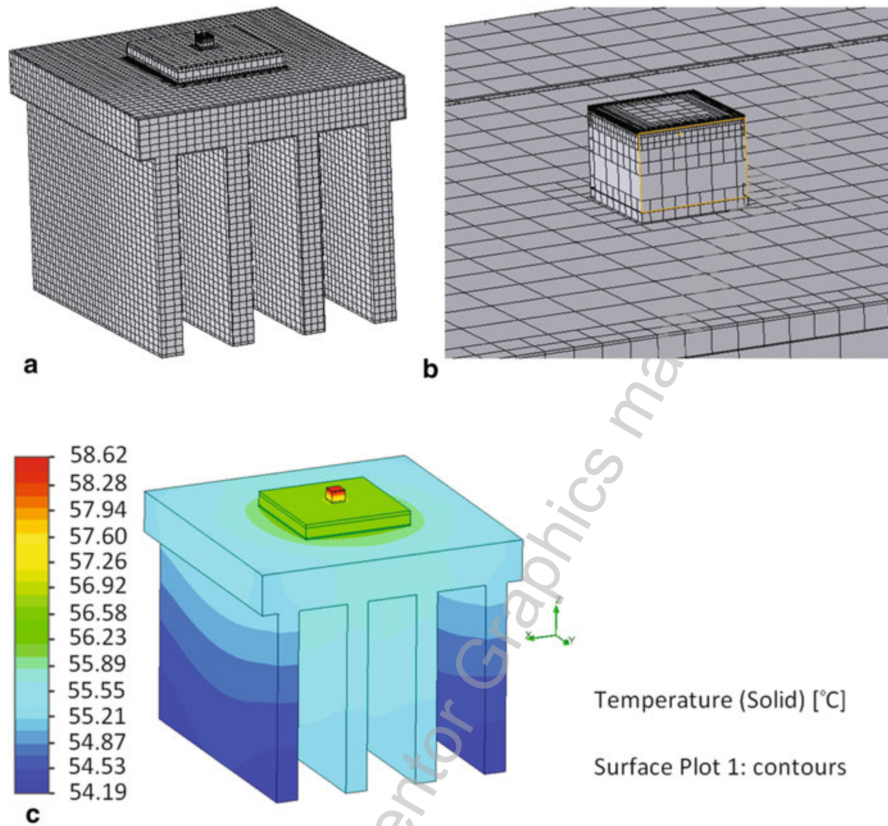


**Fig. 4.2** An LED device on heat sink: **a** detailed thermal model, meshed for a finite difference solver (FloTHERM), **b** close-up view of the model at the LED chip, **c** results of the CFD simulation using this model

For internal use by Mentor Graphics ma

Creating compact models is not too simple either. In classical electronics, thermal management and modeling techniques were developed in the last two decades and became formally standardized recently. In case of LEDs, however, compact modeling is still evolving; it is far from a mature state that one could call standard. A survey on LED compact modeling status is provided in Chap. 6 on standardization.

Figure 4.3 shows an LED device packaged and a heat sink to be attached to the "case" surface. Fig. 4.4 shows different possible model topologies—which are in practical cases nodes assigned to surfaces of more or less uniform temperature and thermal resistances between these.

A compact model approach helps in interpreting measurement results, and we shall mainly use it for this purpose in this chapter. It also enables understanding the interaction of the device (represented by RL, RR, RP) and the environment (represented by R1, R2, R3 in Fig. 4.5).

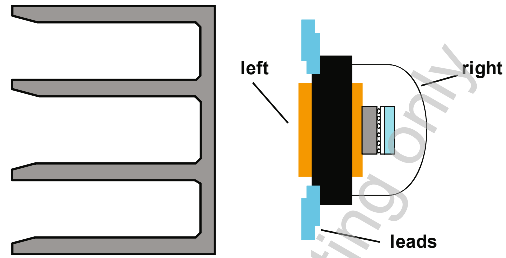


**Fig. 4.3** A real package: LED packaged and a heat sink to be attached

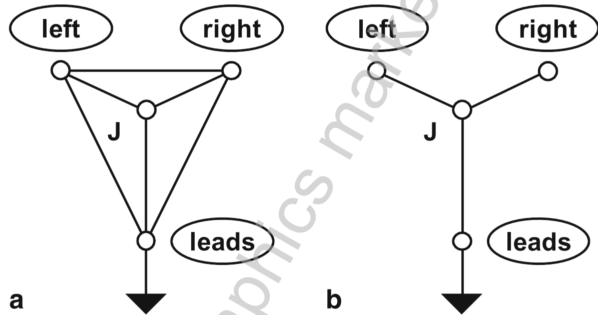


**Fig. 4.4** **a** General, **b** simplified model network topology of a packaged device. (*Lines* represent graph edges, *small circles* represent graph nodes)

Applying an extremely good cooling on the "case" or "left" surface and applying known power on the LED, we can identify the measured thermal resistance as the classic junction-to-case value (RL). Replacing this extreme cooling by a heat sink for which a catalogue claims R1 at still air condition, we shall measure more or less RL + R1 thermal resistance. Rather less, as all other elements of the model (if it is correct) will be "active" in this new situation, the air cannot be so "still"—and we shall see later on that even the package section represented by RL will behave in a very different way.

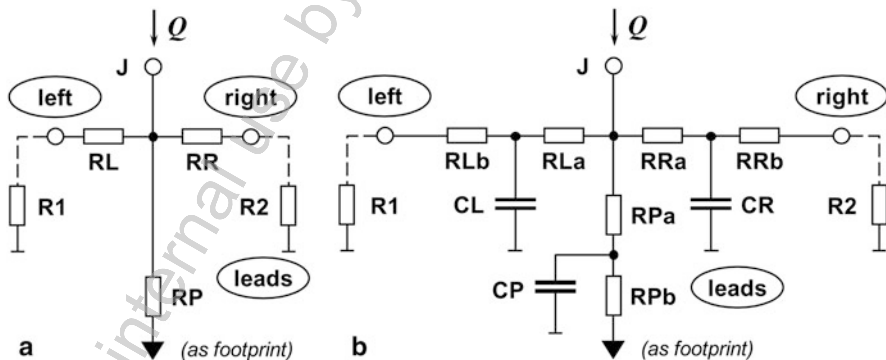


**Fig. 4.5** **a** Static, **b** dynamic compact model of a packaged device according to the model topology shown in Fig. 4.4b

For internal use by Mentor Graphics marketing only

Usually, model values derived for a given topology strongly depend on the actual environment. Models containing more elements such as in Fig. 4.5a show less dependence on actual boundary conditions.

Instead of single thermal resistance values, major semiconductor companies nowadays offer compact models that can be used in design tools like board or system-level thermal simulators. It is expected that a thorough optimization step yields acceptable values for a broad range of actual boundary conditions (*boundary condition-independent* models), see also [1].

Besides packaged devices, other system elements such as heat sinks, fans, heat pipes, etc. may also have compact models derived from measurements and simulations [2].

## 4.3 Thermal Measurements

We can summarize the consequences of the previous section as follows:

- Measurements can be done for component or for system characterization.
- They can be steady-state or transient measurements.

In this chapter, we mainly focus on *transient measurements*.

As we will see in later sections, besides the primary information of the temperature at selected points; the heat propagation starting from the heaters in the system also reveals structural details of the assembly, comparable to ultrasonic or X-ray investigation. In such a way, transient measurements and their evaluation serve *multiple purposes*. They:

- Yield essential data to application engineers in format of data sheets or compact model libraries.
- Characterize the thermal behavior of components at package, board, and system level.
- Help production engineers to perform quality checks on packaging, die-attachment.
- Give feedback to designers of packages or luminaires on the actual performance of constructions.
- Help design engineers to evaluate thermal properties of package, thermal interface, and board materials.

As we can see, some measurement tasks serve research and development (R&D), or can help perform structural FA and production monitoring as part of a quality assurance (QA) process.

Applying a steady low power level to the device and then instantly switching to a higher level (Fig. 4.6), we can observe a heating transient. Similarly, switching from a higher level to a lower one, we can monitor the cooling of the device.

For internal use by Mentor Graphics marketing only

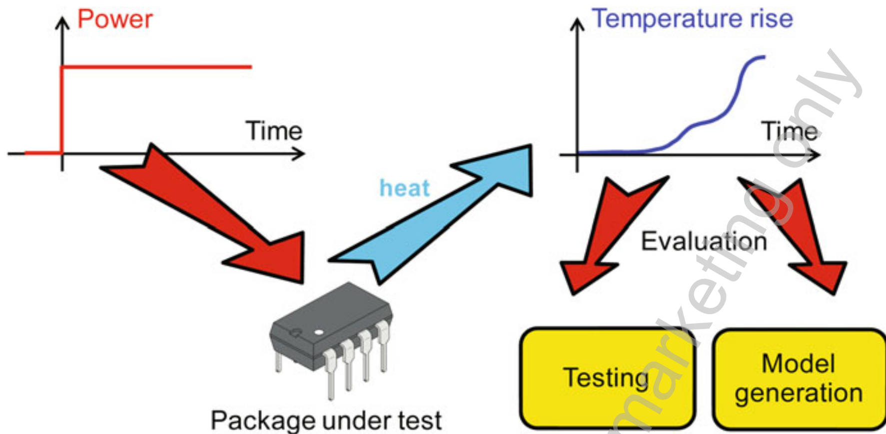


**Fig. 4.6** Thermal transient testing of electronics parts (with heat generation only)

At R&D and FA, the time spent for each measurement doing transient analysis is not critical. At these measurements, we are in the fortunate situation that we can completely capture the transients up to steady-state level. This practice can also be followed at QA if we restrict investigations to a few selected samples.

When aiming at a broader characterization performed on all manufactured samples, the time per measurement is much more limited; i.e., we have to carry out short transients and search for correlation between short time and complete transient behaviors. Some results related to this problem in case of LEDs are presented in a couple of conference papers [3, 4]. Figure 4.6 illustrates testing of semiconductor devices with a single-energy transport mechanism, all electric energy flowing towards the device will be transformed at the end to heat.

In Fig. 4.7, we see a case where a portion of the input electric energy is converted to some other sort of energy: in case of LEDs, laser diodes, etc. this is typically emitted light. While recording the temperature transient, this other quantity can also be recorded. Further consequences of this type of measurement will be discussed in Sect. 4.3.7.

### *4.3.1 Device Categories and Their Features*

Semiconductor devices can act as *heaters* by applying appropriate voltage and current at some of their internal structures. They can also act as *sensors* using their *temperature-sensitive parameters* (further referenced as TSP, for more details see Sect. 4.3.8 on the TSP calibration of devices).

Dedicated thermal test chips have separate heater (dissipator) and sensor structures (Fig. 4.8d).

For internal use by Mentor Graphics marketing only

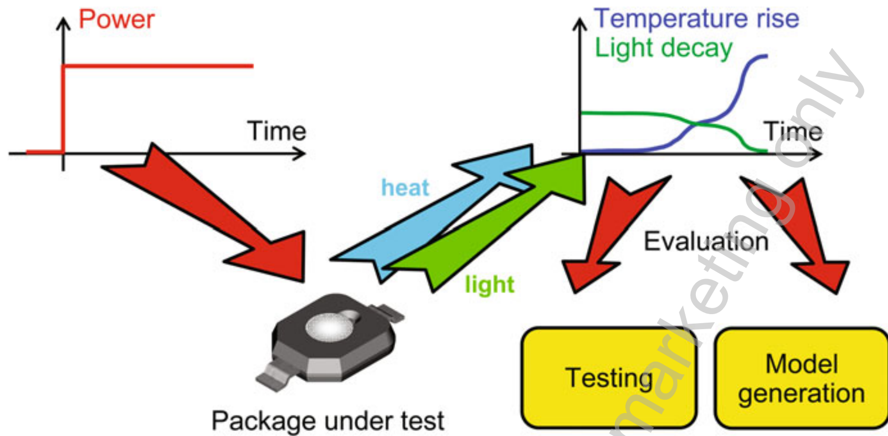


**Fig. 4.7** Thermal transient testing of LEDs (with heat generation and light emission)

**Fig. 4.8** Heater/sensor structures used in thermal testing: **a** MOS transistors, **b** bipolar transistors, **c** pn-junction or diodes, **d** separate heaters and sensors

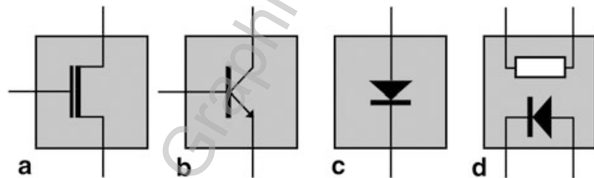


For internal use by Mentor Graphics marketing only

The most common three-pin semiconductor devices like MOS field effect transistors (MOSFET) and bipolar junction transistors (BJT; Fig. 4.8a, b) have an inherent feature of sensing temperature—parameters influenced by the temperature such as $V_{BE}$ or $V_{GS}$ voltages can be measured. These three-pin devices have at least partially separated ports for heating and sensing, e.g., heating can be applied across collector and base electrodes, while the emitter-base junction can be used for sensing purposes. The power step can be induced by a sudden change in the collector-base voltage $V_{CB}$ (voltage jump) or in the emitter current $I_E$ (current jump).

Diode-type discrete devices (Fig. 4.8c) have only one pair of pins, the port used for heating and sensing is the same. The typical powering mode is "current jump," switching between a larger heating current and a smaller sensing or measurement current. At heating, the voltage on the diode changes significantly during the transient (which is the effect we use for measurement actually). Preferred measurement mode is cooling, at a small measurement current. This ensures a suitable $V_F$ forward voltage, which can be used for sensing purposes. In case the power level at cooling is very small, it can be considered to be constant zero. (See considerations of proper choice of the measurement current later.)

Standard silicon integrated circuits can be measured in a "dull" way with their inherently present substrate diodes; such falling into category c. MOSFET devices also can be measured using their reverse diode structures.

A more sophisticated way of measuring integrated circuits is powering heating structures, which dissipate at normal operation. The same structure can act as sensor in many cases. Also, input protection diodes or output parasitic diodes can be used for multiple point sensing. In this case, selecting a proper low sensor current is essential so that the voltage on eventual series resistors can be neglected compared to the forward voltage on the small diode.

### *4.3.2 Basic Approach*

In further sections, we shall give an exhaustive treatment of standards and techniques. In order not to be lost in the details here, we want to emphasize that relevant thermal information can be gained even with a multimeter, thermocouple, and other simple devices. Of course, advanced methods give a much deeper insight into device structure and failure locations.

All methods have to comprise the following steps:

1. Calibration: measurement of the TSP at more temperature values.
2. Heating by applied electric power.
3. TSP measurement at low power.

In production lines, thermal testing is often simplified to a *static method* recording one or a few characteristic temperatures.

In a measurement targeting steady-state *thermal metrics* such as junction-to-ambient *thermal resistance*, step 3 has to be carried out twice, once in hot state, just after switching off the heating power, and once near cold steady state. The measured TSP values yield the "hot" and "cold" temperatures using the calibration values from step 1. This calibration is sometimes carried out just for a few samples of a manufacturing lot.

In a correct static measurement, the cold steady state is reached after a longer equalization time,

- Either just before switching on the power, or
- Using the same long equalization time at the end of a cooling transient (which is not measured).

The critical question is how the time point "just after switching off" is found.

Production line testers often arbitrate just based on one or few "hot" temperature values in go-no go tests.

With "*continuous transient*" *methods* (sometimes, as a result of ill-formed terminology of an old thermal testing standard [5] mistakenly referred as static), step 2 has to be applied for an equalization time and then step 3 has to be carried out more times at a certain sampling rate. The first and the last sample yields the "hot" and "cold" temperatures, the temperature change in between provides device structure-related information.

For internal use by Mentor Graphics marketing only.

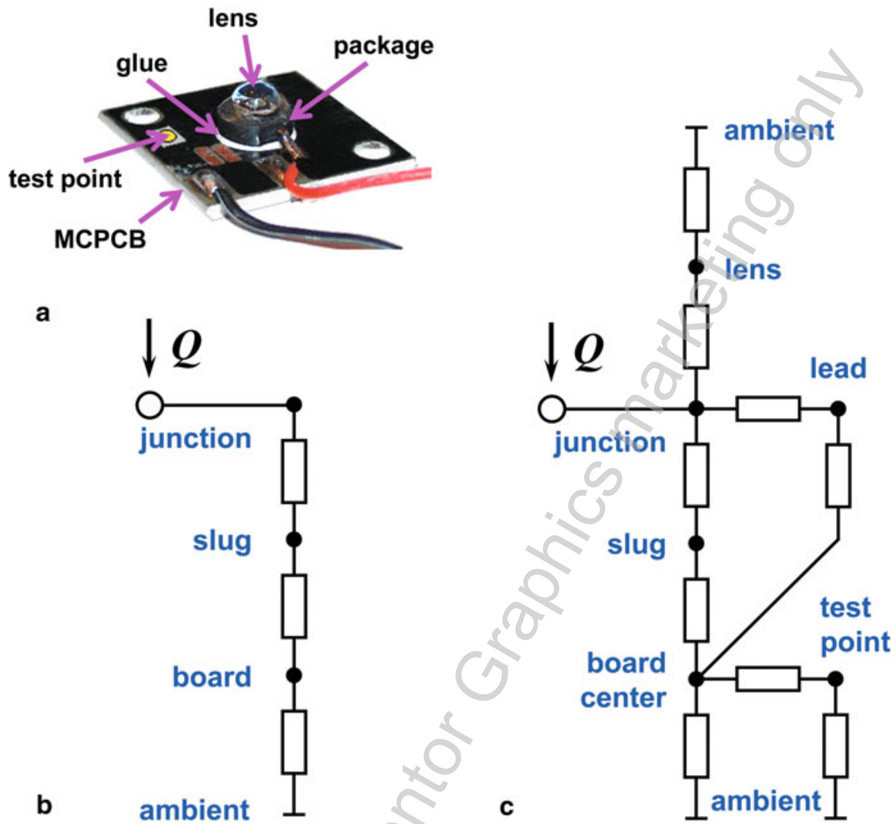


**Fig. 4.9** LED device on metal core PCB with thermal testing point, **a** photograph, **b**, **c** compact models of different accuracy and complexity

For internal use by Mentor Graphics marketing only

While at simple static and "continuous transient" methods step 2 and step 3 last for a time long enough for reaching temperature equalization, *pulsing methods* repeat step 2 and step 3 for each sampling. Here, actually step 3 has to be carried out before and after each heating pulse.[3]

For large-scale testing, often simple comparison measurements are used.

In Fig. 4.9, we see a power LED mounted on a metal core printed circuit board (PCB) used as heat spreader having a thermal test point. LED manufacturers often specify the safe operating area of the LED in terms of test point temperature—allowing their end-users to perform a very simple temperature measurement at this point, often considered as the final thermal testing of their LED application.[4]

[3] Measurement waveforms for the static test methods are depicted in Fig. 6.20 of Chap. 6; (see also [6] and [7]). A concise summary of thermal measurement of diodes is given in [7, 8, 9]. A more detailed analysis is provided in Sect. 4.3.6.

[4] The *junction-to-test point* thermal characterization parameter is a thermal metric, which can help relate junction temperatures to test point temperatures. Discussion of such simple tests is not the main target of this chapter.

For LEDs of this construction (Fig. 4.9a), application notes suggest a compact model as presented in Fig. 6.16 of Chap. 6.

The model in the application note is rather simplified and corresponds approximately to Fig. 4.9b. Although it can be used well despite its simplicity, partial thermal resistance values and internal node temperatures cannot be measured.

Instead, at certain powering, the chip temperature can be derived using one of the methods described before. The package, lead, and test point temperatures can be measured by attaching a thermocouple there.

The more detailed model suggested in Fig. 4.9c hints that such simple static methods yield information on junction, lead, and test point temperatures. However, test point temperature can significantly differ from board temperature under the LED, depending on the cooling mount attached.

In comparative tests, the measurement restricted on leads and test point already provides basic information like "some failure occurred in the chip–submount–heat slug–glue–distributor plate" heat conduction path. Temperature of internal elements in the device and structural information can be gained by transient measurements.

### *4.3.3 Thermal Testing Standards*

Repeatability of a measurement on the same device, moreover the reproducibility among systems at different sites serving the same purpose are key issues in all measurements. In case of thermal characterization, this can be ensured provided the *measurement technique*, *boundary conditions (test environments)*, in some cases, *test devices* along with the *measured quantities (thermal metrics)* are defined by widely accepted standards.

Since 1990, the Joint Electron Device Engineering Council (JEDEC), under the Electronic Industries Association (EIA), has been creating a set of thermal measurement standards for semiconductor device packages. The JEDEC JC-15 committee (Thermal Characterization Techniques for Semiconductor Packages) has been formed by over 40 member companies, among them semiconductor, packaging, and software companies.

The JEDEC thermal testing standards recommend specific environmental conditions, measurement techniques, fixturing, heating power, and data reporting guidelines. Most recently, compact thermal modeling guidelines and LED thermal testing guidelines have been developed and published. (For details on these latter, refer to Chap. 6 on standardization.)

Further in this chapter, we provide details on the basic concepts of thermal testing of packaged semiconductor devices (keeping in mind what is important for LED thermal testing). The basics of thermal testing are described in the JEDEC JESD51 document [10], which is the so-called overview document of the thermal characterization of packaged semiconductor devices. The family of pertinent JESD-51 standards is shown in Fig. 4.10. This figure is an updated version [11] of the chart published in the original JESD51 document [10]. (The most recent update on the

For internal use by Mentor Graphics marketing only.

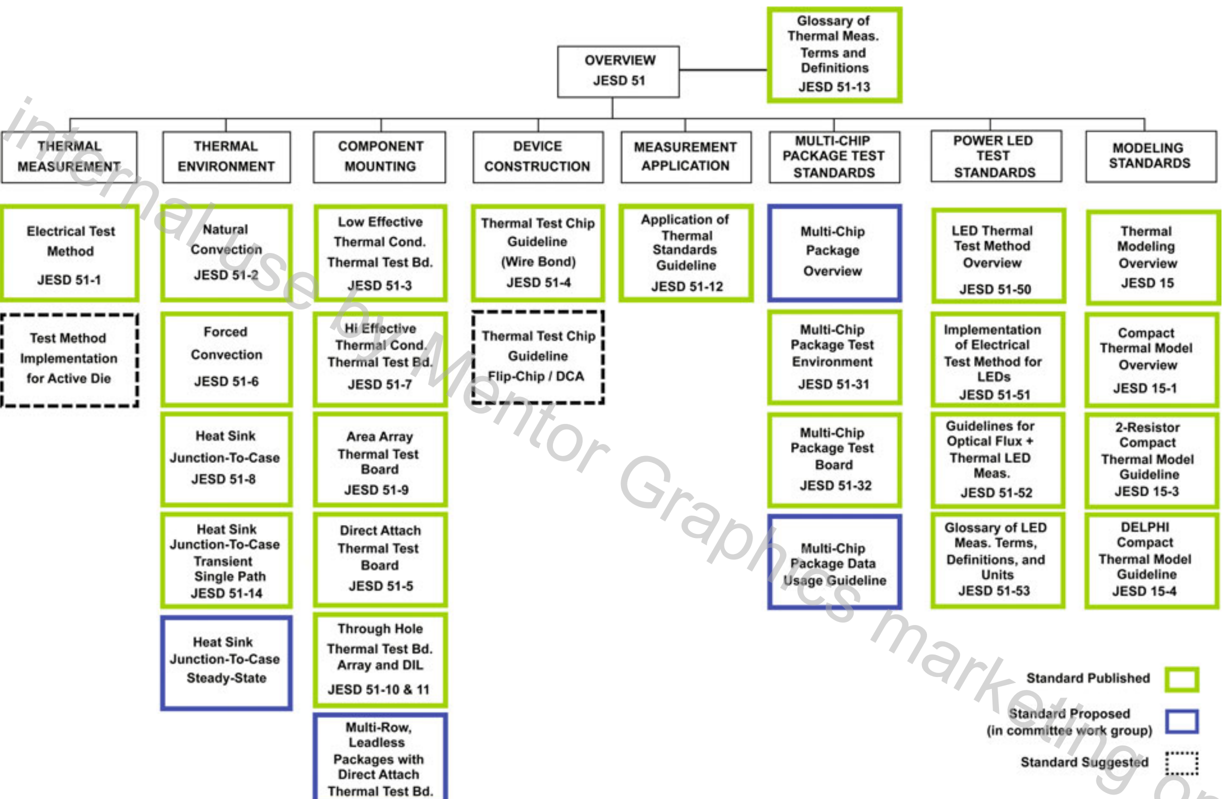


**Fig. 4.10** An updated version of the JEDEC thermal testing standards overview chart of the JESD51 document [10]. (Chart provided in private communications by Bruce Guenin, chairman of the JEDEC JC15 committee. Reproduced with permission of Bruce Guenin)

For internal use by Mentor Graphics marketing only

| | |
|---|---|
| *Temperature measurement technique*: | Electrical test method |
| *Boundary*: composed of | |
| *Test environment*: | Natural convection |
| *Component mounting*: | Low conductivity test board for surface-mount leaded package |
| *Device construction*: | Wire bond thermal test chip |

standardization activities of the JC15 committee is provided in [12]. More details on JEDEC's LED thermal testing standards are given in Chap. 6).

The series of the JESD 51 standards is based on a modular approach. A testing protocol for a particular measurement problem can be composed by selecting the appropriate documents describing the measurement method, the test environment, component mounting, device construction, and the data reporting. For example, a process can be built up on the following elements:

The measurement process yields one or more standardized *thermal metrics*, which need to be reported with information recommended by the data reporting guidelines and according to the specific requirements of the given test method.

The modular approach of the JEDEC thermal testing standards is explicitly described in the JESD51 document by mentioning possible addition of new documents as the need arises.

JEDEC thermal metrics types aim to express power-induced temperature change. The measurement occurs between the point where the powering occurs (driving point, "*junction*") and some reference point or reference surface or reference environment.

The first type of thermal metrics is based on a stricter definition and is called *thermal resistance*, denoted as $R_{thJX}$ or $\Theta_{JX}$. Supposing that all heat generated by $P_H$ heating power at the $J$ driving point (usually referred to as *junction*) flows through an isothermal surface in the measurement arrangement called $X$; we define $R_{thJX}$ as

$$R_{thJX} = \frac{T_J - T_X}{P_H} \tag{4.2}$$

In thermal design, we still often use the term *junction* for the thin region on the top of the semiconductor chip where dissipation occurs. The term is inherited from the time of discrete components having a large pn-junction as source of dissipation. In case of LEDs, it is really the pn-junction where most heat is generated.

Usually, the $X$ surface is not a plane. $T_J$ and $T_X$ are the temperatures of the driving point and the reference environment.

In many cases, it is not possible to find an isothermal surface where all heat passes. In such cases, a less rigorous thermal metric type is defined, called *thermal characterization parameter*, which is denoted as $\Psi_{JX}$.

Supposing the heat generated by $P_H$ power at the $J$ driving point flows through more alternative heat conducting path sections, and there is a well-defined *point* in the measurement arrangement called $X$, $\Psi_{JX}$ is defined as

$$\Psi_{JX} = \frac{T_J - T_X}{P_H} \tag{4.3}$$

For internal use by Mentor Graphics marketing only

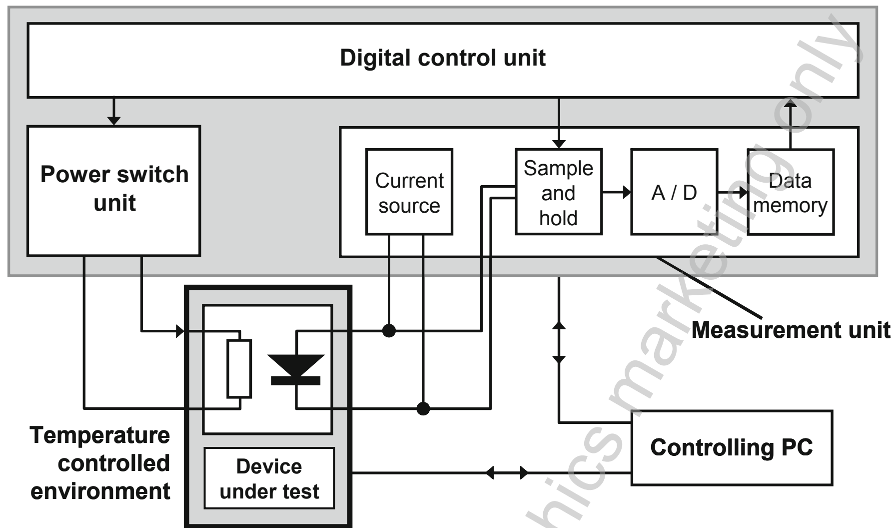


**Fig. 4.11** The general scheme of the tester and test environment

For internal use by Mentor Graphics marketing only

$T_J$ and $T_X$ are the temperatures of the driving point and of the reference point. The test point in Fig. 4.9 can serve for producing such a thermal characterization parameter in comparison measurements.

For further details on standardization of thermal characterization of LEDs, consult Chap. 6 of this book. Some new thermal testing standards are presented for power semiconductor devices in [13] and for power LEDs in [6, 14].

### *4.3.4 Measurement Instruments and Environments*

As shown before, we have to use controlled voltage and current sources to apply the appropriate power levels. For measuring the *junction temperature* by *electrical test method*, we also need fast and accurate amplifiers and data acquisition, at least in transient testing. Powering, sampling, and data acquisition is integrated in *thermal transient testers*.

Another task related to the thermal testing of semiconductor devices is the realization of *repeatable boundary conditions*. The JEDEC JESD 51 series of standards define *convective* and *conductive* environments.

Convective boundaries are typically realized by still air chambers, wind tunnels, and liquid baths. Conductive environment is realized by different cold plate structures.

Plates and baths can be programmed to force different temperature values to the device under test. Using them with the tester equipment, these can be also applied to calibrate the temperature-sensitive parameter of the devices (Fig. 4.11).

The thermal transient testing system consists of:

- The tester hardware,
- Software elements for measurement control and data acquisition,
- Software elements for the subsequent postprocessing and display of data measured.

The measurement control software applies programmed power excitations to the dissipator element and records the complex temperature responses.

Relevant radiometric and photometric standards (listed in Chap. 6) prescribe an appropriate temperature-stabilized environment for LED measurements, e.g., an integrating sphere with temperature-stabilized fixture. In Sect. 4.3.7, we present a combined methodology for radiometric/photometric and thermal testing.

### *4.3.5 The Differential Measurement Principle*

Formerly, when steady-state thermal measurements predominated, usually the *absolute measurement technique* was used. This technique takes the meaning of Eq. (4.2) literally.

One has to apply a $P_H$ heating power and then has to measure the absolute $T_J$ and $T_X$ values separately. The advantage of this measurement is that it can be carried out by very simple means, like a multimeter. On the other hand, this approach unleashes a lot of problems in measurement and calibration (referred later in this section).

One can get rid of most measurement errors using a *differential technique* for measuring quantities, which are by nature differences.

For example, at junction-to-ambient measurements, we can apply two different level of the heating power $P_{H1}$ and $P_{H2}$, and measure the temperature after equalization in each case. We shall get:

$$T_{J1} = P_{H1} \cdot R_{thJA} + T_A \tag{4.4}$$

$$T_{J2} = P_{H2} \cdot R_{thJA} + T_A \tag{4.5}$$

$$(P_{H1} - P_{H2}) \cdot R_{thJA} = T_{J1} - T_{J2} \tag{4.6}$$

$$R_{thJA} = \frac{(T_{J1} - T_{J2})}{(P_{H1} - P_{H2})} \tag{4.7}$$

As shown before, the temperature-sensitive element is in most cases a pn-junction (or a resistor), needing some bias (usually a constant current) to produce a temperature-dependent voltage. The temperature sensitivity of these structures has typically good linearity over a large temperature interval, thus, if the $V_{F0}$ reference value of the forward voltage is known for the $T_{J0}$ reference value of the junction temperature, the forward voltage at any junction temperature can be expressed with a linear relationship:

$$V_F(T_J) = V_{F0} + S_{VF} \cdot (T_J - T_{J0}) \tag{4.8}$$

For internal use by Mentor Graphics marketing only

where the $S_{VF}$ sensitivity slightly depends on the $I_M$ bias current, too. With this, for $R_{thJA}$, we get

$$R_{thJA} = \frac{V_F(T_{J1}) - V_F(T_{J2})}{S_{VF} \cdot (P_{H1} - P_{H2})} = \frac{\Delta V_F}{S_{VF} \cdot \Delta P_H} \tag{4.9}$$

The differential principle offers a lot of advantages. There is no need to directly measure $T_A$, just $T_J$. Even when doing the calibration for getting the $S_{VF}$ sensitivity for Eq. (4.8), only a differential measurement is needed. All offset problems at measurement and calibration cancel out.

In the literature, often the $K = 1/S_{VF}$ reciprocal sensitivity factor is used. Therefore, the calibration process for finding the value of $S_{VF}$ is also called *K-factor calibration*. With the K-factor, Eq. (4.9) reads as

$$R_{thJA} = K \cdot \frac{\Delta V_F}{\Delta P_H} \tag{4.10}$$

The results apply to transient measurements, too. Here, a full capture of $\Delta T_J(t)$ time function (i.e., using the voltage of the temperature-sensitive structure) is needed between the equilibrium at $P_{H1}$ and that at $P_{H2}$. It is often thought that one of the power levels, $P_{H2}$ for example, has to be kept low in order to avoid self-heating of the device. Using the differential technique, this effect is only of minor importance; even the effect on the K-factor calibration can be neglected.

$P_{H1}$ and $P_{H2}$ can be applied in many ways, such as changing $V_{CB}$ on a transistor, or changing the clock frequency of a processor.

If in Eq. (4.10) we consider the $\Delta V_F(t)$ time function of the change of the forward voltage, we obtain $R_{thJA}(t)$—a time dependent thermal resistance value referred to as $Z_{thJX}(t)$ thermal impedance, see also Sect. 6.1.4.1 of Chap. 6.

$Z_{thJX}(t)$ impedances, i.e., thermal impedances towards a point different than the ambient can be derived similarly, by measuring $T_J$ and $T_X$ at two power levels. Here, all offset problems cancel out again.

For internal use by Mentor Graphics marketing only

## 4.3.6 Current Jump Measurements on Two–Pin Devices

At diode-like devices (including LEDs), the usual way to apply the $P_{H1}$ and $P_{H2}$ power levels is to change the current bias. While maintaining a constant $I_{sense}$ sensor current, a sudden jump in the power level can be generated by switching on and off an $I_{drive}$ heating current. Throughout the JESD51 series of thermal testing standards the $I_{sense}$ sensor current is also known as $I_M$ *measurement current* and the sum of $I_{sense}$ and $I_{drive}$ currents is called $I_H$ *heating current*.

### 4.3.6.1 Continuous Cooling Measurements

With this measurement technique, the switching from the $I_H$ *heating current* to a smaller $I_M$ *measurement current* occurs only once, as shown in Fig. 4.12.

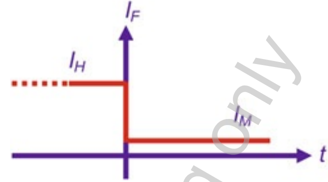


**Fig. 4.12** Stepwise change of the forward current on the diode under test

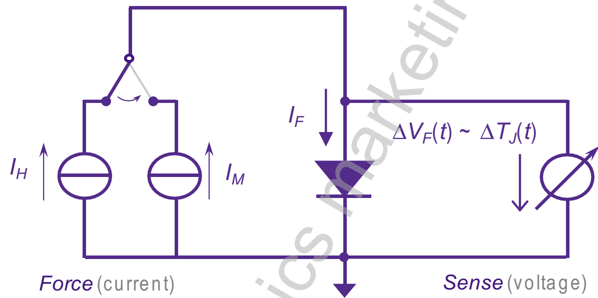


**Fig. 4.13** Diode measurement scheme as defined by JESD51-1 and JESD51-51

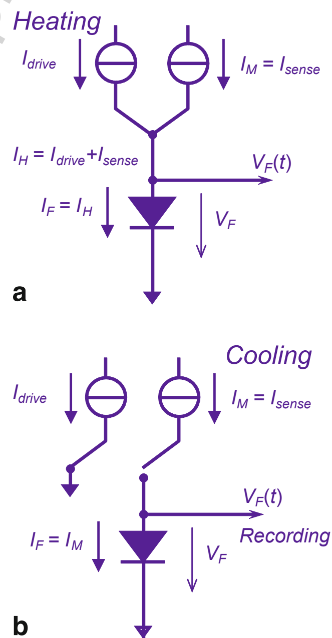


**Fig. 4.14** Practical realization of the diode measurement scheme: **a** applying heating current, **b** applying measurement current

For internal use by Mentor Graphics marketing only

Figure 4.13 shows the theoretical measurement arrangement as recommended by the classical technical literature [7] and the JEDEC thermal testing standards [5, 10]. In Fig. 4.14a, b, the practical realization of the switching is shown.

The $I_H$ heating current is provided as a sum of the currents of the $I_{drive}$ and $I_{sense}$ current sources, thus, in the heating period (Fig. 4.14a) both currents are applied on

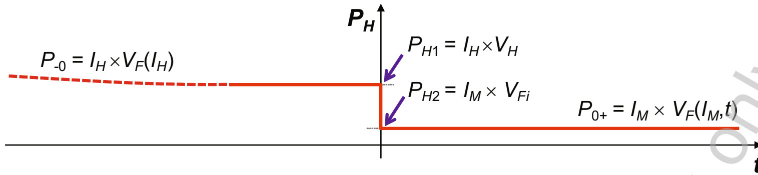


**Fig. 4.15** Power change before and during the cooling measurement on a diode

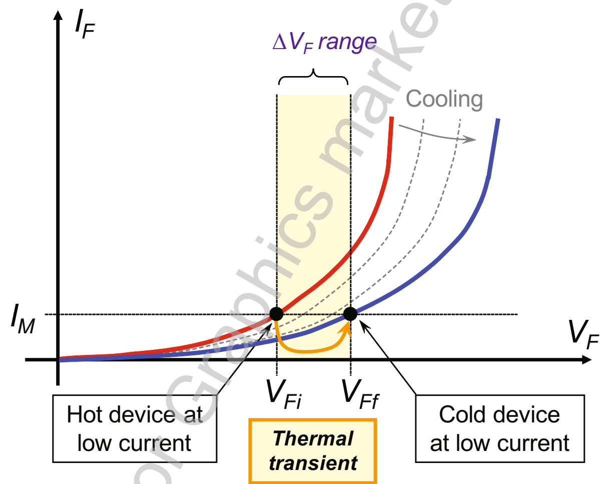


**Fig. 4.16** Thermal (cooling) transient of the diode at constant measurement current shown in its I–V characteristics

For internal use by Mentor Graphics marketing only

the device for an equalization time of appropriate duration. When the device reached "hot" steady state, the drive current will be switched off and the transient recording of the cooling will start (Fig. 4.14b) at the $I_M$ measurement current provided by the $I_{sense}$ current source only.

Diodes have negative temperature sensitivity ($S_{VF} \approx -1$ to $-2.5$ mV/°C), so during the heating period the temperature increases and the $V_F$ forward voltage diminishes. As the current is constant, $P_{H1}$ also diminishes during the heating (Fig. 4.15), it has to be measured just before switching out. We can state that

$$P_{H1} = I_H \cdot V_H, \;\; P_{H2} = I_M \cdot V_{Fi} \tag{4.11}$$

and

$$\Delta P_H = P_{H1} - P_{H2} = I_H \cdot V_H - I_M \cdot V_{Fi} \tag{4.12}$$

where $V_H$ is the forward voltage of the hot diode biased with the $I_H$ heating current (heating voltage) at the time instance of switching, $V_{Fi}$ is the initial value of the forward voltage at the beginning of the cooling transient when the diode is supplied with the small $I_M$ measurement current only (for notations see Fig. 4.16).

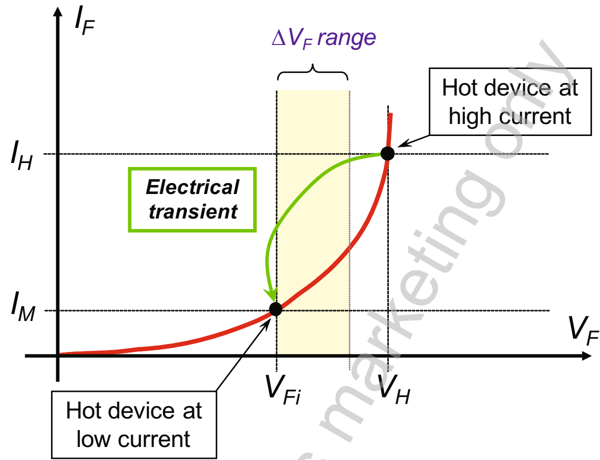


**Fig. 4.17** Electrical transient of the hot diode shown in its I–V characteristics, switching from the heating current to the measurement current

For internal use by Mentor Graphics marketing only

During the cooling period, the $V_F$ forward voltage will grow, it nearly repeats the change that took place during the equalization, but now in the opposite direction. The slightly changing power during cooling can be expressed as

$$P_{H2} = I_M \cdot V_{Fi} + I_M \cdot \Delta V_F(t) \tag{4.13}$$

If the $I_M$ measurement current is significantly lower than the $I_H$ heating current, then the *power change* during cooling can be neglected.

For a simple estimate on an LED measurement, let us program $I_H = 350$ mA and $I_M = 5$ mA. Assuming a forward voltage of about 3 V at $I_H$ and 2.9 V at $I_M$, the total power step will be (350 mA × 3 V) – (5 mA × 2.9 V) = 1.035 W.

If the temperature sensitivity is –2 mV/ °C at the measurement current and the temperature change during the transient is 50 °C, then the temperature-induced forward voltage change is 100 mV. The error term (power instability during the cooling) will be $I_M \cdot \Delta V_F(t) = 0.5$ mW, which is about 0.5 % of the total power change. Thus, at low $\Delta V_F$ and low $I_F$ the change of the heating power is a secondary order effect only. In such a way, at cooling, we could realize a nearly perfect *power step*.

After switching off first, we can observe a sudden large voltage jump on the diode—the $V_F$ forward voltage sinks from the $V_H$ value belonging to the “hot” diode characteristics at $I_H = I_{drive} + I_{sense}$ to the lower $V_{Fi}$ value belonging to the “hot” diode characteristics at the smaller $I_M = I_{sense}$ only (Fig. 4.17).

This change, referred to as electrical transient, can be many hundred millivolts for diodes, for diodes with higher series resistance[5] even more than 1 V. The voltage change can be slow (10–100 μs), as large amount of stored diffusion charge has to be removed from the forward biased pn-junction (see also [7]).

After this electric transient, we can capture the thermal transient, as the $V_F$ forward voltage slowly increases from its $V_{Fi}$ initial value when the operating point moves

[5] The effect of the series resistance is discussed in detail in Chaps. 2 and 6 and in papers [15, 16].

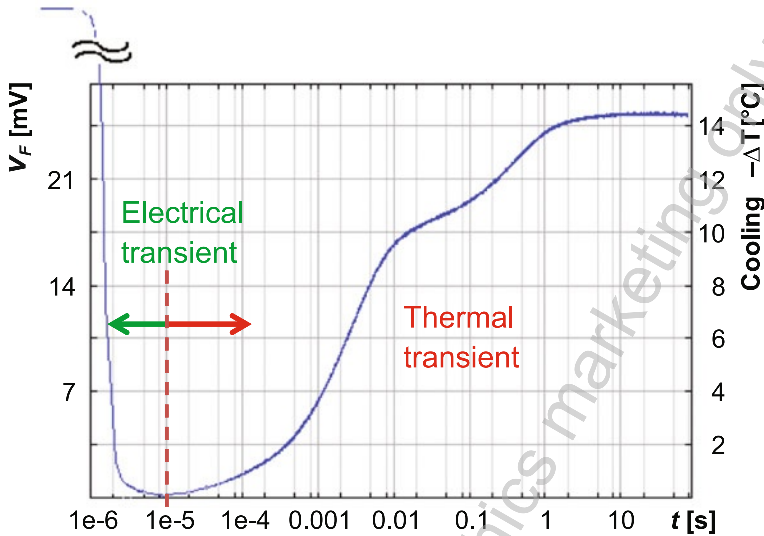


**Fig. 4.18** Recorded transient of an actual diode, scaled in voltage (on the *left*) and in temperature (on the *right*)

from the "hot" to the "cold" diode characteristics, reaching its final, $V_{Ff}$ value, always at $I_M$ bias (Fig. 4.16).[6]

Selecting a measurement range of a few millivolts (shown in Fig. 4.16 as $\Delta V_F$ *range*), we always capture first the end of the electric transient at early times (intersection of $\Delta V_F$ *range* and the electric transient), and then the thermal transient.

In Fig. 4.18, a recorded transient of a diode is presented; the electric transient finishes at approximately 10 μs.

#### 4.3.6.2 Selecting the Heating Power

As thermal testers are typically sensitive, for just analyzing the structure integrity, we need a power level that can ensure a few centigrade temperature elevation. For reliability testing, normal operational power has to be ensured. For accelerated reliability testing, higher than normal power has to be applied unto the device.

#### 4.3.6.3 Selecting the Measurement Current

A common mistake in the literature is that the sensor current should be kept low in order to avoid self-heating of the component. In reality, the self-heating has only some minor influence in the *absolute* measurement technique, and can be nearly neglected

[6] Voltage and current notations correspond to the notations used the JESD51-5x series of standards, see also Chap. 6.

For internal use by Mentor Graphics marketing Only

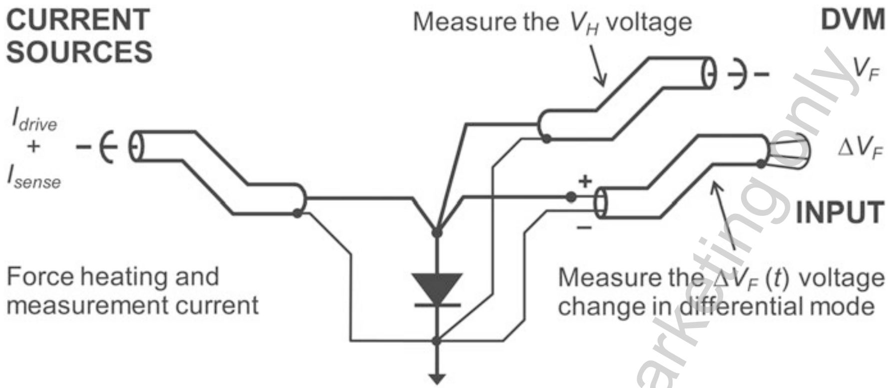


**Fig. 4.19** Force/sense measurement of a diode. (Connection diagram of a thermal transient tester)

For internal use by Mentor Graphics marketing only

in the *differential* technique. In this case, we have great freedom for selecting the sensor current.

One of the advantages of selecting higher sensor currents is smaller and faster electric transients.

As we will see in Sect. 4.3.8, semiconductor diodes biased at different current level obey the

$$(V_{F1} - V_{F2}) = V_T \cdot \ln(I_1/I_2) + R_S \cdot (I_2 - I_1) \tag{4.14}$$

law. The first term of the equation describes the ideal diode equation of the junction. For calculating the change of the voltage caused by this term, we can use the approximate values as $V_T = kT/q \approx 26$ mV (at room temperature) and ln (10) ≈ 2.3. The result is that at a measurement current ten times lower than the heating current the voltage change during the electric transient is approximately 60 mV. Similarly, at a measurement current hundred times lower than the heating current the voltage change during the electric transient is approximately 120 mV.

The second term in Eq. (4.14) is practically dependent on the heating current only; the influence of the measurement current can be neglected.

Using forward voltage of diodes as temperature-sensitive parameter, we experience lower noise at higher measurement current. The physical background of the effect will be given later in Sect. 4.3.9.

In actual current jump measurements, a *four-wire* force/sense arrangement (as shown in Fig. 4.13) is preferred for correct power calculation, not adding the dissipation on the wires to the powering of the device.

Up-to-date testers can measure separately the high $V_F$ value on a DVM unit for calculating the power and the small temperature-induced $\Delta V_F$ change on a sensitive differential measurement channel (Fig. 4.19).

An actual thermal measurement arrangement with the tester and the equipment realizing the thermal boundary is shown in Fig. 4.20.

As continuous heating measurements and pulsed measurements suffer from serious drawbacks in LED measurements and in such a way their use has limitations, we discuss these below only briefly.

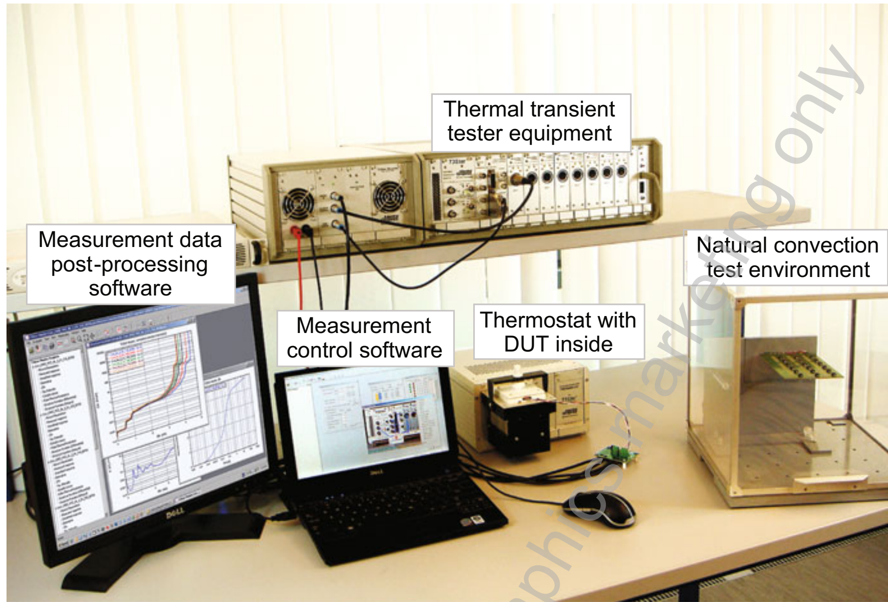


**Fig. 4.20** Typical thermal measurement arrangement: test equipment, thermostat for K-factor calibration or to be used as a cold plate, natural convection test environment and measurement control, and data processing software running on a PC

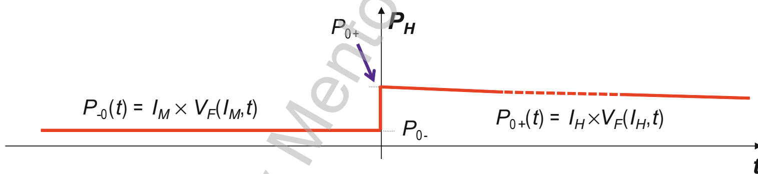


**Fig. 4.21** Power change before and during the heating measurement on a diode

For internal use by Mentor Graphics marketing only

### 4.3.6.4 Continuous Heating Measurements

In these measurements, only the sensor current is applied to the device for an equalization time of appropriate duration. When the device reached "cold" steady state (the equilibrium at $P_{H1} = I_M V_{F1}$), the drive current will be switched on, too, and the transient recording of the heating will start.

Most considerations introduced for the cooling operate in the same way. However, here we experience a larger power change on the hot device during recording time, approximately the opposite forward voltage change, which we saw at cooling measurements occurs now at high current. The powering is far from an ideal step (Fig. 4.21).

This problem can be mathematically handled, but it is easier to use the cooling for the thermal measurements of two pin devices.

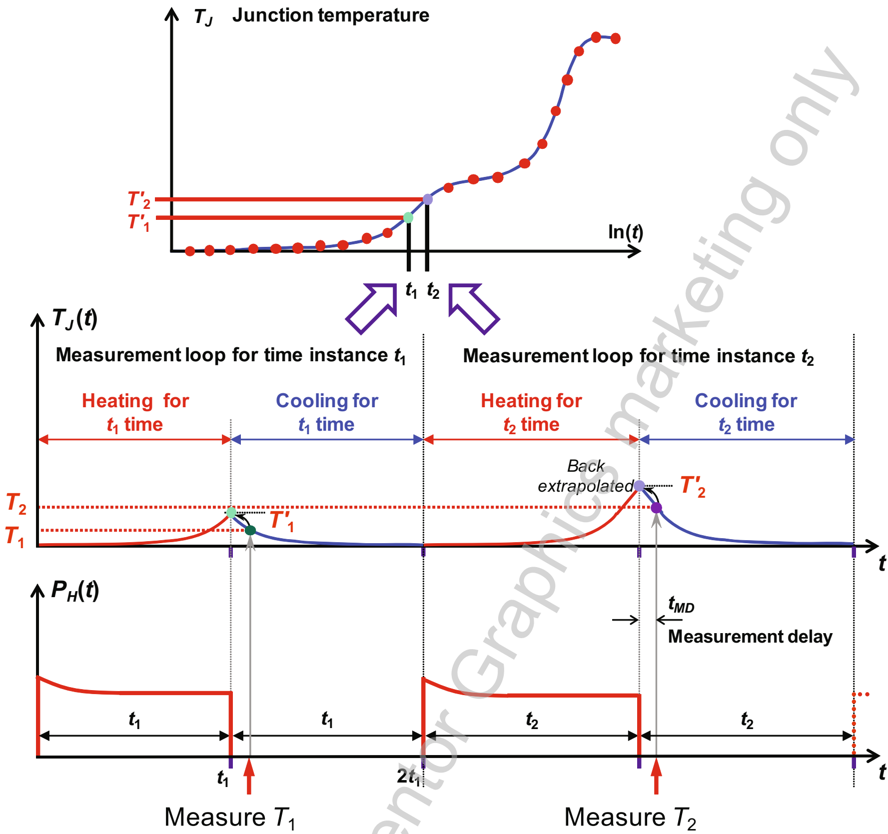


**Fig. 4.22** The principle of the JEDEC JESD51-1 dynamic test method: **a** the series of heating pulses and corresponding temperature responses, **b** heating curve composed of individual temperature values measured at the end of the heating pulses

Both the cooling and the heating measurements described up to this point correspond to the transient extension of the JEDEC JESD51-1 “static” test method,[7] defined in [5] and Chap. 6.

### 4.3.6.5 Pulsed Measurements

The JEDEC JESD51-1 standard [5] also defines the so-called “dynamic” method. The measurement principle is illustrated in Fig. 4.22. In this method, the measurement

[7] This extension was first defined in details in the JEDEC JESD 51-14 standard [13]. This proposes a transient method for the measurement of the junction-to-case thermal resistance of power semiconductor device packages with a single heat flow path and with an exposed cooling surface—such as power LED packages. JEDEC JESD 51-14 also prefers the cooling mode transient measurement for diodes since the error introduced by the slightly changing power after switching is negligible in this case (as we also pointed out by a numerical example). The most recent LED thermal testing standard JESD51-51 [6] also recommends the cooling mode measurement if the task is to measure the real $Z_{th}(t)$ thermal impedance of an LED package.

For internal use by Mentor Graphics marketing only

is based on a series of high current pulses for heating and switching back to low current for temperature recording: the temperature value $T_1$ corresponding to $t_1$ time instance is measured such that a power pulse with a duration of $t_1$ is applied to the device under test. When $t_1$ time is elapsed, the power pulse is switched off (switching from $I_H$ heating current to the $I_M$ measurement current) and with a short delay $t_{MD}$ (called the measurement delay) the value of the TSP (forward voltage) is measured and through the K-factor is converted to junction temperature. Then, the device under test needs to cool down, the cooling time must be at least as long as $t_1$. Then, the process is repeated for a longer pulse width $t_2$, etc.

The test result (referred to as heating curve) is composed from these responses to individual heating pulses of different length. This technique distorts each recorded point by an electric transient and the data correction problem (back extrapolation of the measured *i*th junction temperature at $t_i + t_{MD}$ time instance to the $t_i$ time instance) is also present at every data point of the composed $Z_{th}$ curve. Moreover, as we see in Sect. 6.5.1 of Chap. 6, these recorded points belong to different heating powers due to temperature-dependent LED efficiency, even if the applied electrical power is kept constant during the entire measurement process. Last but not least: the physical time needed for the measurement by the dynamic test method is by orders of magnitude longer than the length of the real cooling transient measured by the transient extension of the static test method.

As such, use of pulsing measurements is very restricted in LED applications: the JESD51-51 standard recommends this only for measuring steady-state thermal metrics such as total junction-to-ambient thermal resistance of a given test setup. The description of this pulsed method as "dynamic" is a bit misleading; all transient measurements of any style are by nature dynamic.

#### 4.3.6.6 Measurement of Devices with Separated Heating and Sensing

Typically, complex systems or thermal test chips have separate leads for heating and sensing. They can also be measured in *current jump* mode with a sudden change in a current of the system. More typically, *voltage jump mode* is used for such devices.

Even simple devices widely used in SSL lighting as current drive stage, such as bipolar transistor or MOSFETs, have a sort of separation between heating and sensing. For example, for transistors, we can maintain a steady $I_E$ emitter current and then switch between a high and a low $V_{CB}$ collector-base voltage value for generating a power step. For sensing purposes, we can capture the voltage change at the emitter-base junction. Then, using different leads, we have good separation of powering and sensing. In such a way, the above mentioned problem of changing power during a heating type measurement is also eliminated.

This measurement mode offers the best resolution when mapping the fine details of the thermal structure, belonging to shortest time constants. Due to the separation, the electric transient is very fast, just a few microseconds.

For internal use by Mentor Graphics marketing only

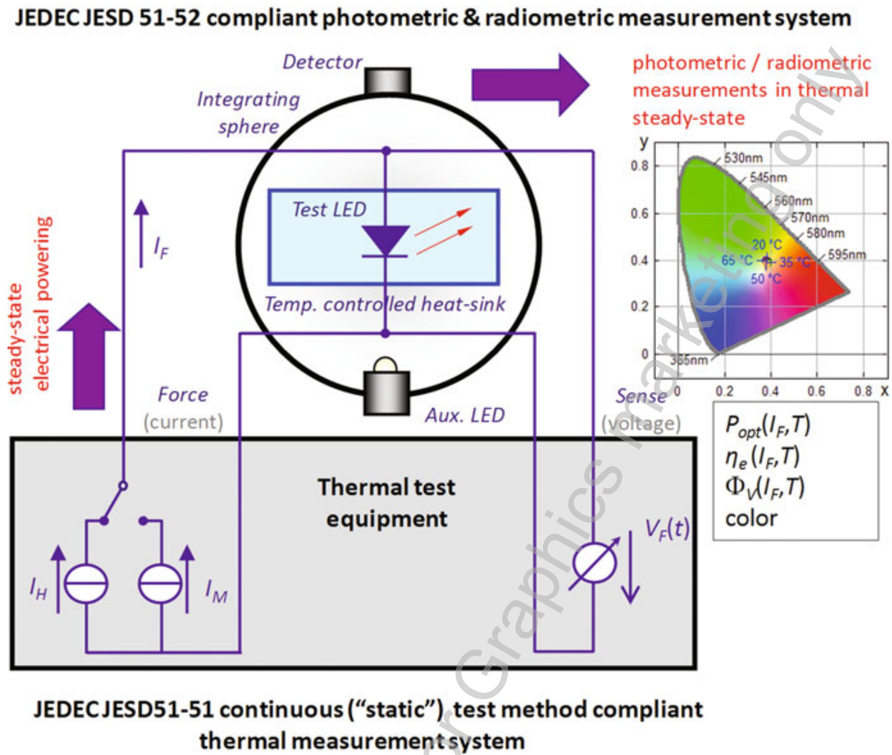


Fig. 4.23 Photometric/radiometric measurement of an LED device in a combined arrangement

For internal use by Mentor Graphics marketing only

### 4.3.7 Combined Thermal and Photometric/Radiometric Measurements

As mentioned before, thermal and photometric/radiometric measurements can be combined for faster and more reliable testing.

In these combined measurements, first the device is mounted on a temperature-stabilized plate, as anyway requested in optical measurements of high-power LEDs and then this plate is fixed to an integrating sphere equipped with detector, filters, spectrometers, etc.

The device is heated by appropriate heating current. When steady state is reached, emitted optical power, luminosity, color coordinates, etc. are provided by the optical test system (Fig. 4.23).

The forward voltage of the device at the heating current is measured by the thermal test equipment. The measured value is stored and used for power calculation. As hinted in Fig. 4.7 "power" can have more interpretations:

- First of all, we can calculate the *input electric power*, $P_{el} = I_F \cdot V_F$
- The radiometric measurement provides the *emitted optical power*, $P_{opt}$
- The heat remaining in the structure $P_H = P_{el} - P_{opt}$ is called *heating power*

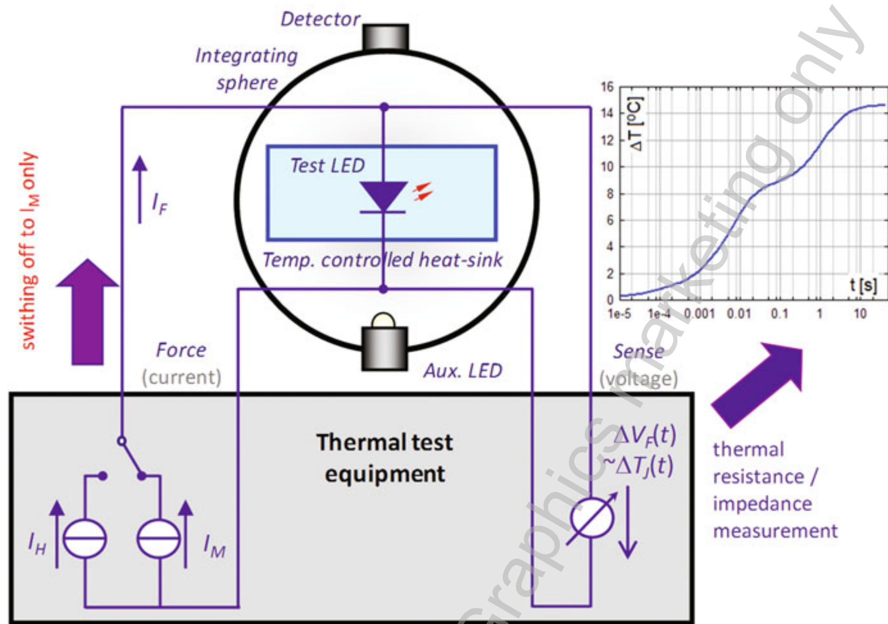


Fig. 4.24 Thermal transient measurement of an LED device in a combined arrangement

For internal use by Mentor Graphics marketing only

$P_{opt}$ is also known as *total radiant flux* and is also denoted by $\Phi_e$.

Finishing the test, we switch down the heating current to a low measurement current and capture the thermal transient (Fig. 4.24) in accordance with the continuous cooling transient measurement technique discussed in Sect. 4.3.6.1.

Now all thermal descriptive functions, which are normalized by the power, will have two different sets with different meaning. Even in the simplest steady-state case, we can define

$$R_{th-el} = \Delta T_J / P_{el} \tag{4.15}$$

as *electrical only* thermal resistance for calculating the thermal stress on the actual device at a certain electrical powering (not considering light emission), and

$$R_{th-real} = \Delta T_J / P_H = \Delta T_J / (P_{el} - P_{opt}) \tag{4.16}$$

as *real* thermal resistance for characterizing package quality, structural details, not influenced by the actual type (color, etc.) of the packaged LED device.

The JESD51-51 standard [6] prescribes measuring the real thermal resistance for package characterization.

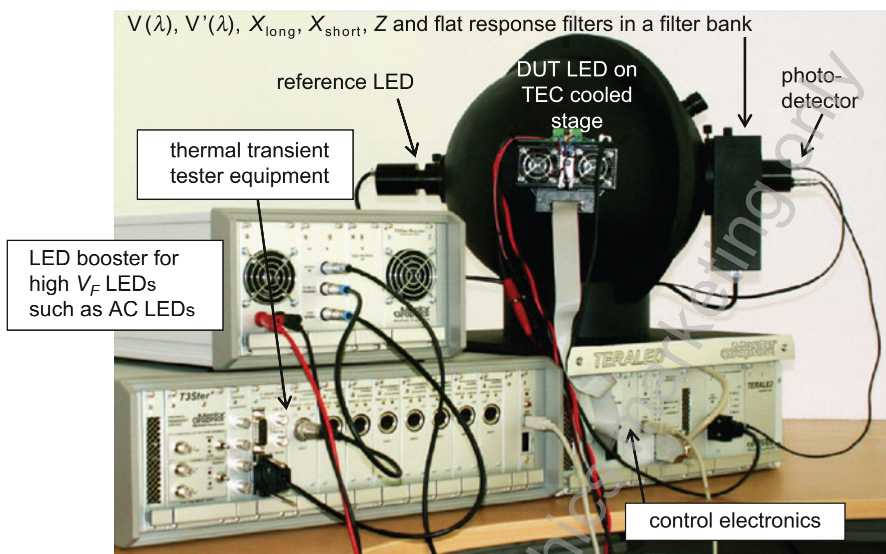


**Fig. 4.25** Realization of a combined thermal and radiometric/photometric LED measurement station

Further analysis of $R_{th\text{-}el}$ and $R_{th\text{-}real}$ thermal characteristics will be provided in Sect. 4.4.

Figure 4.25 shows a practical realization of a combined thermal and optical LED measurements station. The device has to be mounted on the temperature-stabilized cold plate only once. The system automatically measures all temperature- and current level-dependent LED parameters, going through a user-defined set of temperatures and currents. After an initial step needed for the optical measurements, the automated measurement is carried out in three embedded loops. The complete measurement sequence is as follows:

1. Dark offset measurement with DUT LED off
2. Self-absorption correction with DUT LED off and reference LED on
3. New temperature is programmed (this can be changed in the slowest way)
   the system waits for temperature stabilization
    4. New current is programmed,
       the system waits for voltage and temperature stabilization
        5/a. radiometric and photometric parameters are measured
             by filters and/or a spectrometer
        5/b. switch from programmed forward current down to the
             measurement current: thermal parameters are measured
             by the thermal transient tester
    Next current is programmed
Next temperature is programmed

For internal use by Mentor Graphics marketing only

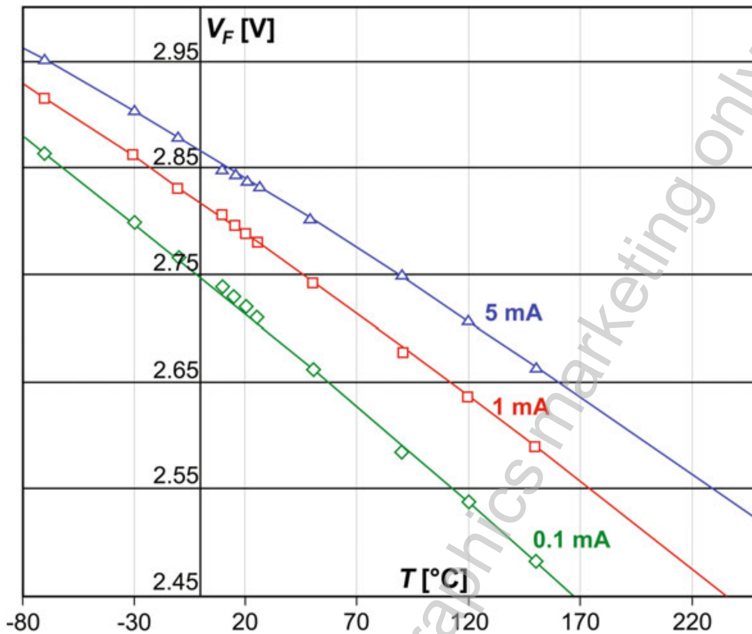


**Fig. 4.26** Temperature dependence of the forward voltage, LED at different bias currents

For internal use by Mentor Graphics marketing only

In step 1, the DUT LED is switched completely off: the dark-level offset measurement of the photodetector (and/or spectrometer) takes place. In step 2, the measurements needed for the self-absorption correction of the DUT LED are performed using an auxiliary reference LED with known and stable parameters. (For further details on this, refer to Sect. 5.2 of Chap. 5).

In a postprocessing step, after making the measurements for every $(I_F, T)$ operating point the real heating power is calculated from the electrical power $(I_F \cdot V_F)$ and the measured radiant flux $(P_{opt} = \Phi_e)$.

With these data, the real thermal resistance can be gained from which the real junction temperature is also calculated back: $T_J = T_{ref} + R_{th\text{-}real} \cdot P_H$, where $T_{ref}$ is the cold plate temperature and $P_H = I_F \cdot V_F - P_{opt}$ denotes the actual heating power.

Plots of temperature- and current-dependent LED parameters are presented in Figs. 6.15 and 6.26 of Chap. 6.

### 4.3.8 The K-Factor Calibration Process

The precise calibration process is of high importance because this step influences the overall accuracy of the measurement. All other steps in thermal measurements are practically voltage and current measurements for which we have instruments of high precision and high time resolution. On the contrary, it is easy to perform a bad calibration and undermine the validity of thermal data.

#### 4.3.8.1 The Temperature-Sensitive Parameter

The most often used parameter for temperature sensing is the forward voltage of a diode-like structure. Temperature sensitivity can be deduced from basic semiconductor theory. We present the case of diodes, which behave nearly ideally in a wide range of temperature and current, but the results are much the same for other device types, too. The forward current ($I_F$)–forward voltage ($V_F$) characteristics of an ideal diode follows the Shockley model of pn-junctions[8]

$$I_F = I_0[\exp(V_F/mV_T) - 1] \tag{4.17}$$

Introducing the $R_S$ internal electrical series resistance (and neglecting the very small—$I_0$ term), we get

$$V_F = mV_T \ln\frac{I_F}{I_0} + I_F R_S \tag{4.18}$$

The $V_T$ and $I_0$ parameters are temperature-dependent

$$V_T = \frac{kT}{q}, \quad I_0 \sim n_i^2 \sim T^3 \exp\left(\frac{-W_g}{kT}\right) \tag{4.19}$$

where $n_i$ is the intrinsic concentration of moving electrons in the pure semiconductor, showing the above dependence on the $T$ absolute temperature of the semiconductor material.

$m$ is a device-specific constant called *ideality factor*. $m$ is 1 in the normal operation mode of an ideal diode.

At very small currents, $m = 2$ because of recombination/generation effects in the depleted junction region. Theoretically, at very high currents $m = 2$, again because of ambipolar diffusion of carriers of both type. These regions generally overlap thus giving an $m$ factor valid for a wide current range. The $m$ factor can be calculated by more methods, the simplest is choosing two appropriate points from the characteristics:

$$V_{F2} - V_{F1} = mV_T \ln\frac{I_{F2}}{I_{F2}}, \quad m = \frac{V_T}{V_{F2} - V_{F1}} \ln\frac{I_{F2}}{I_{F1}} \tag{4.20}$$

In practical cases, Eq. (4.17) is suitable for the description of the diode behavior for a wide range of the forward current with an appropriate selection of the ideality factor $m$.

The temperature dependence of the forward voltage (temperature sensitivity) can be calculated from the above equations. An often-used form is

$$S_{VF} = \frac{dV_F}{dT} = \frac{\left(V_F - 3mV_T - \frac{Wg}{q}\right)}{T} \tag{4.21}$$

[8] See also Chap. 2 on the physical basics of LEDs.

For internal use by Mentor Graphics marketing only

**Table 4.1** Major properties of some semiconductor materials

| Properties | Si | Ge | GaAs |
|---|---|---|---|
| Atoms/cm$^3$ | $5.0 \times 10^{22}$ | $4.42 \times 10^{22}$ | $4.42 \times 10^{22}$ |
| Density [g/cm$^3$] | 2.32 | 5.32 | 5.32 |
| Bandgap energy at 300 K [eV] | 1.12 | 0.66 | 1.424 |
| Intrinsic carrier concentration [cm$^{-3}$] | $1.45 \times 10^{10}$ | $2.4 \times 10^{13}$ | $1.79 \times 10^{6}$ |
| Lattice constant [nm] | 0.543 | 0.564 | 0.565 |
| Minority carrier lifetime [s] | $2.5 \times 10^{-3}$ | $\sim 10^{-3}$ | $\sim 10^{-8}$ |
| Optical phonon energy [eV] | 0.063 | 0.037 | 0.035 |
| Specific heat [kJ kg$^{-1}$K$^{-1}$] | 0.7 | 0.31 | 0.35 |
| Thermal conductivity at 300 K [Wm$^{-1}$K$^{-1}$] | 150 | 60 | 46 |

**Table 4.2** Bandgap energy of some color LEDs

| Color | Wavelength [nm] | Bandgap energy [eV] |
|---|---|---|
| Deep red | 700 | 1.77 |
| Red | 660 | 1.88 |
| Orange | 623 | 1.99 |
| Amber | 594 | 2.09 |
| Green | 523 | 2.37 |
| Cyan (verde green) | 501 | 2.47 |
| Deep blue | 470 | 2.64 |
| Violet | 410 | 3.02 |

For internal use by Mentor Graphics marketing only

where $W_g$ is the bandgap of the semiconductor. Important material parameters (including bandgap energy) for some semiconductors used in electronics are listed in Table 4.1. Table 4.2 lists bandgap energies of LEDs emitting light in different spectral ranges. The tables show values at room temperature (300 K), at actual operating temperature they can be significantly different.

Figure 4.26 shows the $V_F$ forward voltage of an LED at different bias current (0.1, 1, and 5 mA). The marks in the plot in the temperature range from 10 to 90 °C show measured $V_F$ values of the actual diode. Using the measured values at 1 mA bias, we calculated the $I_0$, $m$ and $R_S$ values and produced analytic curves (solid lines) for other bias than 1 mA and an extrapolated temperature range (− 80 to 250 °C).

The curves, corresponding to the analytic equations above, are obviously nonlinear, but show only very small nonlinearity over a broad temperature range.

Previously, we used a symbolic form for the same temperature dependence of the temperature-sensitive parameter in Eq. (4.8)

$$V_F(T_J, I_M) \cong V_{F0}(I_M) + S_{VF} \cdot (T_J - T_{J0}) \tag{4.22}$$

Thermostats produce highly repeatable boundary conditions at various temperature levels. So they can be used for *temperature–voltage calibration*, which means *recording* $V_F$ forward *voltage* (or other parameter) values *at different component temperatures*.

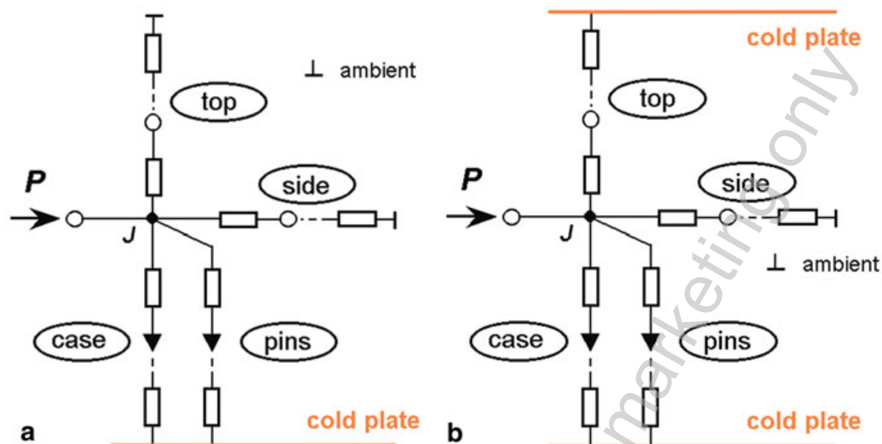


**Fig. 4.27** Calibration of a component mounted on single and dual cold plate

For internal use by Mentor Graphics marketing only

We have to make a difference between *absolute* and *relative* calibration. The former means mapping the $V_F(T, I)$ function, the latter deriving the $S_{VF}$ sensitivity parameter only.

Absolute calibration has theoretical limitations. For operating our component, we need some $P$ power applied on it. Supposing all paths in the heat conduction path arrive at the same temperature-controlled surface named $X$, we experience a

$$T_J = P \cdot R_{thJX} + T_X \tag{4.23}$$

junction temperature. Even with the $P$ power kept low, the junction temperature will differ from the controlled temperature.

Relative calibration has practical limitations only. As we saw in Sect. 4.3.5 for the differential measurement principle, we only need the $S_{VF}$ sensitivity value (or its reciprocal, the K-factor).

#### 4.3.8.2 Calibration on a Cold Plate

Components having a large cooling surface (case, tab) where most heat flows through can be measured and calibrated when mounted on a cold plate (Fig. 4.27). This is actually an easy process:

- Set the cold plate temperature to several values.
- Record the corresponding $V_F$ forward voltage.

Despite its simplicity, we have to be aware of some important issues for doing the calibration correctly:

- As the $S_{VF}$ sensitivity introduced in Eq. (4.8) depends on the operating point; always *apply the voltage and/or current* on the component to be calibrated, which *corresponds exactly to the transient measurement* circumstances.

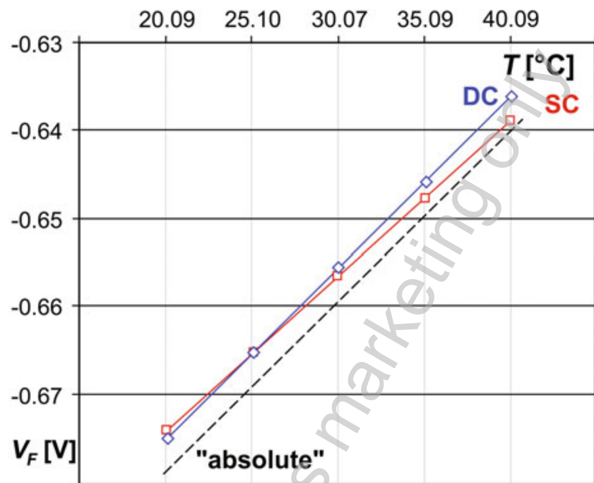


**Fig. 4.28** Example on the absolute calibration error

For internal use by Mentor Graphics marketing only

- For cooling measurements, this should be the lower, for heating the higher powering of the two levels used in the differential method.
- For diode-type components, this practically means applying the sensor current only if cooling (or pulsed method) is the selected transient type. The same is true for other devices in current jump mode.
- If the power sinking capability of (liquid circulator-driven) cold plates is high, even the calibration at high power needed for heating can be carried out easily.

Figure 4.27 shows the simplified model of a surface mounted device (SMD) component mounted on a single and on a dual cold plate. The figure reveals that some surfaces of the package are terminated by the ambient (room temperature) rather than by the temperature-controlled plate. The junction temperature is "downscaled" by the appropriate thermal resistances in the thermal circuit; it does not follow exactly the setpoint of the plate.

Figure 4.28 shows the consequences. The dashed line labeled as "absolute" shows the $R_{thJX} = 0$ case ("chip not packaged, just attached to the cold plate"). The solid SC curve corresponds to the forward voltage of the packaged component on a single cold plate, while the solid DC curve corresponds to the dual cold plate case. The temperature axis is scaled in the measured *cold plate temperature*. $V_F$ is negative (calibration of an anode grounded device).

If the cold plate is set to room temperature (25 °C in the figure), then the SC and DC curves coincide. The junction-to-ambient thermal resistance can be derived from the plot, using the $T_J = P \cdot R_{thJA} + T_A$ equation. At all other temperatures, the junction is between the ambient and the cold plate temperature and we underestimate the actual $S_{VF}$ sensitivity.

Figure 4.27 also hints that if a large portion of the heat leaves through the pins (package with small tab and many pins), a good thermal contact is also needed between the wires feeding the package through the pins and the cold plate.

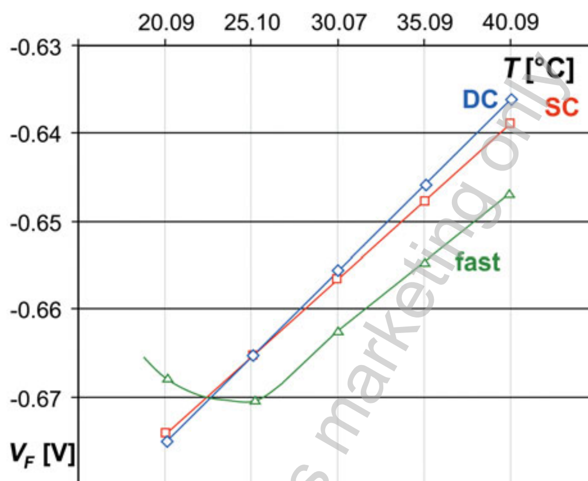


**Fig. 4.29** Example on the dynamic calibration error

For internal use by Mentor Graphics marketing only

The calibration process can be manual or automatic, using calibration software. In both cases, the following steps have to be carried out:

- Select four or five temperature setpoints, spanning the whole temperature range of the future measurement.
- Apply the appropriate power on the device.
- Program the lowest temperature value and wait for $t_1$ time until the cold plate temperature stabilizes.
- Check the component voltage, wait for $t_2$ time until the voltage stabilizes.

The $t_1$ and $t_2$ waiting times are needed because the "thermal resistance" elements shown in Fig. 4.27 are complex impedances and their capacitive part expresses heat storage in different material sections (see Sect. 4.4.4). If $t_2$ is too short, we face the problem shown in Fig. 4.29. The component voltage (dynamic curve labeled "fast" in the figure) follows the cold plate with some delay, at the lowest temperature point, we also see the previous cooling from room temperature.

Even waiting for long $t_2$ times, we cannot completely get rid of the dynamic effect. On the other hand, even with long $t_1$ times, we experience small changes in the cold plate temperature also due to the control loop of the liquid circulator. The best practice to minimize these effects is:

- Record the actual temperature of the cold plate after a $t_1$ stabilization time instead of the programed setpoint temperature (as in Fig. 4.29).
- Omit the first voltage reading at lowest temperature.
- Try to read all voltage values at equidistant $t_1 + t_2$ times (in such a way the dynamic curve runs parallel to the SC or DC curve).

**Example 1—K-factor calibration**

A flat SMD package with exposed cooling surface (tab, heat slug) is calibrated in a single-side cold plate setup.

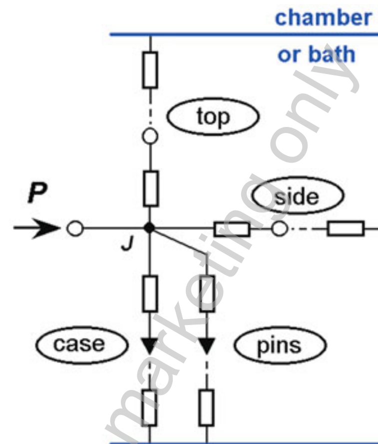


**Fig. 4.30** Calibration of a component in closed chamber or bath

For internal use by Mentor Graphics marketing only

Suppose that in the model of Fig. 4.27 the junction-to-top resistance is approximately 10 K/W and the still air cooling on the top surface corresponds to approximately 20 K/W.

The parallel path composed by the junction-to-case and junction-to-pin resistance is 2 K/W, the spreading in the cold plate is below 0.1 K/W. The wires towards the pins are in good thermal contact with the cold plate. The junction-to-side path is approximately 200 K/W.

Without detailed calculations, we can see that nearly 10 % of the heat leaves towards the ambient, we underestimate the sensitivity by almost 10 % in this setup.

In the dual cold plate setup, we have some heat loss towards the sides only. However, as there is a thin air gap between the two temperature-stabilized metal plates, the air is practically of the same temperature as the cold plate. The side resistance is connected to the cold plate temperature rather than to room temperature.

#### 4.3.8.3 Calibration in a Closed Chamber or Bath

In case all branches of the heat conduction path end at the same temperature, many problems of the previous section are automatically solved. This is the case when using a closed chamber with thermoelectric heating and cooling, or a liquid bath (Fig. 4.30).

Otherwise, the way of programming temperatures and reading voltages is much the same as in case of cold plate calibrations.

The $t_1$ and $t_2$ equalization periods are not fixed values. Instead, we should accept the state as thermal equilibrium if the changes of the chamber temperature remain below a given limit in a given time window, and after reaching this, also the measured voltage does not change more than a predefined limit for a similar time window.

For cold plates and chambers, the actual liquid or plate temperature can be different from that of the sensor used for controlling the system. In real life, 3–5 % repeatability can be expected for TSP calibration.

As mentioned before; all other steps in thermal tests need some sort of voltage and current measurement instruments, which are of high accuracy and stability. Recalibration of these is also only very rarely needed. Calibration thermostats need regular recalibration using stable reference devices.

### *4.3.9 Electrical Noise Calculation*

The electrical noise in thermal measurements has two distinct sources: internal noise (shot noise in case of diodes) and external noise from the sensor current source.

For the latter, the noise calculation is very simple. From Eq. (4.17), the differential resistance of the diode is simply inversely proportional to the measurement current, $r_d = V_T/I_M$. As a consequence, the more shunted the external noise is, the higher is the measurement current.

The internal shot noise comes from the thermal equations, at a certain $\Delta f$ bandwidth of the measurement it is:

$$i = \sqrt{4kT\Delta f/r_d} = \sqrt{4kT \cdot (qI_M/kT) \cdot \Delta f} = \sqrt{4qI_M\Delta f} \tag{4.24}$$

where $k$ is Boltzmann's constant in J/K, $T$ is the absolute temperature in K, and $r_d$ is the dynamic resistance. The $\Delta f$ is the bandwidth of the measurement, $q$ is the charge of the electron, and $I_M$ is the steady current (measurement) through the diode.

However, testers measure the device voltage, along with the noise voltage. As $u = i \cdot r_d$, the noise voltage shows square root decrease with higher measurement current.

Electrical noise calculation plays an important role in tester construction, but also has importance for a broader audience when selecting the measurement current for thermal transient measurements.

In practical cases, we select the lowest measurement current with already acceptable noise. For a broad category of silicon devices, 1 mA and for LEDs 10 mA is an acceptable value.

## 4.4 Evaluation of the Thermal Transients: Theory and Practice

The world of thermal transient measurements could be explored in a fully theoretical way. Now, we rather select some practical examples to show the highlights of the evaluation of thermal measurements characterizing power LEDs.

**Example 2—Thermal impedance of a high-performance 1 W white LED**
An Osram Dragon LED was selected for measurement. For characterizing the package, we selected a set of measurements at two different boundaries.

For internal use by Mentor Graphics marketing only

**Fig. 4.31** Sketch of the two boundaries: with TIM layer ("wet" condition) and without TIM layer ("dry" condition)

**Table 4.3** Measurement settings and powering data of LED of Example 2

| Programed parameters | Measured parameters | Calculated parameters |
|---|---|---|
| $I_H = 0.700$ A | $V_H = 3.33$ V | $P_2 = 2.30$ W |
| $I_M = 0.010$ A | $V_{Fi} = 2.68$ V | $P_1 = 0.03$ W |
| $t_{max} = 20.0$ s | $t_{corr} = 20$ µs | $P_{el} = P_2 - P_1 = 2.27$ W |
| $T_{coldplate} = 25$°C | $P_{opt} = 0.55$ W | $\eta_e = P_{opt}/P_{el} = 0.24$ |
| Sampling rate: 200/octave | | $P_H = 1.75$ W |

The difference in boundaries was realized by different thermal interface at the exposed cooling surface of the package as suggested in the JEDEC JESD 51-14 standard [13].

The measurement was carried out in an integrating sphere, in a combined thermal and radiometric/photometric arrangement (Fig. 4.25). During the measurement, effective cooling was assured by the cold plate mounted on the side of the sphere. The two boundary conditions were realized as (Fig. 4.31.):

- Mounting the LED on the dry plate surface (which always implies a thin insulating air gap between the faces); and then
- Mounting the same LED on the plate wetted by thermal grease.

For calibrating the *temperature-sensitive parameter,* we put the device in a closed thermostated chamber and recorded the forward voltage at different temperatures with $I_M = 10$ mA applied (Fig. 4.31).

The measured temperature sensitivity of the forward voltage was approximately $S_{VF} = -1.21$ mV/°C.

Then, we placed the LED on the cold plate of the integrating sphere and connected the device to the appropriate connectors of the *thermal transient tester*.

A few trial measurements were carried out to find the measurement time needed to reach steady state and the proper sampling rate of the tester. The power level was chosen to achieve several degrees Celsius of temperature change. The selected parameters are listed in the first column of Table 4.3.

Cooling measurements were carried out. The power was applied on the diode by switching on a higher $I_{drive}$ current, as an addition to the $I_M$ measurement current, which had been already used in the calibration step. The LED was left to reach its hot thermal steady state powered by the $I_H = I_{drive} + I_M$ heating current.

For internal use by Mentor Graphics marketing only

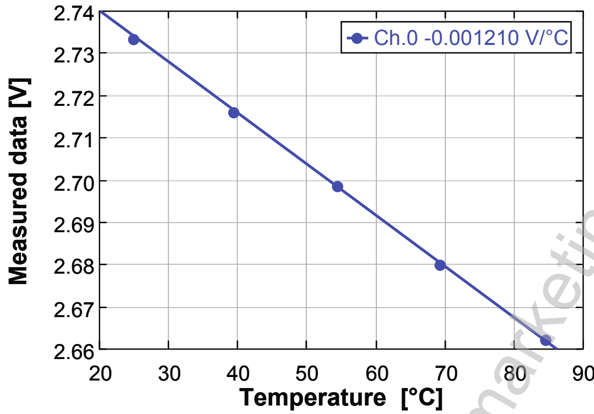


**Fig. 4.32** Calibration curve of a power LED at 10 mA

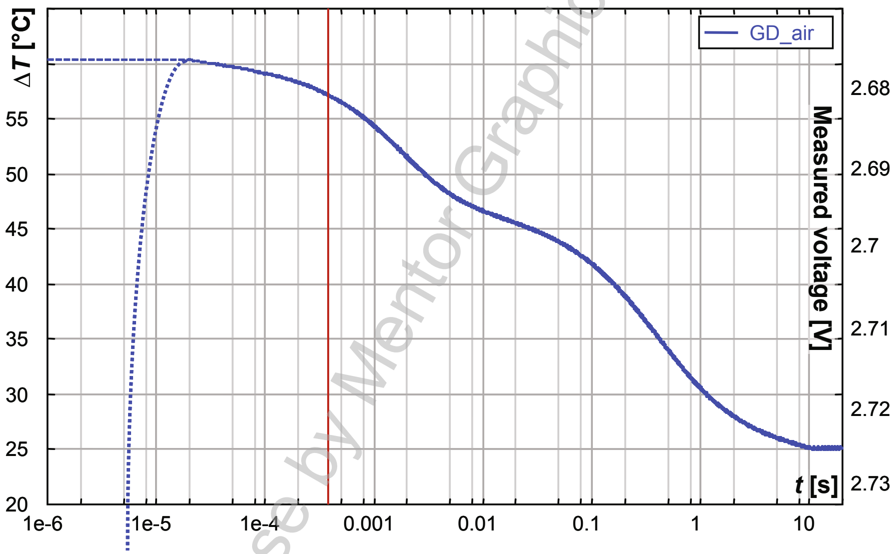


**Fig. 4.33** Raw cooling transient: 1 μs to 20s with initial correction

For internal use by Mentor Graphics marketing only

At the start of the cooling, the current was switched from $I_H$ to $I_M$ only. Before switching off, $V_{FH} = 3.33$ V was measured on the hot diode at 700 mA bias. Immediately after switching off, the forward voltage dropped to 2.68 V at 10 mA bias. So the *electric* power step was $P_{el} = (3.33 \cdot 0.7)\text{W} - (2.68 \cdot 0.01)\text{W} = 2.27$ W.

The radiometric measurement yielded $P_{opt} = 0.55$ W emitted optical power resulting in a radiant efficiency of $\eta_e = P_{opt}/P_{el} = 0.24$ and $P_H = 1.75$ W heating power.

Figures 4.32 and 4.33 show the recorded transient as change of voltage and temperature.

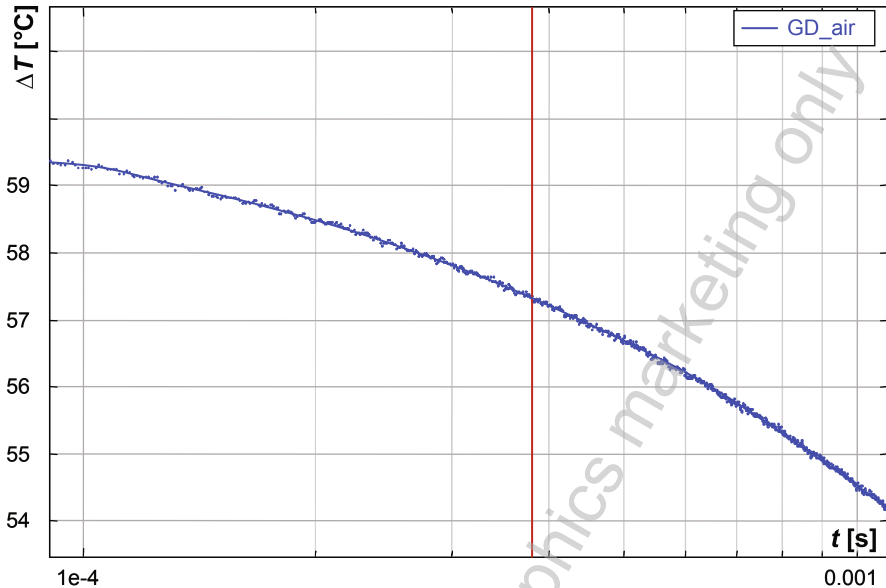


**Fig. 4.34** Excerpt of the raw cooling transient, 100 μs to 1 ms

For internal use by Mentor Graphics marketing only

In the 1 to 20 μs interval, we see the electric transient of the diode as the voltage sinks from 3.33 towards 2.68 V. (Reference directions of the picture have been selected in a way that moving up in the plot represents diminishing voltage—so cooling is shown in the usual way).

The electric transient of the device finishes at 20 μs, after this point, we see the temperature-induced voltage change, the real thermal transient.

The excerpt in Fig. 4.33 demonstrates that for subsequent postprocessing a good-quality transient record is needed. The precise sampling at as high as 200 samples/octave rate produces many thousand points. (An octave is a 1:2 time span, such as 100 to 200 μs, etc.). Moving average over the samples serves good noise suppression.

### 4.4.1 Temperature Change Plots

Figure 4.34 presents the relative temperature change of our Dragon LED at the two selected boundary conditions. Here, and in all subsequent plots, GD_air denotes the curve belonging to a dry condition with the inherent air gap when no thermal interface material (TIM) is applied and GD_grease denotes the curve belonging to a wet condition with applied grease on the package cooling surface.

A cooling (or heating) plot already yields a lot of useful information. Usually, the *time axis is logarithmic*, this helps analyze the thermal behavior of the packaged

device, we see the *early time details* that *characterize the chip, package, and pin region* and later we can identify the cooling mount.

However, this information is very specific, it describes the component behavior on cold plate, at $P_{el} = 2.27$ W power step only. We want to find descriptive functions that predict component behavior at *different boundary conditions, different power waveform and magnitude*, etc.

Fitting the cooling curves at their hottest point in Fig. 4.34, we find that the cooling is *not influenced by the actual boundary condition* until 20 ms and all curves coincide perfectly. This can be easily explained stating that until 20 ms the thermal changes occur inside the package; we still did not reach the outer thermal interface.

A beautiful world of powerful description tools can be entered assuming that *the behavior of our thermal systems is linear*. Luckily, the material parameters of the components show only a small dependence on temperature. However, e.g. LEDs' radiant efficiency shows a stronger change.

In silicon devices, linearity assumption is typically valid over a 50 °C temperature rise. A study on handling nonlinearity is presented in [17]. As shown in Fig. 6.32 of Chap. 6, assuming temperature-independent material properties for LEDs in a temperature range of 60 °C is also valid for power LEDs. Similar experimental evidence for LEDs can be found in the technical literature too (see, e.g., Fig. 11 of [18]).

### 4.4.2 $Z_{th}$ Curves

The first evident step of generalizing our temperature measurement result can be done by *normalizing* it by the applied power. This normalized temperature transient is the $Z_{th}$ curve also known as *thermal impedance curve*.[9]

In the world of silicon (single-energy transport) devices, all input electric energy is converted into heating power: $\Delta P_H = \Delta P_{el}$, thus: $Z_{th}(t) = \Delta T_J(t)/\Delta P_{el}$.

The power step can be negative (cooling) resulting in a negative change of the junction temperature as well or the power step and the junction temperature change can be positive (heating); in both cases, the thermal impedance curve will be a monotonically increasing function, therefore we usually consider the direction of the heating as positive in $Z_{th}$ curves.

The curves shown in Figs. 4.36 and 4.37 come from dividing the measured cooling curves (Fig. 4.35) by $P_{el} = -2.27$ W.

In silicon devices, the approximate junction temperature transient for any power step can be easily gained from the $Z_{th}$ curve, simply multiplying each time point by the actual power.

This process has a small error as linearity is not perfect. At higher temperature, the cooling is generally better, turbulent convection is more effective, radiation grows quickly. If we apply on our system an actual power, which is higher than the one used

[9] In electronics, the impedance is interpreted in the frequency domain, not in the time domain as a step-response function. In Sect. 6.1.4.1 of Chap. 6, the thermal resistance concept is generalized to thermal impedances.

For internal use by Mentor Graphics marketing only

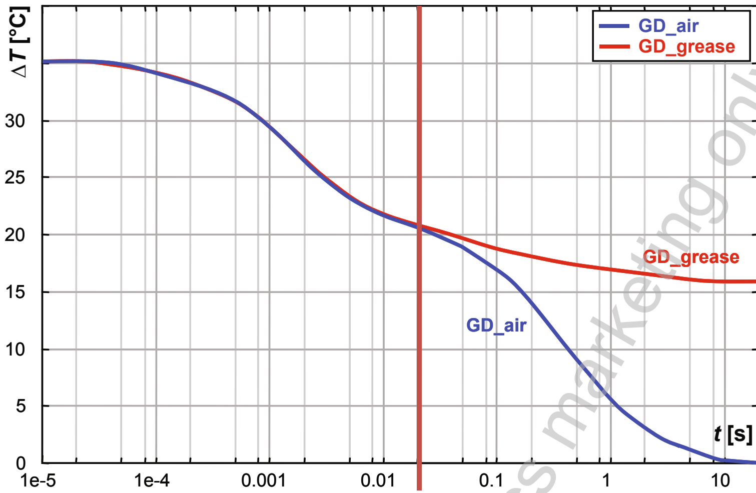


**Fig. 4.35** Smoothed response curves matched at hot point

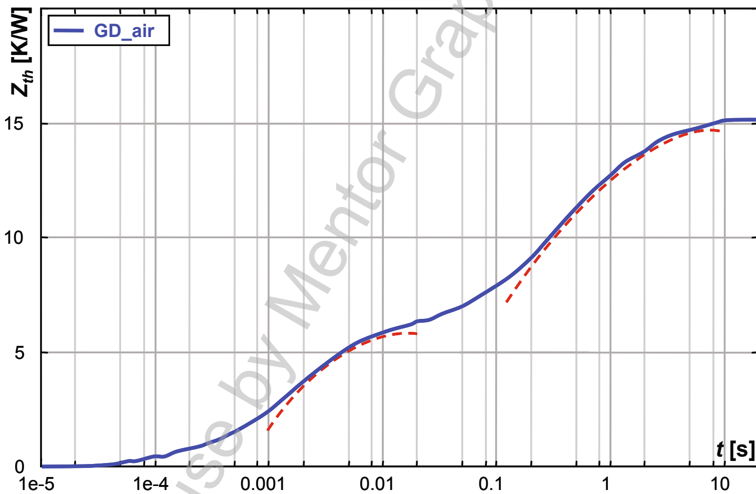


**Fig. 4.36** $Z_{th}$ curve (without correction of emitted optical power), LED component on cold plate, dry surface. Two possible exponential components shown

during the $Z_{th}$ measurement, the actual temperature elevation will be lower than the calculated. In such a way, the error is made on the safe side.

From the beginning, the $Z_{th}$ curve was used for analyzing device structure. As we can see in Fig. 4.36 the $Z_{th}$ curve is "bumpy," we see the heating of structural elements (chip, submount, heat spreader) superposed. The height and position of a bump can be used to check the structural health of the device or for identifying failures.

For internal use by Mentor Graphics marketing only

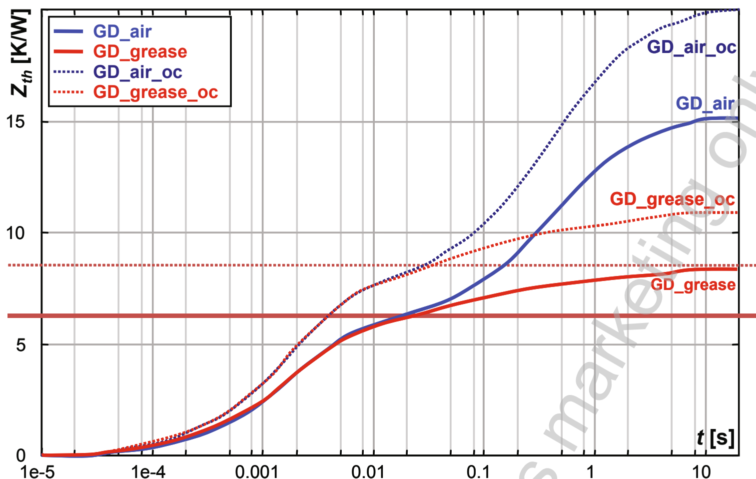


**Fig. 4.37** $Z_{th}$ curves with and without correction for the emitted optical power, LED measured twice with different case-to-cold plate thermal interfaces

In Fig. 4.37, we compare more $Z_{th}$ curves constructed from the cooling curves of Fig. 4.35. Dividing the cooling curves by $P_{el}$, we get the GD_air and GD_grease "electrical only" $Z_{th\text{-}el}$ curves of Fig. 4.37.

Using $P_H = P_{el} - P_{opt}$, we get the GD_air_oc and GD_grease_oc "real" $Z_{th\text{-}real}$ curves, where the postfix _oc stands for "optical power corrected".

Putting the question which one is the "good" $Z_{th}$ curve, the answer is that all of them are correct but they have different information content and may serve different applications.

Repeating the $Z_{th}$ measurements at different power level or ambient temperature, we will see that the real $Z_{th\text{-}real}$ curves fit nearly perfectly; they reflect only the possible temperature dependence of material parameters and the cooling mount characteristics.

As exposed many times in this book, the $\eta_e = P_{opt}/P_{el}$ radiant efficiency depends on the LED's forward current and junction temperature. In the range of interest, the efficiency is higher at lower currents and lower temperatures.

According to the above, $Z_{th\text{-}el}$ is valid only for one current and one specific ambient temperature. Therefore, publishing it in product data sheets is correct only along with these conditions.

Both curve types can be relevant in proper context. In the data sheet of an LED module or luminaire where practically one optimal driving current is specified, and all other use is limited to dimming at smaller current; $Z_{th\text{-}el}$ gives answer to questions like "after switching on or off the unit what will be the junction temperature at a certain point in time."

However, in an R&D project where LED packages or LED light output properties have to be compared, $Z_{th\text{-}real}$ can be used for adequate comparison. Also, this is the

For internal use by Mentor Graphics marketing only

thermal metric to be used in thermal simulation—allowing modeling of application scenarios with any electrical and thermal conditions.[10] As presented later in this section, postprocessing $Z_{th\text{-}real}$ can reveal structural details and can identify failure locations in a correct way.

Looking at the GD_air and GD_grease “electrical only” $Z_{th\text{-}el}$ curves in Fig. 4.36, we can observe in the plot that until the point we proceed in the internal structures of the heat conduction path a bit more than 6.3 K/W (reached at 20 ms), the $Z_{th}$ curves coincide. Leaving the cooling slug, we step into the thermal interface region. The measured curves show 15 K/W total change with the LED on dry surface and 8.2 K/W on the surface with thermal grease applied.

This way, we identified the “electrical only” junction-to-case thermal resistance as $R_{thJC\text{-}el} = 6.3$ K/W.

The “effective” junction-to-ambient thermal resistance is 8.2 and 15 K/W for the two boundaries, interpreting “ambient” as the end of the cold plate–liquid-based thermostat system.

The corresponding “real” quantities are 8.3, 11, and 20 K/W, respectively. These bigger numbers for the real impedance or resistance values underline the importance of proper standardization. The requirement of reporting these values on product data sheet does not leave any room for possible misleading of inexperienced end-users.

Figure 4.36 already proves that a drastic change in the structure provokes a visible change in the transient thermal behavior, but quantitative statements are limited on one specific point only. The $Z_{th}$ curves can be used as starting point for more “views” of the same measurement, which provide much clearer picture of the device and its environment. The most refined way for structure identification will be presented in Sect. 4.4.4.

A basic statement of linear system theory is that knowing the system response to a short pulse (Dirac-$\delta$ pulse) or to unit step (Fig. 4.36 or 4.37) we know all possible transient responses. The transient change caused by any excitation of any waveform can be easily calculated using the so-called *convolution integrals* [20].

A closely related problem is studying system response on periodic excitations at different frequencies. The result is that time domain transients can be converted to frequency domain response using the *Fourier transformation*.

Descriptive functions of such nature are now common in data sheets regarding electric parameters, and are more and more important for the thermal parameters.

### *4.4.3 Thermal Time Constants*

A further way of representing the thermal system is highlighted in Fig. 4.36. The $Z_{th}$ curves are of “bumpy” nature. This is natural, at heating we can observe how we first heat up the chip, then internal package elements, followed by the package body, the board, etc.

---

[10] See Sect. 6.5.2.2 of Chap. 6 for an overview of LED multidomain modeling.

For internal use by Mentor Graphics marketing only

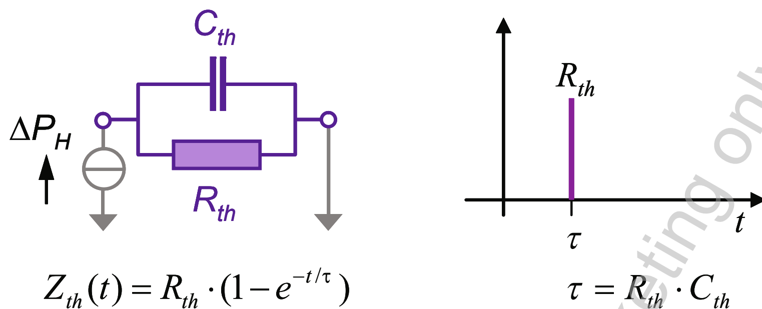


**Fig. 4.38** The simplest dynamic thermal model: a parallel thermal resistance and thermal capacitance and its discrete time constant representation. (Source: [13] © JEDEC, reproduced with permission)

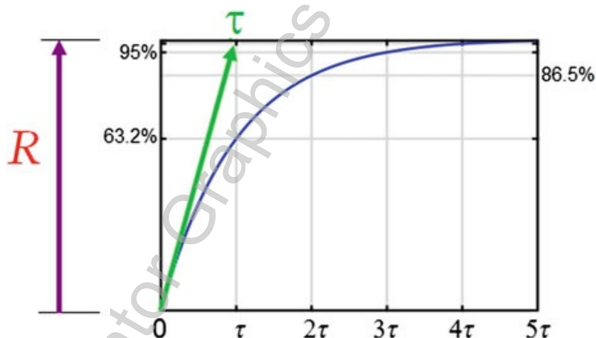


**Fig. 4.39** Time response of a single RC stage to a step function excitation with its magnitude and time constant shown

For internal use by Mentor Graphics marketing only

Such a curve can always be interpreted as a sum of exponential components. This exponential composition automatically yields a simple one-dimensional dynamic compact model, a series or chain of parallel connected thermal resistance–capacitance pairs.

In the simplest case, our system can be represented by a single thermal resistance expressing heat conduction and a parallel thermal capacitance expressing energy storage (Fig. 4.38).

Applying a step-wise power change to this equivalent network, the temperature quickly grows until $t = R_{th} \cdot C_{th}$ time, then gradually stabilizes at the $T = P_H \cdot R_{th}$ value following the $T(t) = P_H \cdot R_{th} \cdot (1 - e^{-t/\tau})$ time function (Fig. 4.39). (In the analogous electric network, power is replaced by current, temperature by voltage.) If 1 W power is applied, we get the $Z_{th}(t)$ curve.

Composing now a $Z_{th}$ curve like the one in Fig. 4.36, we have to sum up such exponential heating curves:

$$T(t) = \sum_{i=1}^{n} P_H \cdot R_{thi} \cdot (1 - e^{-t/\tau_i}) \tag{4.25}$$

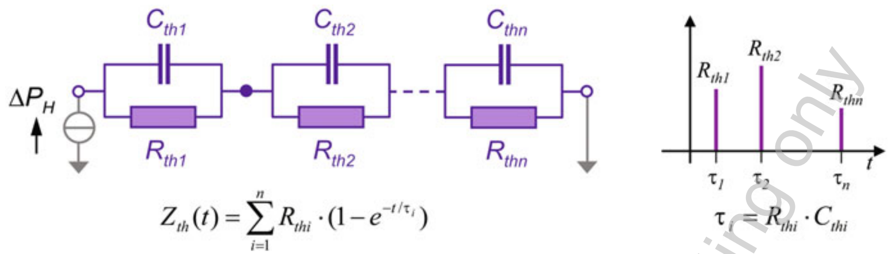


**Fig. 4.40** A popular behavioral dynamic thermal model: a chain of parallel thermal resistance and capacitance stages its discrete time constant representation. (Source: [13] © reproduced with permission)

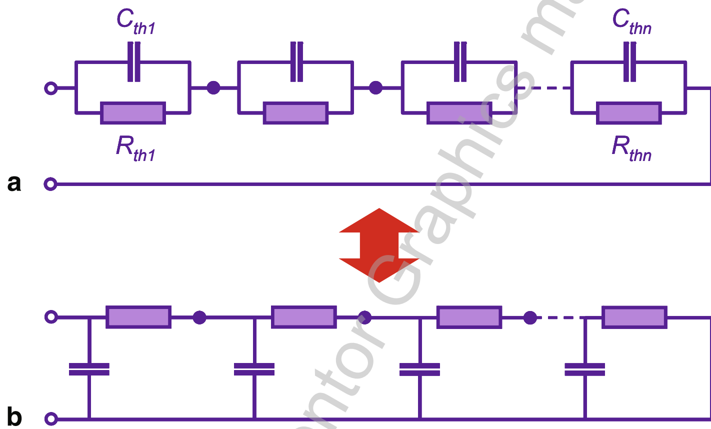


**Fig. 4.41** **a** *FOSTER* type and **b** *CAUER* type representations of a driving point[12] thermal impedance. (Source: [13] © JEDEC, reproduced with permission)

The addition of temperatures corresponds to model network composed as a chain of parallel RC stages as shown in Fig. 4.40: the same power ("current") flows along the chain, and the total temperature ("voltage") is calculated as the sum of the components. At 1 W power, we get the $Z_{th}(t)$ curve again.

We could quantitatively describe the chain model with a large table of $R_i$ and $C_i$ pairs. For the visual representation, it is practical to give the $R_{thi}$ and $\tau_{\mathrm{i}} = R_{thi} \cdot C_{thi}$ values instead (see on the right in Fig. 4.40), because $R_{thi}$-s give direct information on the magnitude of the given component, and $\tau_i$-s on the place of the "bump" along the time axis.

The network model shown in Fig. 4.40 is called the *FOSTER model* of the impedance. As this model perfectly describes the time response of the thermal impedance, it can be considered as a black box model of the thermal impedance.

It would be misleading to associate these thermal resistances and capacitances to the different physical regions of a heat conduction path structure. The FOSTER model is unsuitable for this since it contains node-to-node thermal capacitances representing no physical reality. An equivalent model exists as well for the RC one-ports: the so-called *CAUER network*. This model is a ladder network, shown in Fig. 4.41b.

For internal use by Mentor Graphics marketing only

This model is excellently matched to the idea of associate the circuit elements with physical regions. This behavior will be the base of the heat flow path identification by means of *structure functions* as will be shown later.

### 4.4.4 Structure Functions

In the late 1990s, the way of interpreting thermal measurement results radically changed. A plausible modification of the time constant representation caused a real revolution that enabled direct investigation of the physical structures, reverse engineering, failure analysis (FA)—instead of just viewing the thermal changes as time behavior of a “black box” system. This change was due to the introduction of the so-called *structure functions*, introduced in thermal testing of packaged semiconductor devices by Székely [21].

We concluded the previous section by stating that CAUER equivalent models of the thermal impedances can be generated from the time constant spectra. The practical problem with such a network model is that 150..200 individual thermal resistance and thermal capacitance values cannot be interpreted. Therefore, after the introduction of further two simple definitions, we can represent the CAUER equivalent model graphically. Thus, the *cumulative thermal resistance* is defined as

$$R_{th\Sigma} = \sum_i R_{thi} \tag{4.26}$$

and the cumulative thermal capacitance as[11]

$$C_{th\Sigma} = \sum_i C_{thi} \tag{4.27}$$

In other words: starting from the driving point (the junction), we cumulate (sum) the partial thermal resistance and thermal capacitance values for all subsequent heat flow path sections. If we interpret the cumulative thermal capacitance as function of the cumulative thermal resistance, we obtain the so-called *cumulative structure function*, often abbreviated as *CSF*

$$CSF = C_{th\Sigma}(R_{th\Sigma}) \tag{4.28}$$

This formal definition is illustrated in Fig. 4.42. The origin of the function corresponds to the *junction*. As all thermal capacitance values are positive, the cumulative

[11] The concept of *cumulative resistance* and *cumulative capacitance* and the concept of the $C_\Sigma(R_\Sigma)$ function were first introduced by Protonotarios and Wing in their fundamental papers about the theory of nonuniform (electrical) RC lines. In the first part, Protonotarios, E. N. [22] they used this function for simplifying the telegraphists’ equations when used in the synthesis of nonuniform RC lines.

For internal use by Mentor Graphics marketing only

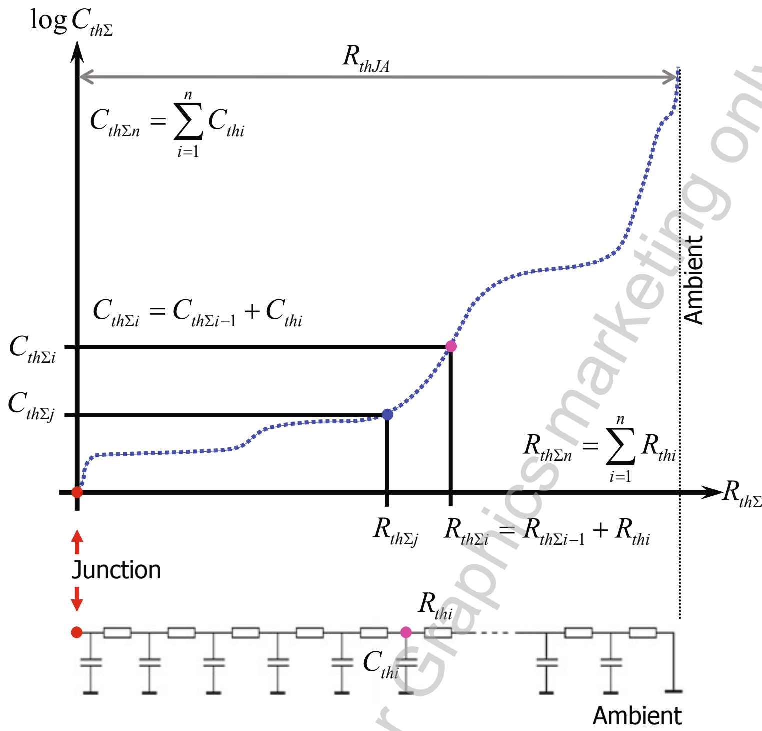


**Fig. 4.42** Cumulative structure function: the graphic representation of the thermal RC equivalent of the system

For internal use by Mentor Graphics marketing only

structure function should be a strictly monotonically increasing function. The heat conduction path ends in the *ambient*, which is characterized by infinite heat sinking capacity, therefore the cumulative thermal capacitance must tend to infinity. This means that the cumulative structure function should end with a singularity (at the location corresponding to the ambient). As a further consequence, the distance of the singularity and the origin is equal to $R_{thJA}$—the junction-to-ambient thermal resistance.

A simple physical model helps understand the meaning of the cumulative structure function. If we have a heat flow through a small portion of material, we shall experience two effects. As shown in Fig. 4.43, there will be a temperature drop *between* two (isothermal) surfaces of the material (assuming an adiabatic condition at the other four faces of the cuboid).

If the material has $\lambda$ thermal conductivity and $P$ power flows through the $a$ and $b$ surfaces, they will have $T_a$ and $T_b$ temperatures, measured from the ambient. We can say that if the slice has a small $dx$ length and a surface with $A$ cross-sectional area then the temperature drop between the two sides can be expressed as

$$T_a - T_b = P\left(\frac{1}{\lambda}\frac{dx}{A}\right) \tag{4.29}$$

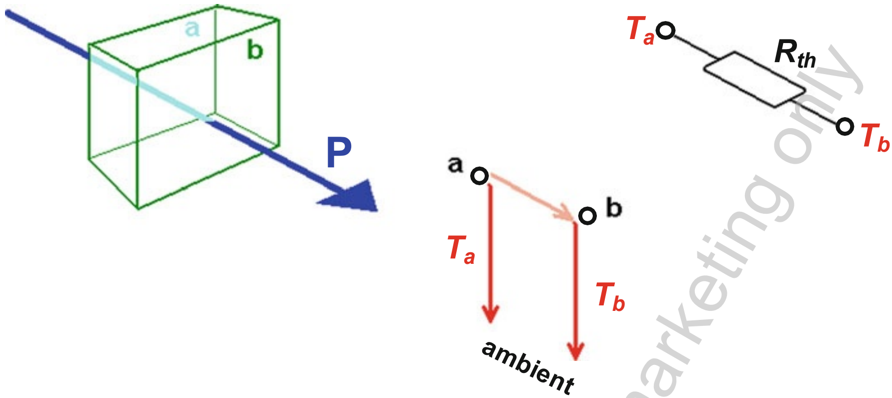


**Fig. 4.43** Heat flow through a material slice

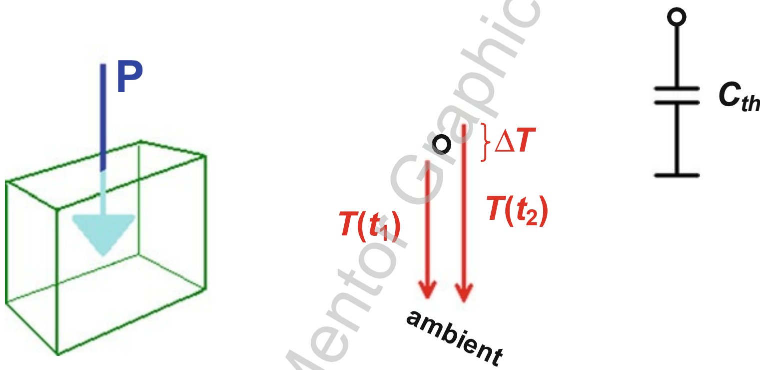


**Fig. 4.44** Heat flow into a material slice

For internal use by Mentor Graphics marketing only

where the expression in the bracket on the right-hand side is the $R_{th}$ thermal resistance between the $a$ and $b$ points corresponding to the two surfaces:

$$R_{th} = \left( \frac{1}{\lambda} \frac{dx}{A} \right) \tag{4.30}$$

On the other hand, the same material slice can store thermal energy (see Fig. 4.44). If we have a heat flow *into* the material, then in a short $dt = t_2 - t_1$ time interval the energy change is

$$dQ = Pdt = C_{th}(T_2 - T_1) \tag{4.31}$$

if $T_1 = T(t_1)$ is the temperature of the material at $t_1$ time and $T_2 = T(t_2)$ is the temperature of the material at $t_2$ time. We can represent the slice by a single point now

[12] Driving point means that heating and measuring the temperature response takes place at the same physical location. See also Sect. 6.1.4.2 of Chap. 6.

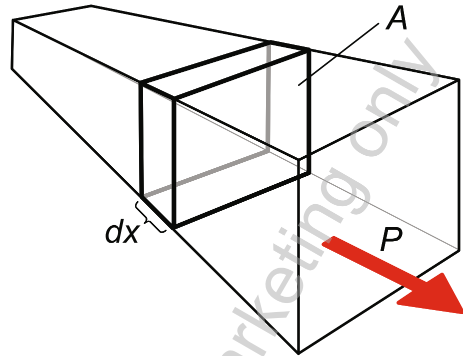


**Fig. 4.45** A section of the heat conduction path

for simplest approach. As $T_1$ and $T_2$ temperatures are again measured from the ambient, Eq. (4.31) defines a $C_{th}$ thermal capacitance between a point representing the material portion and the ambient. The value of this $C_{th}$ thermal capacitance can also be expressed trough material parameters

$$C_{th} = c \cdot m = c \cdot \rho \cdot dx \cdot A \text{ or } C_{th} = c_V \cdot V = c_V \cdot dx \cdot A \tag{4.32}$$

where $c$ denotes specific heat, $m$ denotes mass, $\rho$ is the density, $c_V$ denotes volumetric (specific) heat capacitance, and $V$ denotes volume.

The cumulative structure function is an excellent graphic tool to analyze the physical structure.

In *low-gradient sections*, a small amount of material having low capacitance causes large change in thermal resistance. These regions have *low thermal conductivity* or *small cross-sectional area*. *Steep sections* correspond to material regions of *high thermal conductivity* or *large cross-sectional area*. Sudden breaks of the slope belong to material or geometry changes.

In such a way, thermal resistance and capacitance values, geometrical dimensions, heat transfer coefficients, and material parameters can be directly read from cumulative structure functions.

In a realistic environment, the heat flow can have various shapes—longitudinal along a beam, radial in a board, conical in a heat sink holding a smaller package. In most cases, we can make a "proper" slicing of the material, on the isothermal surfaces, perpendicular to the direction of the flow. These slices must be narrow, but not always of very small cross-sectional area (Fig. 4.45) and the surfaces are usually not planes.

It is sometimes easier to identify the interface between the sections using the derivative of the cumulative curve: the differential structure function. Here, peaks correspond to regions of high thermal conductivity like the chip or a heat sink and valleys show regions of low thermal conductivity like die attach or air. Interface surfaces are represented as inflexion points between peaks and valleys.

For internal use by Mentor Graphics marketing only

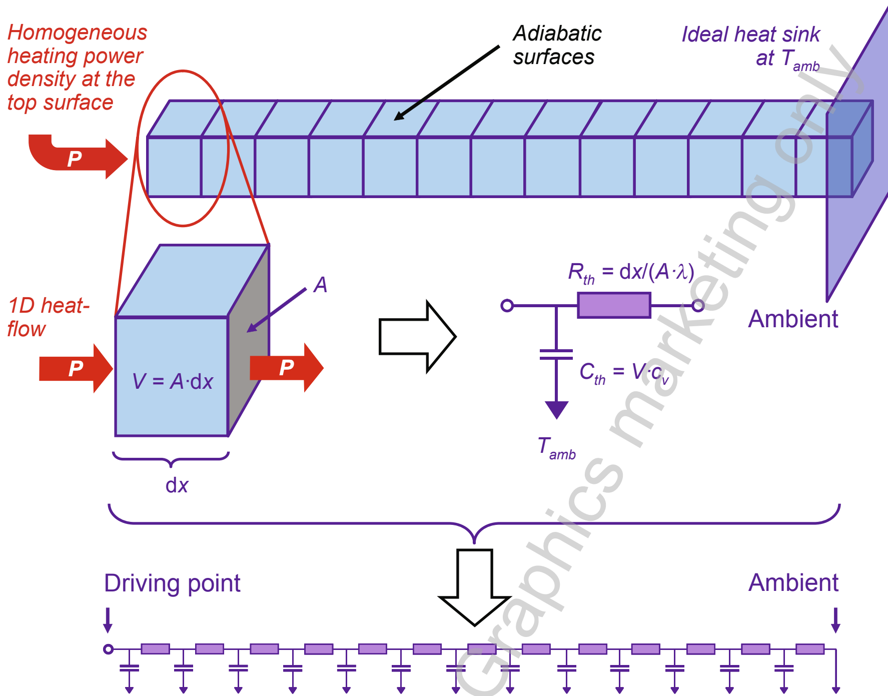


**Fig. 4.46** The RC model of a narrow slice of the heat conduction path with perfect one-dimensional heat flow and the CAUER-type network model of the thermal impedance of the entire heat flow path

For internal use by Mentor Graphics marketing only

From Eq. (4.31) and Eq. (4.32), we can say:

$$DSF = \frac{dC_{th\Sigma}}{dR_{th\Sigma}} = c_V \cdot dx \cdot A \cdot \left(\frac{1}{\lambda}\frac{dx}{A}\right)^{-1} = c_V \cdot \lambda \cdot A^2 \tag{4.33}$$

This is called *differential structure function* (frequently abbreviated as *DSF*), which also yields information on the cross-sectional area along the heat conduction path.

As summary, let us consider a homogeneous rod with thermal boundary conditions as indicated in Fig. 4.46. This rod can be considered as series of infinitesimally small material sections as discussed above. Consequently, the network model of its thermal impedance would also be a series connection of the single RC stages as shown in Fig. 4.46. Thus, with this slicing along the heat conduction path, we create a ladder of lateral thermal resistances between two thermal nodes and thermal capacitances between a node and the ambient.

Since we assumed homogeneity, the ratio of the elementary thermal capacitances and thermal resistances in the network model shown in Fig. 4.46 would be constant. This means that the cumulative structure function of the rod would be a straight line—its slope is determined by the $C_{th}/R_{th}$ ratio of the network model and its differential structure function would be a constant pn-junction $C_{th}/R_{th}$ ratio of the element values, as shown in Fig. 4.47.

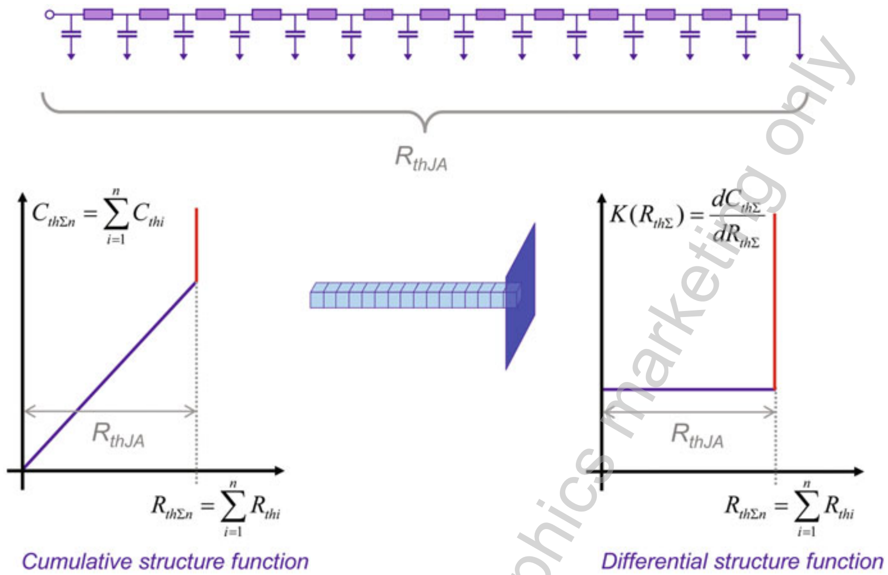


**Fig. 4.47** The cumulative and differential structure functions of a homogeneous rod

For internal use by Mentor Graphics marketing only

With this rod example, we can demonstrate that the features of the structure functions are in a one-to-one correspondence with the properties of the heat conduction path.

Let us assume that in a given section in the middle of the rod the $C_{th}/R_{th}$ ratio is doubled. This results in a steeper middle section in the cumulative structure function (with the slope doubled) and in a peak in the differential structure function (which is twice as high as the constant value of the other sections). This is illustrated in Fig. 4.48.

**Example 3—optical correction and TIM quality in structure functions**

In Fig. 4.49 and Fig. 4.50, we converted our previous $Z_{th}$ curves (presented in Fig. 4.37) into structure functions.

Figure 4.49 presents the cumulative structure functions at two boundaries when the normalizing factor in the calculation was the $P_{el}$ electric power and the emitted optical power was not taken into consideration. The technique used for producing the curves emphasizes small differences; we can see the divergence of the curves much clearer than in Fig. 4.37.

The curves are steep around the divergence, we can read an $R_{thJC\text{-}el} = 6.3$ K/W junction-to-case thermal resistance unambiguously. However, if the boundary change is applied on a larger surface in the structure then the divergence is less pronounced. For correct interpretation of the measured data, it is indispensable to specify the $\varepsilon$ threshold value at which we consider the structure functions belonging to different boundaries to be separate.

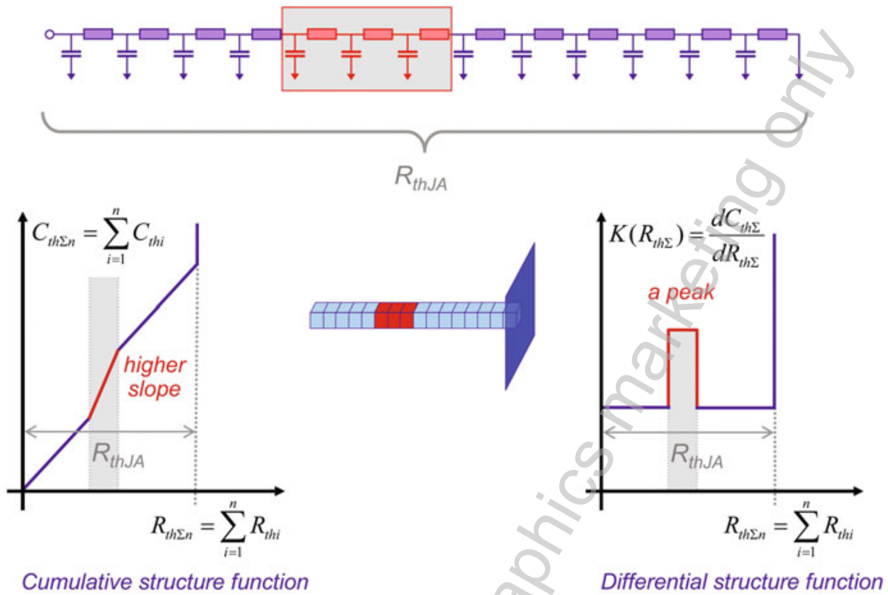


**Fig. 4.48** Structure functions indicate the changes in the $C_{th}/R_{th}$ ratio along the heat conduction path

For internal use by Mentor Graphics marketing only

In case we start our calculation from the $Z_{th\text{-}real}$ thermal impedances with the emitted optical power considered, we get those structure functions that are scaled in the real physical thermal resistances and capacitances (Fig. 4.50, curves with postfix _oc).

In this plot, we can read partial resistances and capacitances easily. We can clearly see the "sandwich-like structure" of the LED, again we can read the junction-to-case thermal resistance as $R_{thJC\text{-}real} = 8.3$ K/W. The curves diverge fast; the value does not change much if we vary the $\varepsilon$ difference threshold. More reference on the standard-compliant definition of the junction-to-case thermal resistance is provided in Sect. 4.5.2.

The steep section until 8.3 K/W can be identified as the cooling slug of the LED; we can measure 18 mJ/K thermal capacitance form the start until the end of it which can be also expressed as 5 mm$^3$ copper calculated from Eq. (4.32).

Figure 4.51 shows the differential structure functions of the same LED measurement examples.

**Example 4—locating structural elements in an LED package**

In Fig. 4.52, we see the optically corrected cumulative structure function of a power LED, mounted on cold plate.

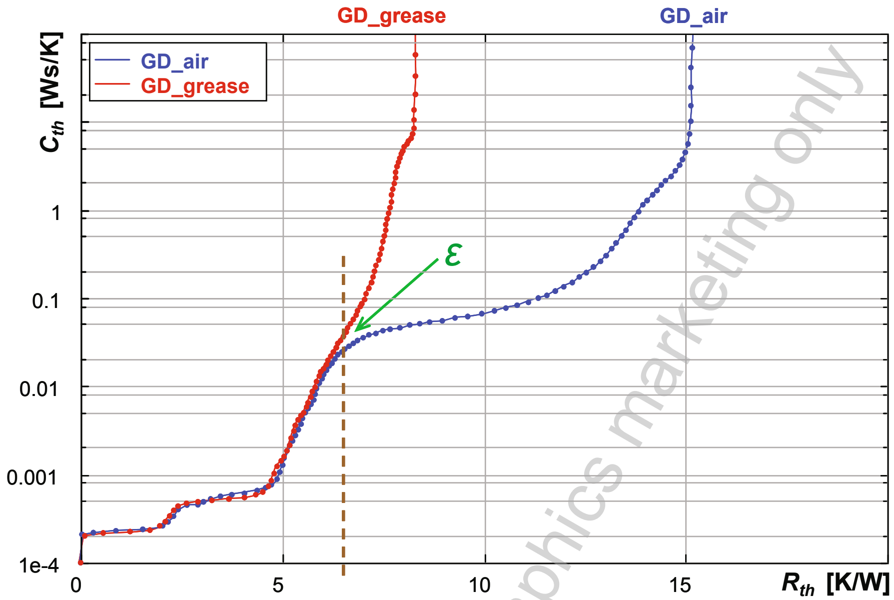


**Fig. 4.49** Cumulative structure functions, LED component at two boundaries, without optical correction

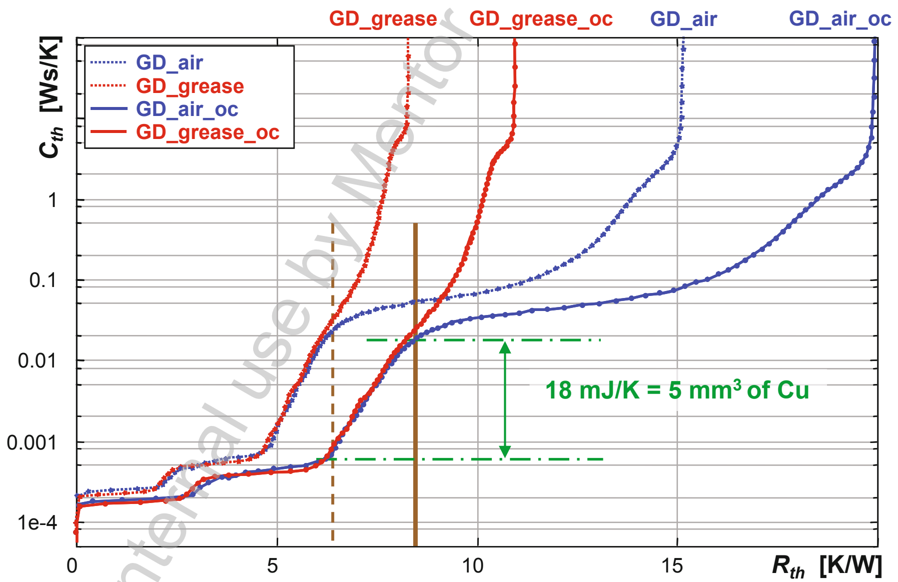


**Fig. 4.50** Cumulative structure functions, LED component at two boundaries, with and without optical correction

For internal use by Mentor Graphics marketing only

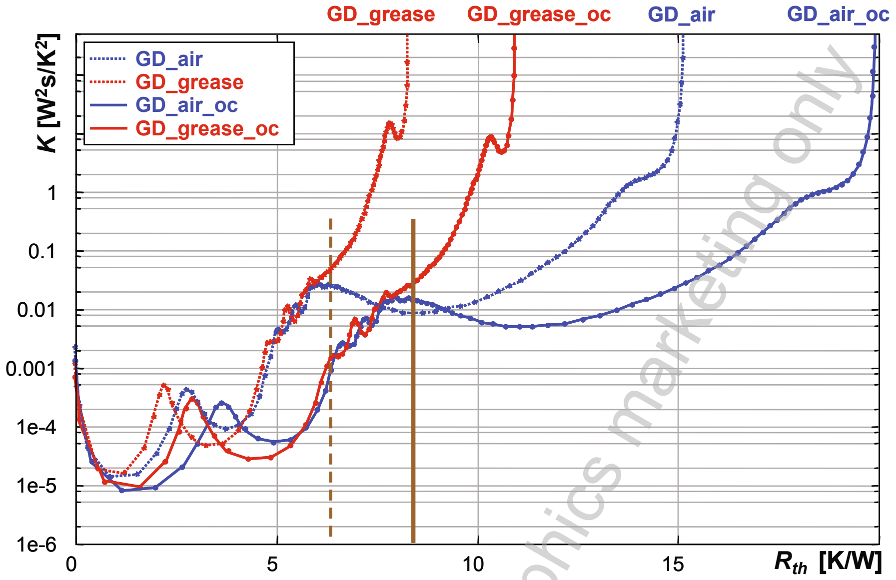


Fig. 4.51 Differential structure functions, LED component at two boundaries

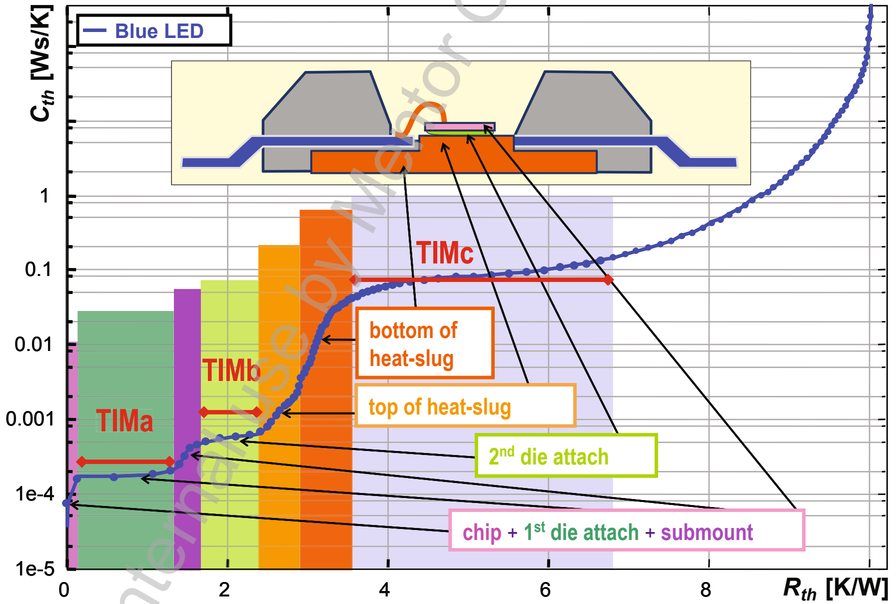


Fig. 4.52 Cumulative structure functions of a power LED with structural elements identified

For internal use by Mentor Graphics marketing only

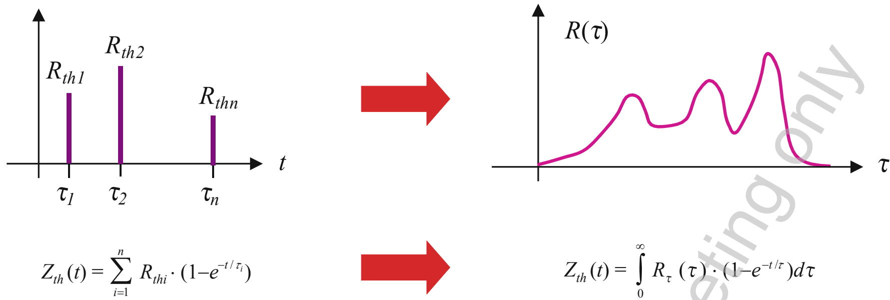


**Fig. 4.53** Distributed, infinite (thermal) RC systems can be represented by the $R\tau\ (\tau)$ time constant spectrum. (Source: [13] © JEDEC, reproduced with permission)

For internal use by Mentor Graphics marketing only

We can identify the sandwich-like structure corresponding to the chip, submount, and the heat slug. The flat sections represent different thermal interface layers (TIMa, TIMb, TIMc).

In case we know the material composition, we can measure the volume of an element through the thermal capacitance difference in the structure function. In case we know the exact geometry of an element, we can measure thermal conductivity and specific heat. For details of such analysis, consult, e.g., [15, 16].

### *4.4.5 Theoretical Background of Thermal Time Constant Spectra, the NID Method and the Structure Functions*

Real thermal systems are infinite, distributed thermal systems, therefore real thermal impedances can be represented not by a set of discrete thermal time constants, but with a continuous spectrum of possible time constants. This representation is called thermal *time constant spectrum*. The $Z_{th}(t)$ function can be expressed in a similar way as presented in Fig. 4.40, but the sum of the exponential terms is replaced by an integral over the entire range of the possible thermal time constants

$$Z_{th}(t) = \int_0^\infty R_\tau(\tau)\cdot(1-e^{-t/\tau})d\tau \tag{4.34}$$

Thus, the discrete $R_{thi}$ magnitude values are replaced by the $R_\tau(\tau)$ thermal time constant spectrum, see Fig. 4.53.

Using logarithmic time scale has advantages. A practical reason is that data acquisition with logarithmically equidistant time intervals greatly reduces the need for data storage. Using logarithmic time in graphical display of junction temperature transients allows visualizing all the details over the entire time constant range: changes corresponding to the chip + submount, heat slug, MCPCB, etc. will be visible. From

data processing point of view, applying logarithmic time scale the relationships between different representations of thermal impedances can be formulated by means of convolution integrals [20, 23].

Thus, by introducing the $z = \ln(t)$ *logarithmic time* and the $\zeta = \ln(\tau)$ *logarithmic time constant* Eq. (4.34) will look as follows:

$$Z_{th}(t) = \int_{-\infty}^{\infty} R_\zeta(\zeta) \cdot [1 - \exp(-t/\exp(\zeta))] d\zeta \tag{4.35}$$

where the $R_\zeta(\zeta)$ logarithmic time constant spectrum is defined as

$$R_\zeta(\zeta) = R_\tau(\exp(\zeta)) \cdot \exp(\zeta) \tag{4.36}$$

In the following, we shall always refer to $R_\zeta(\zeta)$ as the time constant spectrum. Simplifying our notation by $a(z) = Z_{th}(t = \exp(z))$, we can further write

$$\frac{d}{dz} a(z) = \int_{-\infty}^{\infty} R_\zeta(\zeta)[\exp(z - \zeta - \exp(z - \zeta))] d\zeta \tag{4.37}$$

Further introducing the notation

$$w_z(z) = \exp[z - \exp(z)] \tag{4.38}$$

we can write

$$\frac{d}{dz} a(z) = \int_{-\infty}^{\infty} R_\zeta(\zeta) \cdot w_z(z - \zeta) d\zeta \tag{4.39}$$

One can easily realize that Eq. (4.39) is a convolution integral

$$\frac{d}{dz} a(z) = R_\zeta(z) \otimes w_z(z) \tag{4.40}$$

where the $\otimes$ symbol denotes the convolution operation. From this, we can deduce a method of obtaining the $R_\zeta(\zeta)$ time constant spectrum, as $a(z)$ is the measured $Z_{th}$ thermal impedance on logarithmic time scale, and $w_z(z)$ is a fixed function:

$$R_\zeta(z) = \left[\frac{d}{dz} a(z)\right] \otimes^{-1} w_z(z) \tag{4.41}$$

where $\otimes^{-1}$ denotes *deconvolution*, the inverse operation of convolution.

Implementation of this calculation is not straightforward. Deconvolution can be performed in time domain, e.g., by *Bayesian iteration* or in the frequency domain by division, also known as *Fourier-domain inverse filtering*. For details of the frequency domain implementation, see, e.g., Annex B of the JESD51-14 standard [13] or refer

For internal use by Mentor Graphics maketing only

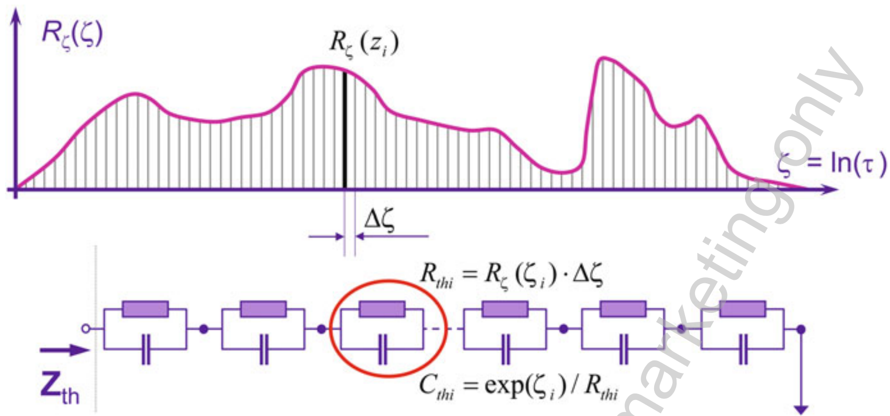


**Fig. 4.54** Discretization of the $R_\zeta(\zeta)$ time constant spectrum and constructing a Foster model of the measured thermal impedance from this. (Source: [13] © JEDEC, reproduced with permission)

to an original paper of Székely et al. [24]. There is another practical aspect of Eq. (4.41): as both the derivation and the deconvolution operations enhance noise, if time constant spectra are to be generated from measured thermal transient curves, these $Z_{th}$ curves must be extremely noise free. Using noisy signals, the obtained time constant spectra would include false values causing misleading artifacts in the results of further postprocessing steps.

Based on this discussion, another, more formal definition of the time constant spectrum can be given as follows [20]:

$R_\zeta(\zeta)\Delta\zeta$ is the magnitude of the components in the thermal impedance (unit-step response) that belong to the time constant range of [exp($\zeta$), exp($\zeta + \Delta\zeta$)].

This formal definition implies a method for discretizing the time constant spectrum and creating a network model of the thermal impedance (Fig. 4.54). Thus, according to this definition the thermal resistance value belonging to the time constant range $[\tau_1, \tau_2]$ can be expressed as

$$R_{th}(\tau_1, \tau_2) = \int_{\ln \tau_2}^{\ln \tau_2} R_\zeta(\zeta)d\zeta \qquad (4.42)$$

and the total steady-state thermal resistance of the measured structure can be calculated as

$$R_{th}(t) = \int_{-\infty}^{\infty} R_\zeta(\zeta)d\zeta \qquad (4.43)$$

The procedure was first applied for the characterization of heat flow path structures of packaged semiconductor devices by Székely [21]. As the method provides

For internal use by Mentor Graphics marketing only

network models of measured thermal impedances through a deconvolution step, it became widely known as *network identification by deconvolution* or *NID method*. The method has some theoretical limits, which are discussed in detail by Székely in his other often cited paper [23]. One needs to add that if the NID method is implemented with care, the method can be widely used in daily practice of thermal measurements, QA, and FA. Another field of application is CFD model validation or LED package compact thermal modeling as will be shown later in this chapter (see also Sect. 6.5.2.2. of Chap. 6).

It is worth mentioning that time constant spectra can be created not only by the deconvolution operation shown by Eq. (4.41) but it is also possible to calculate them directly in any thermal simulation program, which is able to calculate thermal impedances in the complex frequency domain [20]. Such calculations have the advantage that time constant spectra obtained this way are free from any distortion of measurement noise and measurement artifacts originating from the cutting and substituting the early electrical transients (see Fig. 4.16 and Fig. 4.18 in Sect. 4.3.6.1).

When converting measured thermal impedance curves to time constant spectra, small differences and noise are further enhanced by the numerical derivation and numerical deconvolution needed to postprocess data using Eq. (4.41).

Based on Eq. (4.41), time constant spectra can also be extracted from simulated thermal impedance curves. In this case, the problems are due to the quantization noise of the numerical results and the possibly too coarse time resolution[13] of such simulated transients. The direct calculation of the time constant spectra as described, e.g., in [20] is a viable alternative to the "brute force" application of the NID method to simulated $Z_{th}$ curves. Unfortunately, commercially available program tools providing this opportunity are no longer available.

As stated already, the $Z_{th}(t)$ thermal impedance function and the $R_\zeta(\zeta)$ time constant spectrum are equivalent, the $R_\zeta(\zeta)$ function also carries all available information about the heat conduction path. Thus, it is worthwhile further transforming it into highly *detailed network models* of the thermal impedance and into other *descriptive functions* for the analysis of different aspects of the junction-to-ambient heat flow path structure. These further representations include the *cumulative* and *differential structure functions*, which were discussed in the previous sections and the *pulse thermal resistance diagrams* described later in this section.

As Fig. 4.54 shows, for further numerical processing, the continuous time constant spectrum obtained by Eq. (4.41) needs to be discretized. For a given discrete time constant value an average $R_{thi}$ magnitude value is assigned using Eq. (4.42). From the discrete time constant and magnitude value, a thermal capacitance value describing the given discretized time constant value is calculated. This way the discretized time constant spectrum is turned into a long FOSTER equivalent model as shown in Fig. 4.54. The discretized version of the continuous time constant spectrum typically contains 150..200 $R_{th}$–$\tau$ pairs, thus, the FOSTER equivalent model consists

[13] Achieving a time resolution higher than 20 points per decade may require unaffordable simulation resources while measuring a thermal transient with about 200 or 400 points per decade resolution is not a problem with the transient extension of the JESD51-1 "static" test method.

For internal use by Mentor Graphics marketing only

of 150..200 stages. In the practical realization of these calculations, the stages are ordered according to the time constant values, starting with the smallest one.

The temperature response of the system described by this model can be calculated by Eq. (4.25). Due to the associativity property of the addition operation, however, the summation in Eq. (4.25) can be carried out by any order of the RC stages of the FOSTER equivalent model. In simple words, this means that the order of the RC stages of the FOSTER equivalent model can be any, it has nothing to do with the physical structure of the heat conduction path described by the model.

This underlines our prior statement that the elements of the FOSTER model are "fictitious": the entire model properly represents the thermal impedance but the individual element values of the model are not related to the physical reality.

To overcome this problem, the FOSTER equivalent model of the thermal impedance is converted into the corresponding CAUER ladder model.

The FOSTER ↔ CAUER conversion is a "standard" technique in case of (passive) linear electrical circuits, but there are practical limits when one tries to implement the conversion algorithms numerically.

Fortunately, we need the FOSTER → CAUER conversion only, which works well for large models with hundreds of stages. The "only" numerical issue in this case is that the standard floating point number representations do not provide the appropriate range of orders of magnitude of values and do not provide enough numbers of decimal digits.[14] Description of the conversion algorithm is out of our scope, it can be found, e.g., in Annex C of the JESD 51-14 standard [13].

As a final result, the $R_\zeta(\zeta)$ continuous time constant spectrum discretized to about 150..200 points is converted into a detailed equivalent CAUER-type RC model of the thermal impedance. If any two RC stages of that model are swapped, the thermal response of the network model would be different, therefore the order of the RC stages of a CAUER-type ladder model is significant; the order and the element values of the RC stages are related to the physical structure of the (essentially one-dimensional) heat flow path.

As a summary regarding structure functions, we can conclude the following. Structure functions are closely related to the theory of the linear RC networks and to their different representations. Strictly speaking, structure functions are representations of impedances of distributed (thermal) RC networks characterized as follows:

- The network is linear and passive;
- Driving point behavior is considered;
- Essentially one-dimensional heat flow is assumed.

Linearity means that the thermal resistance and capacitance are independent of the temperature itself. In other words: both the thermal conductivity and heat capacity are constant values, without temperature dependence. In reality, this theoretical condition is not met exactly but in practical situations it is a reasonable approximation.

[14] This problem can be overcome by using special math libraries in the implementation, which provide any number of digits both for the exponent and for the mantissa.

For internal use by Mentor Graphics marketing only

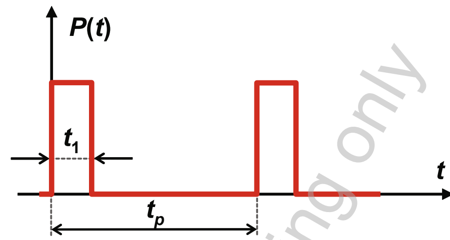


**Fig. 4.55** Periodic heating pulse sequence

The subject was discussed in detail by Székely and Rencz [17] and is also touched in Sect. 6.5.2.2 of Chap. 6.

Driving point behavior means that the same location of the structure is heated (by, e.g., a power step) and measured for its temperature response; see also Sect. 6.1.4.2 of Chap. 6.

*Essentially one-dimensional* heat flow (besides longitudinal flow) includes more complex heat spreading, which with some coordinate system transformation can be mapped to longitudinal flow in a Cartesian coordinate system. This includes *radial spreading* in disc-like structures such as an MCPCB under a power LED or in a JEDEC standard thermal test board, *cylindrical spreading* or *conical spreading* (e.g., in a copper heat slug of a power LED package).

A heat flow path is called essentially one-dimensional path if it is formed as "series connection" of the regions with the above described heat spreading characteristics, which is often the case with real semiconductor device packages. Only the splitting of the heat flow path poses questions. When the splitting point coincides with the driving point of a main and a parasitic heat flow path and the total thermal resistance of the parasitic path is known, there is a possibility to eliminate the effect of the parasitic path from the structure function [25]. Even if such a correction is not possible because the parasitic shunting resistance is not known or the splitting point differs from the driving point, still an "equivalent" physical structure can be derived, but without direct mapping to the real physical structure in such a case.

### 4.4.6 Pulse Thermal Resistance Diagrams

In case we apply a square wave power profile (such as shown in Fig. 4.55) on a device for a long period of time, we can expect it to reach a stationary state: the junction temperature will also follow a periodic function and its waveform becomes stable. Examples for such stabilized junction temperature waveforms are shown in Fig. 4.56.

The most important quantity at such excitations is the peak temperature reached in stationary state. One way of getting this value is really programming different pulses of different length and amplitude and measuring the transient temperature changes (for practical reasons in the "off" state).

For internal use by Mentor Graphics marketing only

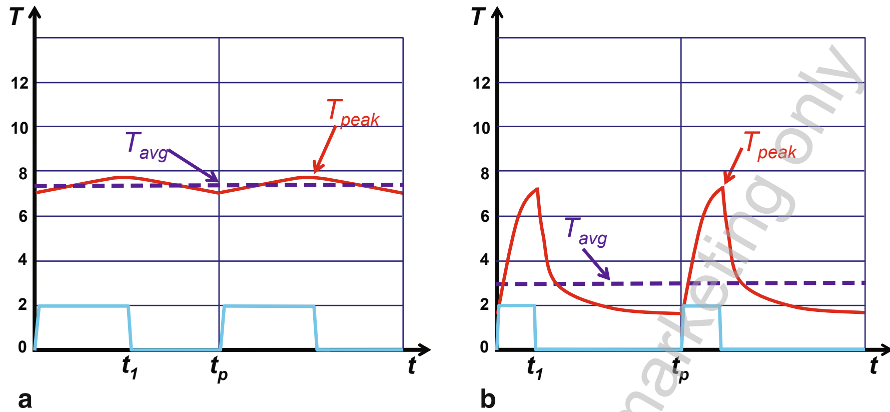


**Fig. 4.56** Junction temperature waveform at different heating pulse series:
**a** $t_1 = 0.1$ ms, $t_p = 0.2$ ms, $\delta = 0.5$, $f = 1/t_p = 5$ kHz, d$T_{peak} = 7.8$ K, d$T_{avg} = 7.3$ K
**b** $t_1 = 1$ ms, $t_p = 5$ ms, $\delta = 0.2$, $f = 1/t_p = 200$ Hz, d$T_{peak} = 6.9$ K d$T_{avg} = 2.9$ K

Carrying out a series of measurements with square wave excitation at many frequencies and duty cycles is a rather tedious task. Instead, we can derive this plot from a single measurement with step excitation, and some mathematical calculation.

Actual temperature waveform can be gained by simulation, making first one of the RC models of the device defined in previous sections and then using a SPICE-like circuit simulator.

A useful plot called *pulse thermal resistance diagram* or *thermal transient impedance plot* yields peak temperature in stationary state directly; it can be easily derived from the time constant spectrum.

Let the periodic pulse load be denoted by the $t_1$ pulse width, $t_p$ period, and the $\delta = t_1/t_p$ duty factor (Fig. 4.55). The curves of the pulse thermal resistance diagram can be calculated from the time constant spectrum by the following convolution operation [20]:

$$Z_{th}(z = \ln t_1, \delta) = R_\zeta(z) \otimes \frac{1 - \exp[-\exp(z)]}{1 - \exp[-\exp(z)/\delta]} \tag{4.44}$$

**Example 5—generating pulse thermal resistance diagrams**
Such a diagram (Fig. 4.57) describes the behavior of the same LED used in Examples 1–3—when excited by repeated pulses of given length and duty cycle. The horizontal axis shows the pulse length; the duty cycle is the curve parameter. The vertical axis shows the peak temperature elevation in terms of an "effective thermal resistance" [K/W].

In case of a stream of very short pulses, the power source can be interpreted as an effective source with a power downscaled by the duty cycle. In case of very long pulses, the temperature has "enough time" to reach the steady-state situation.

For internal use by Mentor Graphics marketing only

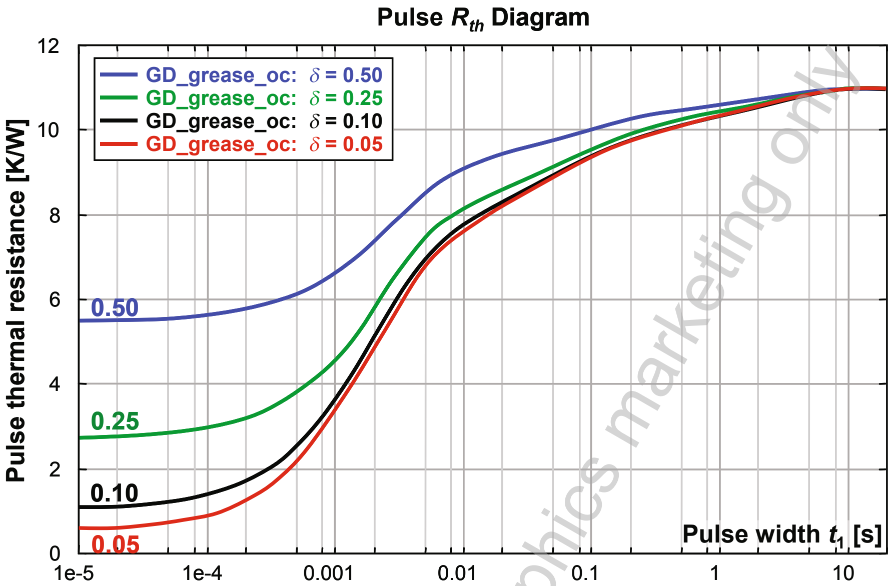


**Fig. 4.57** Pulse thermal resistance diagram of the Dragon LED on cold plate, thermal grease applied, emitted optical power considered

For internal use by Mentor Graphics marketing only

Accordingly, in Fig. 4.57, we get back for pulses of very long $t_1$ again the peak temperature elevation corresponding to 11 K/W as in previous "views." At 50 % duty cycle, the peak temperature behaves like at driving a 5.5 K/W thermal system for a long time, at 10 % like driving a 0.11 K/W heat conduction path, etc. The really informative part of the figure is in between, where we have no instant guess on the peak temperature.

This curve is extremely useful for producing data sheets for devices and designing switching-type power supplies (pulse width modulation [PWM] LED drives).

The powering scheme shown in Fig. 4.55 is typical in case of dimming LEDs with pulse width modulation (PWM dimming) where the average luminous flux is controlled by the duty factor.

## *4.4.7 Complex Loci*

The frequency domain representation of the thermal impedance can be provided in different ways. Based on the $Z_{th}(t)$ function, it can be by transformed into the $Z_{th}(\omega)$ function

$$Z_{th}(\omega) = \int_0^\infty Z_{th}(t) e^{-j\omega t} dt \qquad (4.45)$$

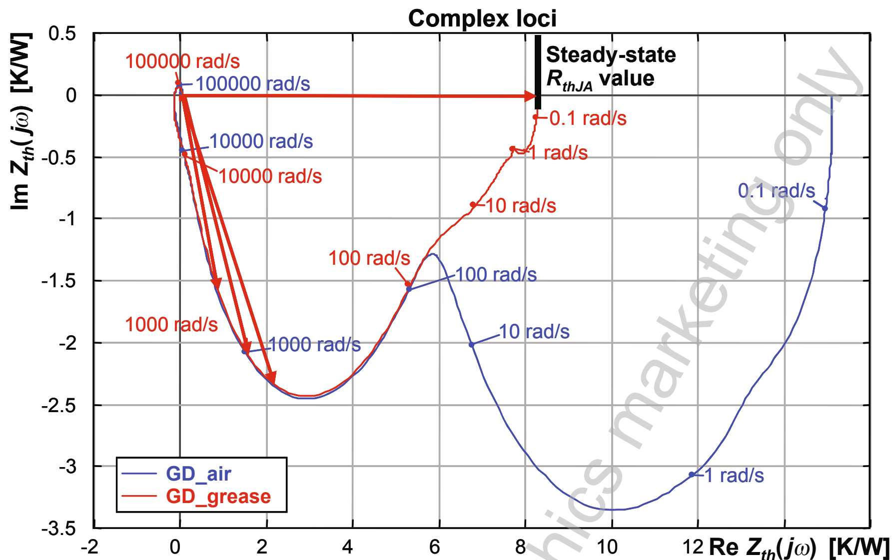


**Fig. 4.58** Complex locus of the frequency domain thermal impedance of the power LED assembly. Harmonic components corresponding to 0, 100, 200, and 300 Hz (0, 628 rad/s, etc.) are shown

where $\omega$ is the angular frequency of the excitation. The resulting $Z_{th}(\omega)$ complex thermal impedance function can be visualized, e.g., by means of a *complex locus* (also known as Nyquist diagram) as shown in Fig. 4.58.

The zero frequency value is the thermal resistance defined in Sect. 4.3.3. In the actual measurement, this is again 8.2 K/W and 15 K/W for the two boundaries when measured along the horizontal axis on the “electrical only” curves.

In case the frequency of the mains *voltage*, is, e.g., 50 Hz, then the *power* will have 100 Hz base frequency and hence, harmonics of 200 Hz, 300 Hz, etc. The corresponding angular frequencies of interest will be accordingly 628 rad/s, 1,258 rad/s, 1,885 rad/s, etc.

The absolute value of the impedance at any frequency is the length of the vector pointing from the origin to the given frequency point on the $Z_{th}(\omega)$ locus (arrows in Fig. 4.58 and Fig. 4.59). The angle between the horizontal axis and the locus shows the phase shift between the sinusoid power component and the temperature change belonging to it.

The length of the vectors shows that the thermal impedance is smaller at higher frequency; their angle proves that the temperature change is delayed to the power. This is also implied by the compact network model of the thermal impedance (Fig. 4.40). The physical meaning of the smaller temperature change on the same power amplitude is that the periodically changing heat can be locally stored and released by the structures near the junction; it does not reach the ambient.

Complex loci are a very powerful representation of the component and its environment when analyzing periodic excitations. An application example is the single valued “AC thermal impedance” of LEDs [26] that will be detailed in Sect. 4.7.

For internal use by Mentor Graphics marketing only

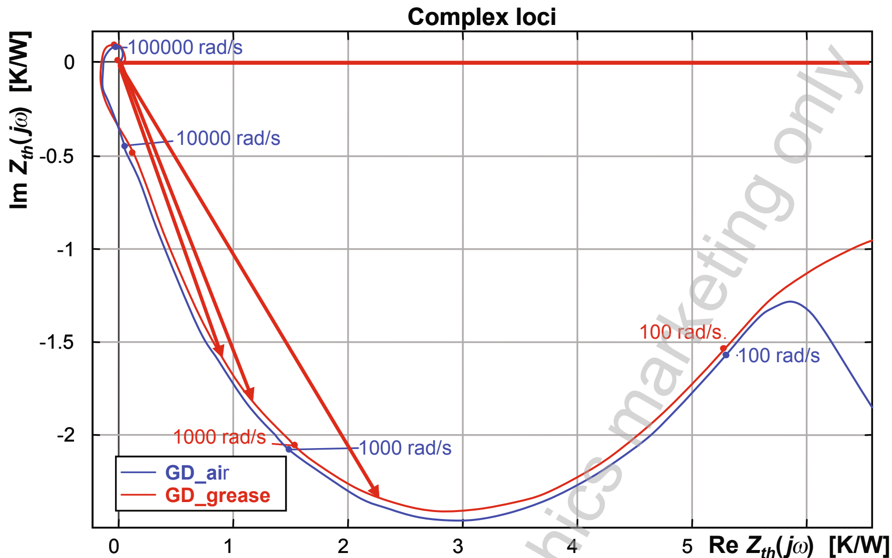


Fig. 4.59 Excerpt of the complex locus in Fig. 4.58

For internal use by Mentor Graphics marketing only

## 4.4.8 Summary About the Different Representations of Thermal Impedances

In Sect. 4.4, we described how the results of thermal transient measurements can be interpreted.

The well-known $Z_{th}(t)$ curve is obtained from the measured junction temperature change $\Delta T_J(t)$: this function is divided by the $\Delta P_H$ real heating power step applied at the device under test (in case of LEDs that is the supplied electrical power less the emitted optical power). The $Z_{th}(t)$ *time domain thermal impedance function* directly provides the junction temperature response if 1 W of heating is applied, therefore it is called *unit-step response*.

We distinguish between driving point thermal impedances (when the heating and the measurement of the dynamic temperature response takes place at the same location) and the transfer impedances (when the heating and the measurement of the temperature response are at different locations).

During the subsequent postprocessing of the measured thermal impedances, logarithmic time scale is assumed by the introduction of the $z = \ln(t)$ transformation. The unit step response in logarithmic time scale is often denoted by $a(z)$ in the technical literature.

The first concept we described was the concept of the continuous $R_\zeta(\zeta)$ thermal *time constant spectra*. The *convolution integral*, which connects the time constant spectrum and the unit-step response, was shown. This relationship provides the algorithm of extracting the time constant spectra from measured thermal impedances. Time constant spectra are interpreted both for driving point and transfer impedances. Time constant spectra of driving point impedances have only positive values, while in case of transfer impedances there are negative values also present in the time constant spectra.

Time constant spectra of driving point thermal impedances can be further processed: after discretization (as a practical step in the numerical implementation of the necessary calculations) *FOSTER equivalent models* (as black box models) and after

a conversion step, detailed *CAUER equivalent network models* (with about 150..200 stages) can be obtained. These detailed network models are yet another representation of the driving point thermal impedances.

The measurement result evaluation method is named *NID* as the process is based on the series of a deconvolution and a network model identification steps.

To facilitate the further analysis of the measurement results, the *cumulative structure function*[15] (*CSF*) is defined as a map or a graphical representation of the thermal capacitance/thermal resistance distribution of the junction-to-ambient heat flow path. We have shown that for essentially one-dimensional heat flow paths the structure functions and the physical structure of the path are in a one-to-one relationship. To further enhance the heat flow path details, the derivative of the cumulative structure function, called the *differential structure function* (*DSF*) is also introduced.

Both kinds of structure functions are powerful tools in finding *partial thermal resistances* (like TIM resistances) or thermal capacitances of different structural elements of a power semiconductor device package. Knowing material properties, volumes and effective cross-sectional areas of different heat flow path sections can be identified; or, if geometrical information about the heat flow path sections is available, material properties can be identified. Some of these properties of structure functions lead to new thermal testing applications like die attach qualification or measurement of thermal conductivity of TIM. Application of structure functions in pre- and poststress analysis of LED's reliability studies was demonstrated recently [28]. This topic is further discussed in Sect. 4.5.4.

Thermal transient measurements and structure functions recently got used in measuring standard thermal metrics of packages like the measurement of the junction-to-case thermal resistance of power semiconductor device packages (see the JEDEC JESD51-14 standard [13]).

Last but not least, there are two further representations of the thermal impedances, which help study the thermal behavior of packaged semiconductor devices under periodic heat load conditions. The *pulse thermal resistance* diagrams can be derived from time constant spectra by using a convolution integral [20]. These diagrams provide information about the effective thermal resistance of the heat flow path when driven with a square wave dissipation with a given pulse duration and duty factor. This information can be useful for the thermal management design of PWM-dimmed LED applications.

*Complex loci* (or Nyquist diagrams) are the graphical representations of thermal impedances in the *frequency domain*. They are defined both for driving point and transfer impedances. With the help of these loci, one can identify the value of the thermal impedance at any harmonic frequency of a sinusoid power excitation. This is very useful information when one needs to characterize the thermal behavior of directly AC mains driven LEDs [26]. This topic is further discussed in Sect. 4.7.

---

[15] In many cases, the adjective "cumulative" is neglected and the *CSF* is simply called the structure function.

For internal use by Mentor Graphics marketing only

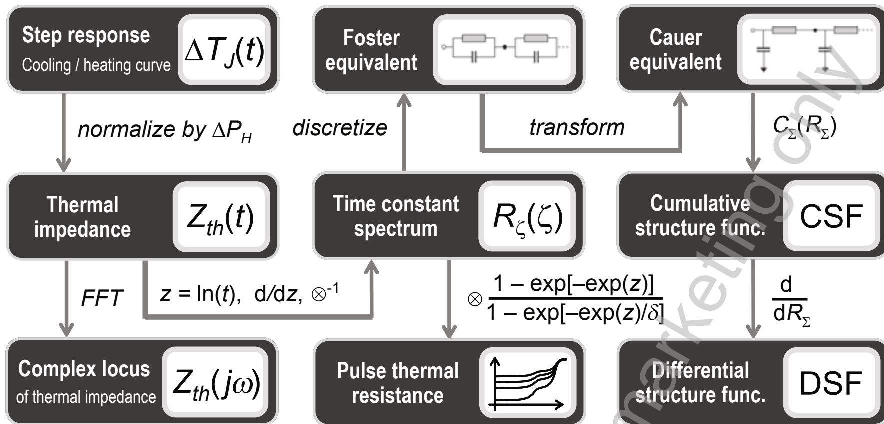


**Fig. 4.60** Summary of the possible equivalent representations of a driving point thermal impedance (after Vermeersch [27])

All these equivalent representations of the thermal impedances and the conversion steps between them are summarized in Fig. 4.60.

## 4.5 Some Applications of Structure Functions

### *4.5.1 In Situ TIM Testing*

As pointed out in Sect. 4.4.4, structure functions can be well used to study material property changes in junction-to-ambient heat conduction paths of different (power) semiconductor devices. As an example, interfaces between mating solid surfaces in a heat flow path are regions usually characterized by a small $C_{th}/R_{th}$ ratio—appearing as long, flat plateaus in structure functions.[16]

Some portions of the LED structure are highly stable (chip, submount, heat slug.) On the contrary, TIM layers, which are applied to fill the small gaps between mating surfaces can show large variation even in samples from the same manufacturing lot. Testing the TIM itself, in bulk or in thin layers (see Sect. 4.5.3) gives no hint on the actual thermal resistance achieved in the fabricated TIM layer. These unavoidable variations can be best studied in structure functions.

Figure 4.61 highlights typical thermal interfaces in an LED application. Their quality can be even measured as the length along the thermal resistance axis of TIMa, TIMb, and TIMc in Fig. 4.51 (Example 4 of Sect. 4.4.4).

There could be many reasons why interfacial thermal resistance changes: temperature change, variation in the thickness of the TIM layer, aging or simply, the TIM quality is changed by purpose. In the subsequent sections, examples will be shown

[16] The analysis technique based on changing $C_{th}/R_{th}$ ratio in the structure function was first suggested by M. Rencz et al. [29] for the study of die attach voiding and for TIM quality assessment.

For internal use by Mentor Graphics marketing only

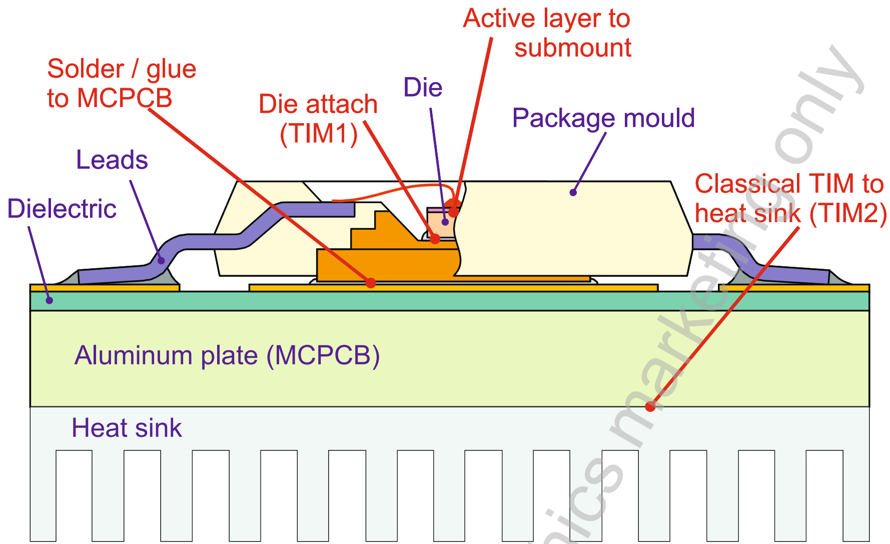


**Fig. 4.61** Different thermal interfaces in the junction-to-ambient heat flow path of a typical LED application

For internal use by Mentor Graphics marketing only

for such cases. The overview of applications of structure functions will be concluded by an example for model calibration.

### 4.5.2 *The Transient Dual Interface Method for the Standard Measurement of the Junction-to-Case Thermal Resistance*

The measurement of the $R_{thJC}$ junction-to-case thermal resistance of (power) semiconductor device packages has always been suffering from different problems. The "classical" method was putting a thermocouple into the cooling mount and making statements on measuring junction temperature and the temperature of an arbitrary point on the "case" surface. The major pain was the repeatability and another issue was accuracy—which became rather severe when small $R_{thJC}$ values had to be measured.

Even small errors in the measurement or its repeatability may cause enormous problems. On one hand, publishing junction-to-case thermal resistance values on the product data sheet underestimated by 10 % may result in liability issues of the semiconductor vendors. On the other hand, the same thermal metric overestimated by 10 % may result in competitive disadvantage if end-users select power semiconductor parts based on the thermal performance measured by this metric.

Application of structure functions in a smart way was a workaround to this measurement problem. Today's new JEDEC standard JESD51-14 [13] is based on the original idea first published by Steffens et al. in 2005 [30], which is the following.

Since structure functions reflect structural changes of an essentially one-dimensional heat conduction path, let us introduce such a change by purpose: let us change the quality of the thermal interface at the "case" surface of a power package. That change must be reflected to some extent by the $Z_{th}$ curves (Fig. 4.37) and much clearer by the structure functions (Fig. 4.50, Fig. 4.51). There are cases when the deviation of the first derivative of the measured $Z_{th}$ thermal impedance function provides a more definite separation, thus allowing a better definition for the $R_{thJC}$ value.

In the original paper, the authors realized the two different qualities of the thermal interface by inserting a thin thermal insulator between the package under test and the cold plate used as a test environment. The present JEDEC standard recommends a more practical approach: it proposes to measure the package "dry" and "wet," as demonstrated in Fig. 4.31.

When applied to LEDs, one has to make sure that in both measurements the heating power is corrected by the emitted optical power, using, for example, the curves with postfix _oc in all characteristic plots.

Finding the separation point of the structure functions is not trivial. After detailed numerical simulation studies and practical experiments, [31, 32] the method got standardized with the requirement of defining a small positive $\varepsilon$ threshold number (Fig. 4.49, Fig. 4.50). This $\varepsilon$ either specifies the *relative difference* of two derivative functions or the *difference* of the cumulative structure functions (depending on the method chosen) where we say, the corresponding $Z_{th}$ value or the corresponding cumulative thermal resistance is equal to the junction-to-case thermal resistance. This $\varepsilon$ value must be included along with the identified $R_{thJC}$ value on the test report. Precise details are presented in the JESD 51-14 standard [13] and in papers [33] or [34].

The required data processing method is implemented in a publicly available software tool (forming an online annex of the standard) as well as in a commercially available software.

Note that the standard was worked out for silicon power semiconductor devices. Before standardization, different aspects of the applicability of the method have been analyzed by Schweitzer et al. [32, 34, 35].

One of the first studies on the applicability of this method to certain high-power LEDs was published by Müller et al. [36].

The great advantage of this transient method is that instead of measuring a *spatial difference* of two temperature values ($T_J$, $T_{Case}$) with two thermometers (the junction itself and a thermocouple attached to the "case" somehow), it takes the *temporal difference* of the junction temperature only (junction temperature transient). This way most of the uncertainty and repeatability issues of the classical steady-state $R_{thJC}$ measurements are inherently eliminated. The completely differential approach used in the $\Delta T_J(t)$ measurement automatically cancels out offset errors and one needs to calibrate the TSP of the device under test only.

For internal use by Mentor Graphics marketing only.

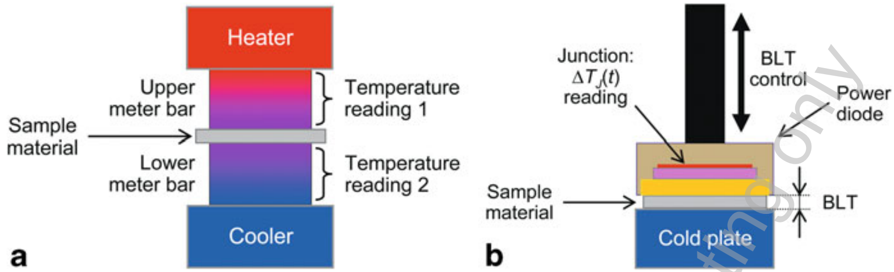


**Fig. 4.62** Possible setups for TIM testing: **a** classical ASTM-like steady-state measurement setup, **b** Dynamic TIM testing setup based on junction temperature transient measurements

For internal use by Mentor Graphics marketing only

### *4.5.3 Structure Functions Used in TIM Testing*

In classical (steady-state) thermal interface material testing (ASTM D-5470-01, see [37]) heat bars with known heat flux are used and the temperature drop difference due to the introduction of the TIM to be tested is measured. Based on this temperature difference, the thermal conductivity of the material can be calculated (Fig. 4.62a).

Uncertainties emerge due to the calibration issues of measuring spatial difference of two temperatures, possible errors in temperature readings of thermocouples used, etc.

A better way of testing thin TIM layers can be built on the transient method used for measuring junction-to-case thermal resistance. The material sample is placed in a dedicated test fixture where one face is the "case" surface of a power diode and the other face is the surface of a cold plate. We measure the $\Delta T_J(t)$ junction temperature transient of the diode at a well specified, preset thickness of the material (BLT—bondline thickness), see Fig. 4.62b. As we change the sample thickness with a precise, dedicated mechanics, the total measured thermal impedance of the complete test setup will change.

The change of the total junction-to-ambient resistance of the test setup is solely due to the changes in material sample thickness, as presented in the structure functions of Fig. 4.63. Therefore, the $\lambda$ thermal conductivity of the sample can be calculated as follows:

$$\lambda = \frac{1}{A} \cdot \frac{\Delta L}{\Delta R_{th}} \tag{4.46}$$

where $A$ is the cross-sectional area of the heat flow path across the sample, $\Delta L$ is the bondline thickness change, and $\Delta R_{th}$ is the corresponding change in the total thermal resistance of the test setup.

According to Eq. (4.46), we can state that the thermal conductivity of the TIM sample tested is directly proportional to the slope of the $R_{th}$–BLT diagram obtained for the sample. Such diagrams are shown in Fig. 4.64.

There are some advantages of this TIM testing method compared to other techniques. For example, there is reduced measurement uncertainty due to the differential

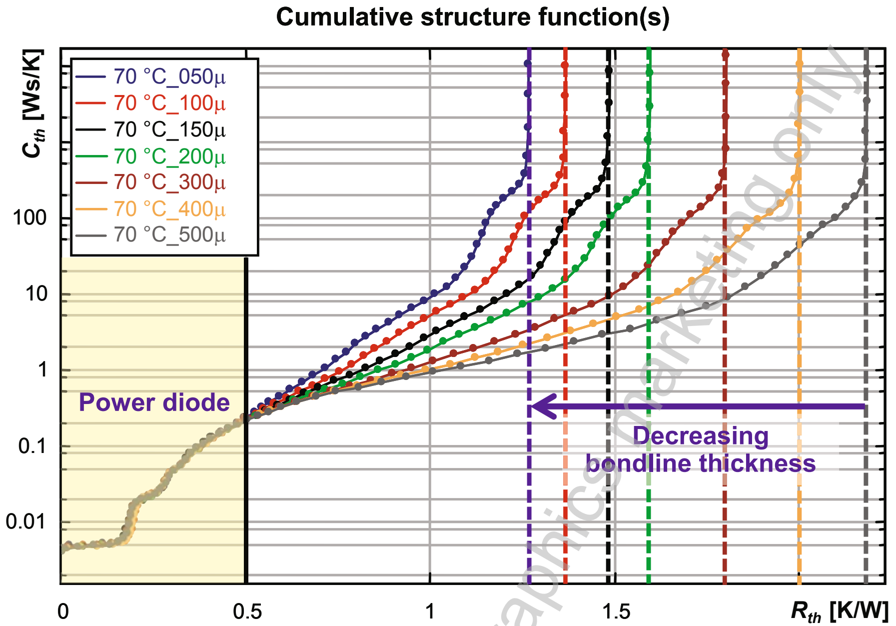


Fig. 4.63 Structure functions of the dynamic TIM testing setup measured at different preset bondline thicknesses of the material tested

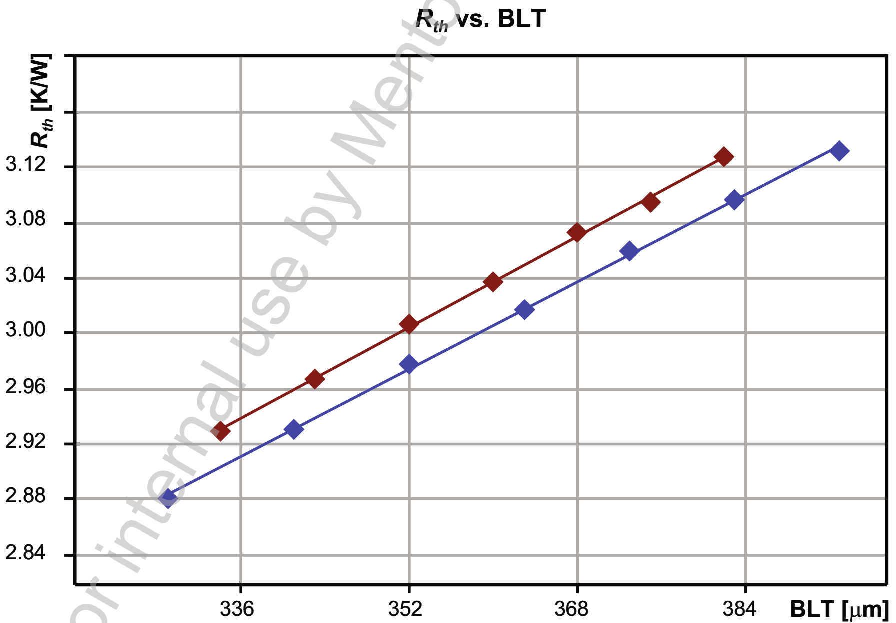


Fig. 4.64 Thermal resistance versus bondline thickness plots obtained for a given material type measured in a dynamic TIM testing setup outlined in Fig. 4.62b

For internal use by Mentor Graphics marketing only

approach. The test method can be considered as a quasi in situ technique as the test fixture resembles the real-life application conditions of TIM materials. Last but not least, every measurement includes an inherent self-test of the measuring system; as based on the obtained structure functions, the structural integrity of the test fixture can always be checked. Such a system is available as an add-on item [38] of a commercial thermal transient tester [39].

A general overview on different TIM testing techniques is given in Chap. 8 on TIMs.

Details of the measurement principle and its realization are presented in papers of Vass-Várnai et al. [40, 47].

### *4.5.4 Structure Functions in Reliability Analysis*

If aging of TIMs manifests in thermal conductivity changes, these changes can thus be well measured by structure functions. Therefore, thermal transient measurements completed by structure function analysis are becoming a popular tool in reliability investigations of complete thermal management solutions both in electronics cooling and in solid-state lighting applications.

The general methodology is as follows.

First, a test heat conduction path setup is created: typically a power semiconductor device is assembled to a cold plate. The purpose of the test could be to test the semiconductor device itself or to test the TIM layer applied between the semiconductor device and the cold plate.

As second step, thermal transient measurement of the test setup is performed before any stress condition of the given reliability/or life time test is applied.

Then, the stress condition is applied. In reliability analysis, typically temperature cycling and/or power cycling are used as a thermal stress condition. Another often applied stress condition is relative humidity (RH) cycling. In case of LED life time testing (LM80 standard [42] compliant tests), the stress condition is realized by operating the LEDs at nominal forward current at elevated environmental temperature (e.g., 85 °C).

Thermal transient measurements of the test structure are usually performed regularly while the stress conditions are being applied: e.g., at 500 h, 1,000 h, 1,500 h etc. in LM80 life time measurements [29].

The first such measurements on power LEDs were published by the team of M.W. Shin [43, 44]. A power LED package was subject to high temperature and high RH conditions, which caused die attach delamination. The delamination process was "monitored" by structure functions taken after 3, 6 and 24 h of stressing. At the end of the experiment, the die attach delamination was confirmed by acoustic microscopy.

**Example 6—structural changes during LM80 tests**

Degradation of these thermal interfaces such as delamination or material aging results in increased thermal resistance, thus in higher junction temperature, which is among

For internal use by Mentor Graphics marketing only

the reasons that lead to luminous flux reduction of LEDs during their life time or even to fatal failures.

End-users of LEDs have no control over the quality of most of these thermal interfaces except the ones introduced at the assembly of the LED-based product. These comprise the LEDs' attachment to a substrate like a metal core printed circuit board (MCPCB) or the so-called TIM2 layer—the TIM used to reduce the interfacial thermal resistance between the MCPCB and the heat sink (luminaire body).

In a series of experiments on aging LEDs performed by the team of Schanda et al. at the University of Pannonia (Veszprém, Hungary), the usual electrical and photometric/spectroscopic measurements during LM80 life time tests have been completed with thermal transient measurements and subsequent structure function analysis [29].

The obtained structure functions indicate all the essential elements of the junction-to-cold plate heat flow path, like the LED chip itself, die attach, the solder/glue between the primary LED package and the MCPCB used for assembly, and the TIM between the MCPCB and the temperature-controlled solid surface of the test chamber (cold plate).

With the regular thermal transient measurements during this experiment, one could observe structural degradation both within and outside the LED package. The most characteristic changes were delamination of the LED package from the MCPCB and the degradation of the applied TIM2 material.

Figure 4.65 provides snapshots for LED samples, which are considered "best" performing devices from the point of view of light output stability (samples A) and for the worst devices (samples B). In Fig. 4.65a, only a slight thermal resistance increase can be observed on samples A, the main contributor to this increase is at the end of the junction-to-cold plate heat flow path. This can be identified as the TIM (conventional thermal grease in this case) between the MCPCB and the test chamber. The increase of 0.9 K/W with respect to the original value of 15.1 K/W means about 6 % change of the total thermal resistance. In Fig. 4.65a, one can also see the high stability of the relative luminous flux of the investigated LEDs.

Figure 4.65b demonstrates that samples B show huge increase in the total thermal resistance as indicated by the structure functions. This increase took place within 500 h of aging time. Since the initial sections of the structure functions in Fig. 4.65b coincide (corresponding to the LED chip and the die attach), probably the increase reveals a delamination of the LED package from the MCPCB. Between 500 and 2,000 h, the same TIM aging took place as seen in Fig. 4.65a.

As one can see, there is a strong correlation between the maintenance of the emitted luminous flux of the LEDs and the structural stability of the junction-to-ambient heat flow path. In case of poorly performing LEDs, the significant increase of the thermal resistance is not the direct reason of the significant drop of the luminous flux.[17] The increased junction temperature resulting from the increased thermal resistance has accelerated those chip-level failure mechanisms, which cause light output reduction. Section 5.5.2 of Chap. 5 presents further details on light output measurement results obtained in this experiment.

For internal use by Mentor Graphics marketing only

[17] In this particular case, about 1.5 % loss can be attributed directly to the increased thermal resistance.

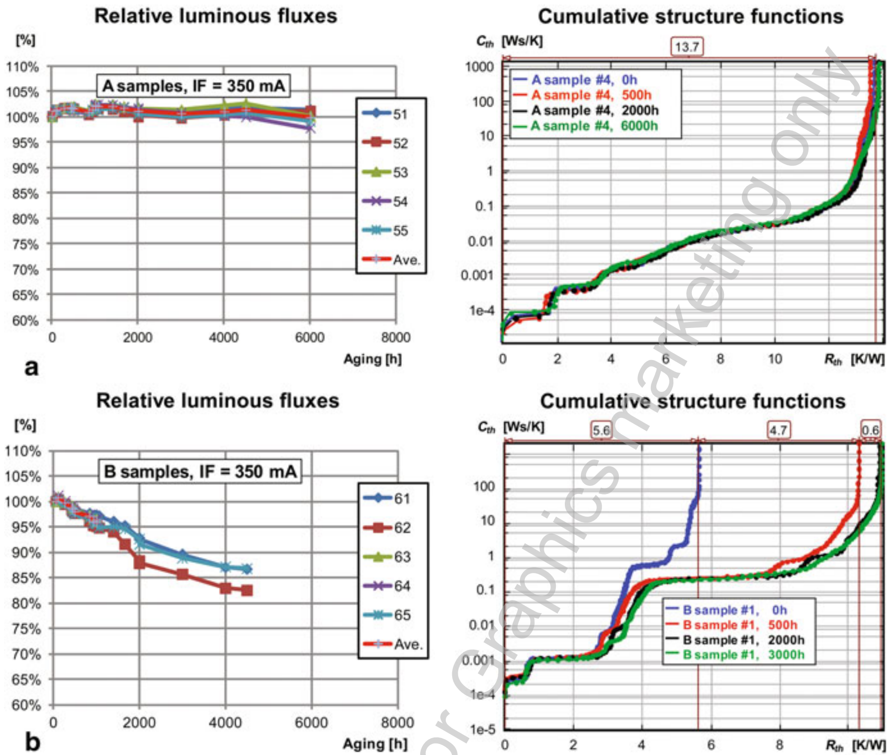


**Fig. 4.65** Change of relative luminous flux and thermal properties of **a** a very stable LED and **b** a poor quality LED during LM80-compliant life time testing experiment [29]

For internal use by Mentor Graphics marketing only

**Example 7—TIM property changes during temperature cycling**
In this case study, the changes of TIM performance were monitored in situ, after repeated reliability tests. In the test arrangement, the TIM material was put between the external cooling surface of a power semiconductor device and a liquid cooled heat sink. The device was fixed to the surface of the heat sink by constant force, maintained by a special fixture.

The test was aimed at the study of the durability of TIM materials for temperature cycling, induced by power cycles applied to the device. After reaching the hot thermal steady state, the high power applied at the device was switched off and the cooling transient was measured by the transient tester. Such test conditions resemble the normal operation of the device: if the quality of the TIM gets worse, the same powering results in higher junction temperatures in each cycle.

The device was trained by approximately 20 W power steps, in 20 s periods of 50 % duty cycle. The surface temperature of the heat sink was set to 40 °C during all measurements. This allowed the junction temperature to rise up to approximately 120 °C in each cycle.

In the original study of Vass-Várnai et al. [45] the thermal behavior of eight different TIM samples was investigated; here we present the case of a nanoparticle filled composite.

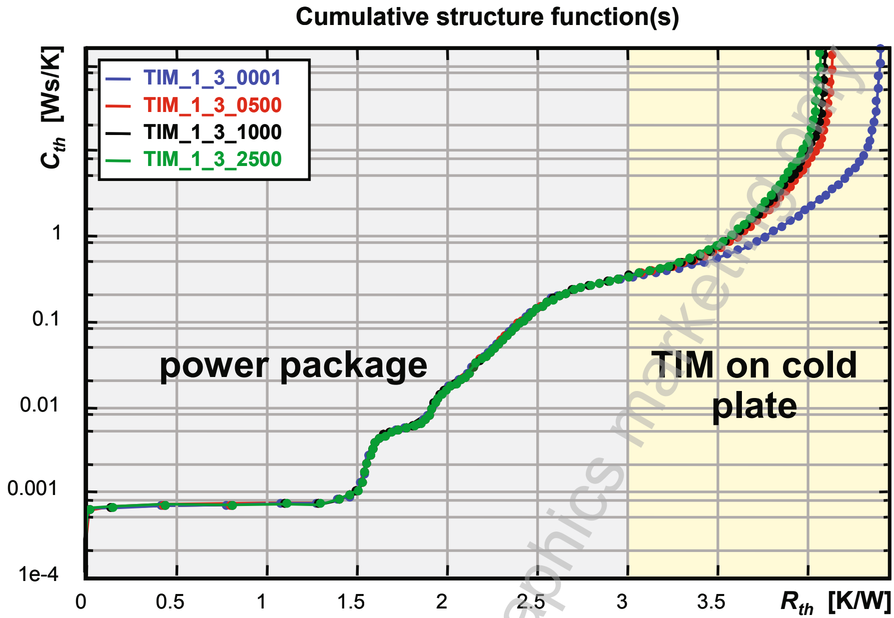


**Fig. 4.66** Sample structure functions obtained from the power/temperature cycling test setup aimed at the study of the long-term behavior of different TIMs

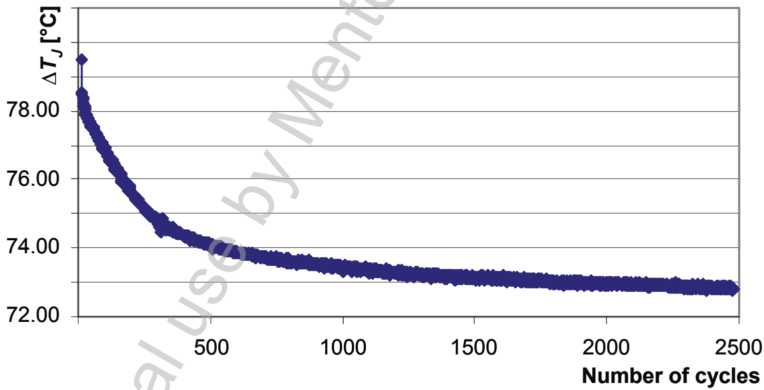


**Fig. 4.67** TIM performance change during power cycling indicated by junction temperature elevation, derived from the structure functions of Fig. 4.66

For internal use by Mentor Graphics marketing only

During the tests of the investigated TIM materials, 2,500 cycles were performed and the cooling transients for every cycle were captured. Structure functions were generated from the junction temperature transients measured in every cycle. As seen in Fig. 4.66, as long as the heat flows in the same structure (the BJT package),

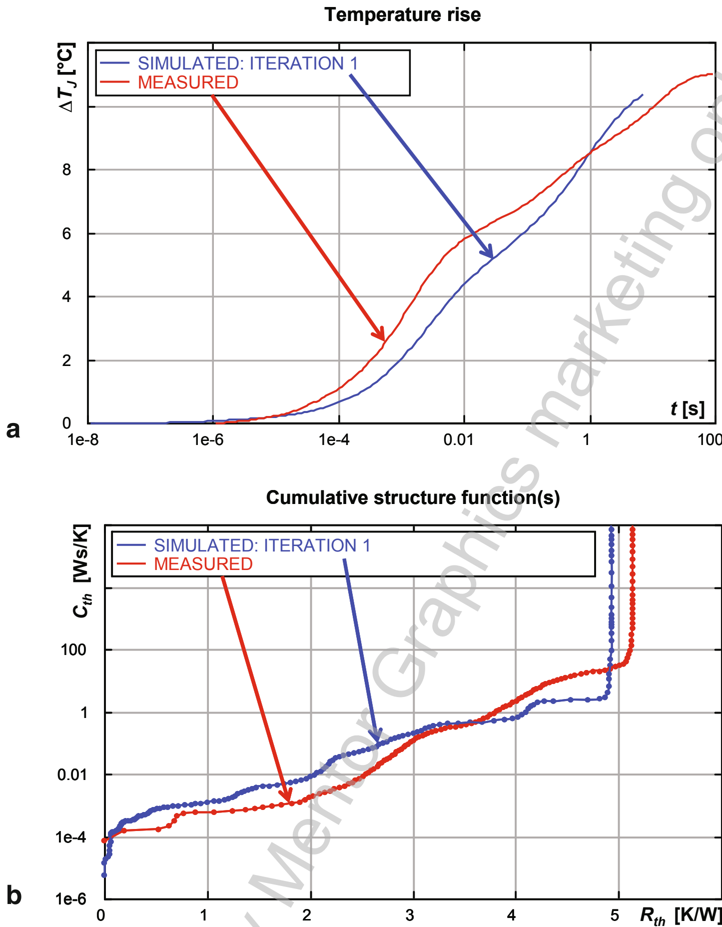


**Fig. 4.68** Measurement and simulation results of a power transistor package: **a** junction temperature transients, **b** cumulative structure functions. Simulation was performed with an initial, uncalibrated detailed model

For internal use by Mentor Graphics marketing only

the structure functions are exactly the same. If the structure of the heat flow path changes, the difference immediately appears on these functions, showing the exact location (thermal resistance value) and magnitude (thermal capacitance value) of the change. In this example, the changes appear in the last section—corresponding to the investigated TIMs.

The reference structure function is the one obtained after the first cycle (the rightmost curve in Fig. 4.66). Further structure functions obtained after 500, 1,000, and 2,500 cycles are also shown in the figure. The observed junction temperature elevations for all test cycles of a selected TIM are shown in Fig. 4.68. In this particular example, the TIM performance has improved during the test.

The original study [45] includes examples in which TIM quality degradation was observed during the temperature cycling.

### 4.5.5 Structure Functions and Thermal Modeling

A simulation model is as good as the available input data: device geometry and material properties. When creating detailed models for CFD simulation tools, this is always an issue, even for semiconductor vendors who in principle must be aware of at least the device geometry. But many times, material parameters and effective volumes or area raise questions. One possible source of uncertainty in detailed thermal simulation models is the interface thermal resistance, both at TIM1 (die attach) and TIM2 (e.g., thermal grease).

Thermal transient testing was already used in the PROFIT project for the calibration of detailed simulation models further used in DELPHI-type compact model generation [46]. Though structure functions were already known as tools of heat flow path structural analysis, in this work they were not yet used: only measured and simulated junction temperature transients obtained for different DELPHI dual cold plate conditions were compared.

The idea behind using structure functions for detailed model calibration/validation is as follows. If both the geometry/material properties in the simulation model and the boundary conditions correspond to the real-life situation, then there should be no differences between the measured and simulated thermal impedance curves. Any small difference due to geometry or material mismatch should be visible in the corresponding structure functions. A paper by Bornoff and Vass-Várnai [47] provides a case study on how a power semiconductor device package model could be fine-tuned with the help of structure functions. We take the example from this paper[18]: creating the calibrated detailed model of BD-242-type transistor housed in a TO-220 package.

In the early iteration steps, the die size and the area of the active (dissipating) chip surface region were matched. With this modification, the first section of the heat flow path model became correct: as seen in Fig. 4.69a. With this, the match between the simulated thermal impedance and the measured thermal impedance became perfect up to a cumulative thermal resistance value of about 2.5 K/W.

After the die attach layer's properties also got modified (interface resistance set to the proper value by adjusting the thermal conductivity of the TIM1 material), the matching of the structure functions became perfect up to roughly 4.4 K/W, see Fig. 4.69b.

The last step in the model calibration was to properly set the thermal resistance of the applied TIM2 layer, see Fig. 4.69c. With this, the model calibration was completed. The remaining difference is attributed to the modeling of the cold plate used.

Trade-offs between simulation and measurement depend on many factors. Paper [48] discusses some of these. A recent approach is to create (dynamic) compact models of packages directly from measurement results [27], leaving out the creation of calibrated detailed CFD models used in standard compact modeling methodologies. For more on this topic, refer to Sect. 6.5.2.2 of Chap. 6.

For internal use by Mentor Graphics marketing only

[18] Measurement and simulation results by courtesy of Vass-Várnai and Bornoff.

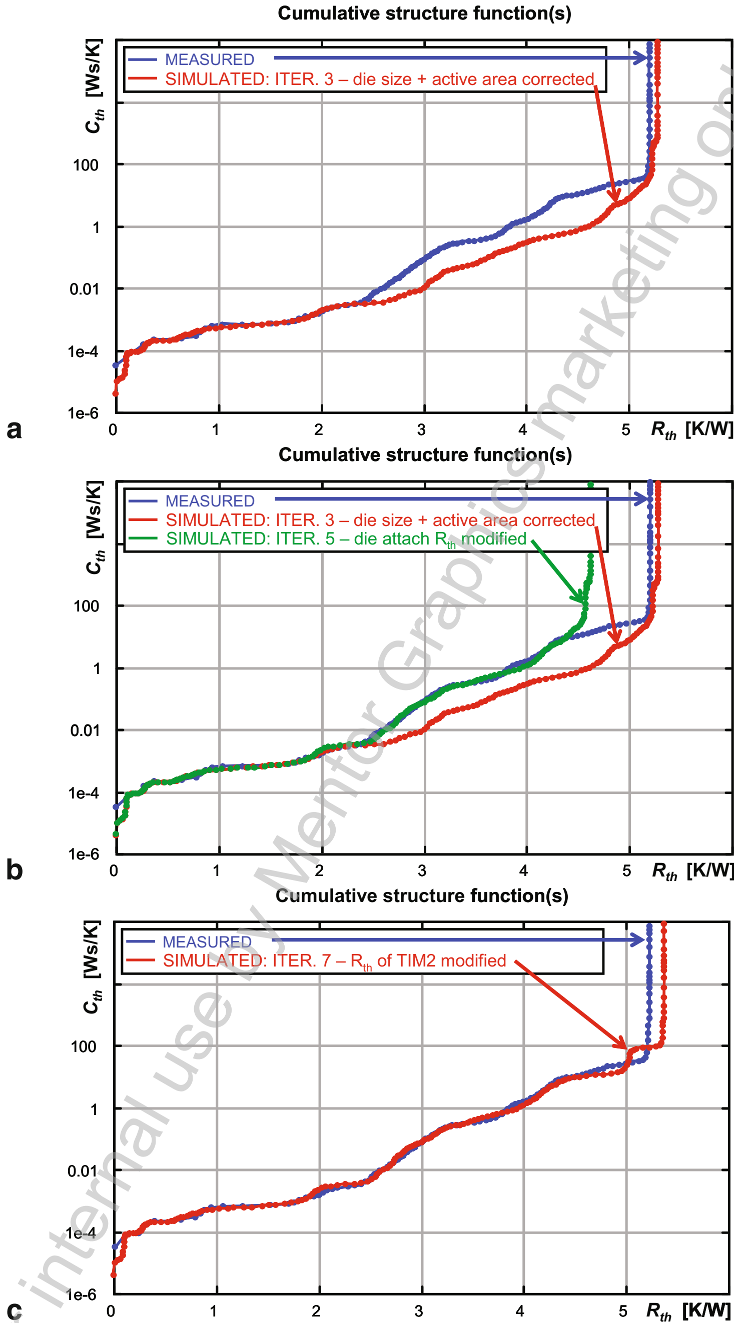

For internal use by Mentor Graphics marketing only

**Fig. 4.69** Major iteration steps of adjusting the simulation model: **a** correction of the die size and the area of the active (dissipating) region, **b** die attach thermal resistance also corrected, **c** final calibrated model with adjusted TIM2 thermal resistance

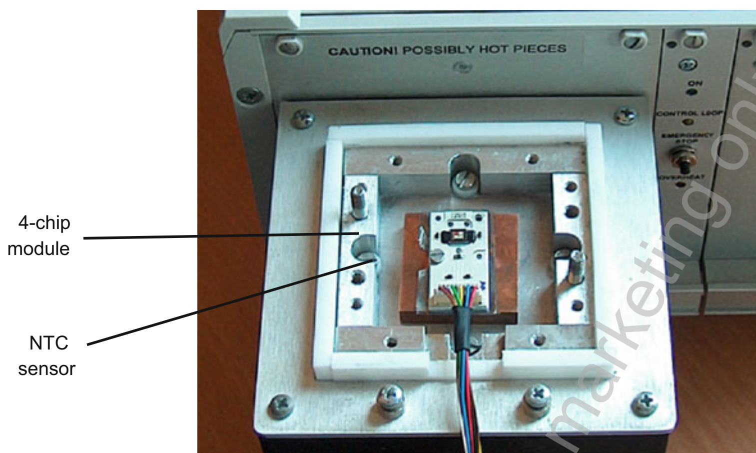


**Fig. 4.70** Ostar module in the calibration chamber also used as cold plate during the measurement

## 4.6 Multichip Measurements

Thermal measurement of multichip modules is discussed systematically in Chap. 6, Sect. 6.1.4.2. Here, we illustrate the features of such measurement in a practical example.

**Example 8—measurement of an RGB module**
We measured a commercially available 4-chip Osram Ostar module built on a surface mount distributor plate. The module contained a 2 × 2 array of a red, a blue, and two green chips.

The plate temperature was separately measured by a negative temperature coefficient (NTC) resistor.

After calibration, cooling curves were recorded and processed in the same way as in previous examples.

Figure 4.70 shows the thermostat with removed lid in which the calibration and the subsequent thermal measurement was carried out.

Figure 4.71 shows the cooling curves of the system. The blue chip was driven by 350 mA, much below the allowed maximum current. We can observe that the run time from the driven blue to the nearby green chips was approximately 3 ms and to the red chip, which was in opposite diagonal position in the array it was 5 ms. The temperature change reached the NTC sensor after 400 ms.

Table 4.4 lists the measured “electrical only” $R_{thJA\text{-}el}$ junction-to-ambient thermal resistance values calculated from the input electric power only. Each row represents a measurement in which one LED was driven by heating current and then the cooling of four LEDs and the NTC sensor were recorded. In the diagonal of the table with bold numbers, we see the self-resistance (temperature change on the LED

For internal use by Mentor Graphics marketing only

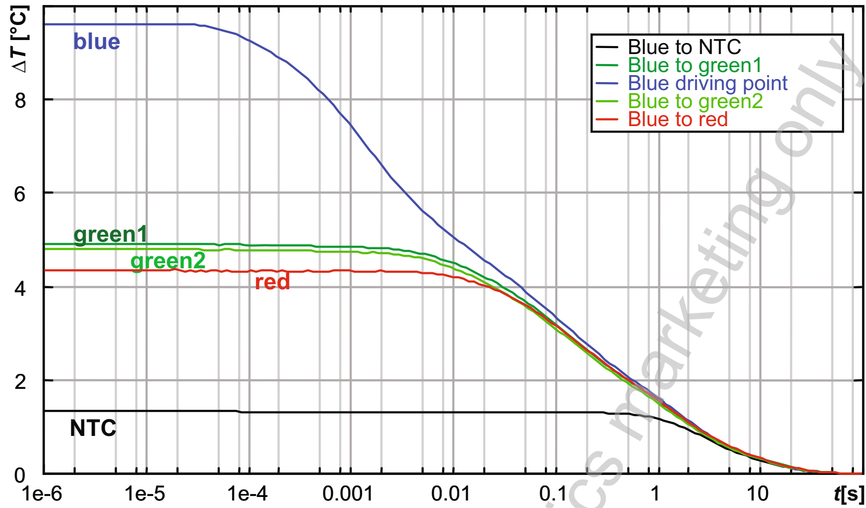


**Fig. 4.71** Cooling curves of the Ostar module, blue chip-driven

**Table 4.4** Measurement results for the RGB module

| LED driven | $R_{ij\text{-}el}$ [K/W] | | | | |
|---|---|---|---|---|---|
| | Channel | | sensed | | |
| | G1 | B | G2 | R | NTC |
| G1 | **10.44** | 4.67 | 4.03 | 4.53 | 1.15 |
| B | 4.21 | **9.24** | 4.13 | 3.73 | 1.14 |
| G2 | 4.00 | 4.54 | **9.95** | 4.48 | 1.14 |
| R | 4.05 | 3.74 | 3.97 | **9.65** | 1.05 |

heated by electric power, also displayed in Fig. 4.72); other cells represent transfer resistance also known as *thermal characterization parameter* (temperature change at an unheated point divided by the input power of the heated LED).

The small asymmetry of the array is caused by the different energy conversion efficiency of the chips of different color.

The next two figures compare the $Z_{th\text{-}el}$ and $Z_{th\text{-}real}$ self-impedances of the four chips. The $Z_{th\text{-}real}$ curves are shifted such that they coincide on the longest section.

Cumulative structure functions composed from the self-impedance also show poor coincidence without optical power correction. Structure functions with correction show difference only in the chip region.

For internal use by Mentor Graphics marketing only

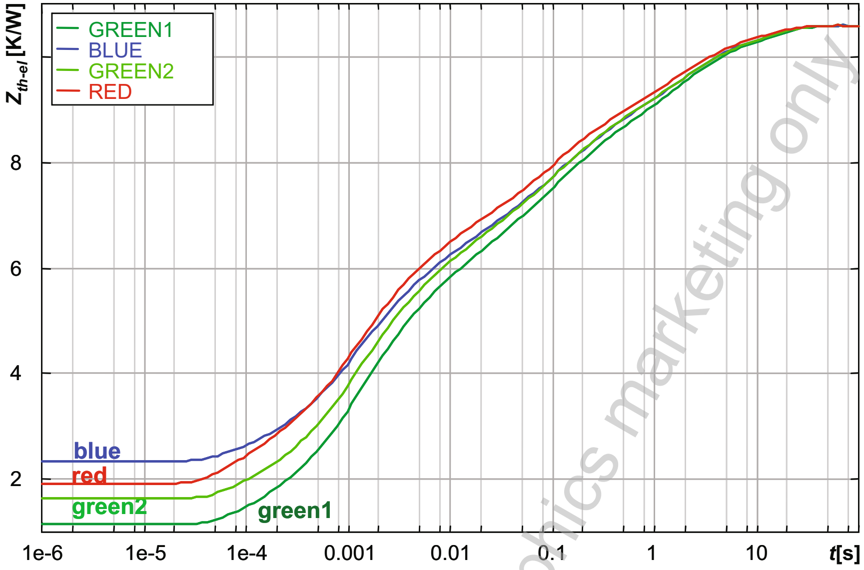


**Fig. 4.72** The $Z_{th-el}$ curves belonging to the self-heating of each LED chip

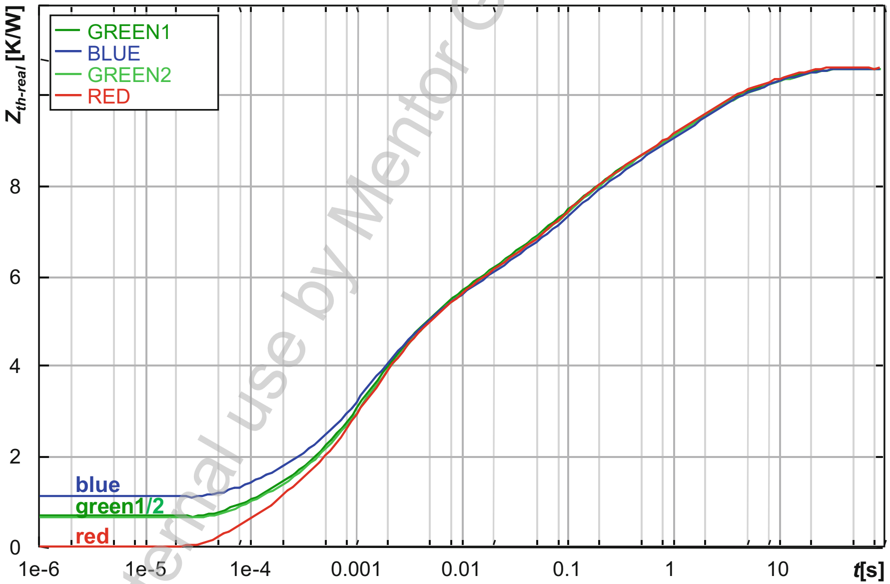


**Fig. 4.73** The $Z_{th-real}$ curves belonging to the self-heating of each chip, magnified along $y$-axis so as to be scaled to Fig. 4.72

For internal use by Mentor Graphics marketing only

## 4.7 Issues of Thermal Testing of AC-Driven LEDs

### *4.7.1 Introduction*

LED lighting applications can be powered either by a constant current LED driver circuit or directly from the AC mains. Such AC-powered LEDs may have different configurations [49, 50, 51]. In directly AC-driven LEDs or LED lamps, the driver electronics is simplified to a small integrated ballast, sometimes a serial resistor only, sometimes a component of reactive nature.[19]

At constant DC, powering LEDs dissipate steady power. This results in a steady junction temperature after a relatively short heating transient. Due to basically one-dimensionalheat spreading in LED components, a single *thermal resistance* value for further system (luminaire)-level thermal design is usually a sufficient model of the steady-state thermal behavior.

The first publications about techniques aimed at measuring the junction temperature of AC-driven LEDs appeared in 2010 [53, 54]. These methods are based on the idea of Zong and Ohno, first suggested for optical testing of DC-driven LEDs at a specified junction temperature [55]. In the following, we present how a single-valued thermal metric of AC-driven LEDs can be identified, based on concepts and testing methods shown for DC-driven LEDs.

As none of these methods provide any thermal metric for packages and cooling solutions of AC-driven LEDs, in the following, we try to fill this gap.

In case of AC-driven LEDs, the sinusoidal mains voltage results in a periodic waveform of the actual heating power, after an initial, transitional period while heating up the LED junctions. Once the shapes of the waveforms of the heating power and the junction temperature do not change any more, we can say that the directly AC-driven LED is in a *stationary state*. As our systems are nearly linear in the thermal domain, the thermally stationary situation can be treated similar to the small signal AC operation of linear electronic circuits.

In AC conditions, the frequency-dependent temperature response is of interest. Using the frequency domain description of the thermal impedance, the temperature can be calculated as:

$$T_J(\omega) = Z_{th}(\omega) \cdot P_{dissAC}(\omega) \tag{4.47}$$

where $\omega$ is (angular) frequency and $P_{dissAC}$ is the AC power dissipation (as we show later, obtaining $P_{dissAC}$ is not trivial). If $P_{dissAC}$ were a purely sinusoidal signal in the form of $P_{dissAC}(t) = P_{\max} \cdot \sin(\omega t)$, the time domain representation of the AC junction temperature response would also be a sinusoidal function:

$$T_{JAC}(t) = T_{J\max} \cdot \sin(\omega t - \varphi),\ T_{J\max} = |Z_{th}(\omega)| \cdot P_{\max} \tag{4.48}$$

where $\varphi$ is the phase shift between the power and the temperature waveforms.

[19] These ballasts usually hamper thermal testing and thus need to be bypassed for the sake of this test.

For internal use by Mentor Graphics marketing only

For fairly good approximate calculations, the dynamic compact network model representation of the thermal impedance (Fig. 4.74c) can be used in formulas (4.47) and (4.48) as usual in the simple small signal calculations of linear electrical circuits:

$$Z_{th}(\omega) = \frac{1}{j\omega C_{th1}} \times \left\{ R_{th1} + \frac{1}{j\omega C_{th2}} \times \left( R_{th2} + \left[ \frac{1}{j\omega C_{th3}} \times (R_{th3} + Z_{hs}) \right] \right) \right\} \tag{4.49}$$

For the element values in Eq. (4.49), notation of Fig. 4.74c was used. $Z_{hs}$ denotes the thermal impedance of the TIM and the heat sink (modeled by $R_{th4}$ and $C_{th4}$ in case of the present example) and the × symbol represents the "re-plus" operation (i.e., resulting in the net impedance/resistance of two parallel branches).

This means assuming constant amplitude of the power the amplitude of the junction temperature changes with the frequency since the value of $|Z_{th}(\omega)|$ vanishes with increasing frequency as it already concludes from Eq. (4.49). This also suggests that the *AC thermal impedance* (yet to be exactly defined in a subsequent section) of thesame AC LED lamp is of different value when operated from a 50 Hz mains or from a 60 Hz mains (see also Fig. 4.74b). Figure 4.74c also helps understand this: the dynamic heat storage in capacity of the different heat flow path sections described by the dynamic compact model act as "shunting branches," which become more effective at higher frequencies.

### *4.7.2 The Harmonic Components of the Periodic Heating Power*

So far, the simple model of a purely sinusoidal dissipated power waveform helps understand the frequency-dependent nature of LEDs' AC thermal impedance. But this simplistic approach does not consider that reality: sinusoid power change does not occur. However, periodic power waveforms have a Fourier decomposition of harmonic changes around a mean (DC) power level. Terms in Eq. (4.50) describe any of these harmonics. The relationship between a periodic dissipation function and its harmonic components is

$$P_{dissAC}(t) = \sum_{n=0}^{\pm\infty} P_n \cdot e^{jn\omega_0 t} \tag{4.50}$$

where the complex number $P_n$ denotes the Fourier coefficient of the $n$th harmonic of the $P_{dissAC}(t)$ "signal." Introducing the notation of $Z_{th_n} = Z_{th}(n \cdot \omega_0)$—where $\omega_0$ refers to the frequency of the base harmonic—the Fourier series expansion of real $T_{JAC}(t)$ time functions can be expressed as

For internal use by Mentor Graphics marketing only

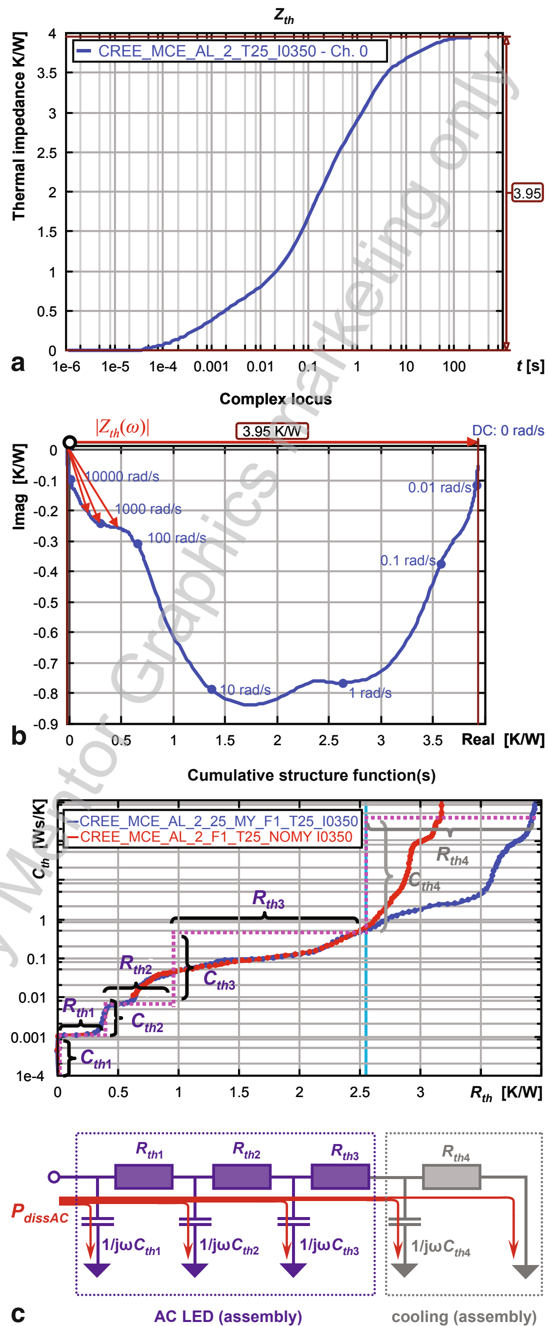

For internal use by Mentor Graphics marketing only

**Fig. 4.74** Different representations of the thermal impedance of a 10 W LED: **a** the usual $Z_{th}$ curve (time domain representation), **b** the complex locus of the $Z_{th}(\omega)$ function (frequency domain representation), **c** cumulative structure function and dynamic compact model representation of the same thermal impedance. (Source: [26] © IEEE, with permission)

$$T_{JAC}(t) = \sum_{n=0}^{\pm\infty} Z_{th_n} \cdot P_n \cdot e^{jn\omega_0 t} \quad (4.51)$$

As introduced by Eq. (4.45) in Sect. 4.4.1.7, the $Z_{th}(\omega)$ function is known once the $Z_{th}(t)$ thermal impedance is measured, thus, the $Z_{th_n} = Z_{th}(n \cdot \omega_0)$ values in Eq. (4.51) can be easily calculated.

### *4.7.3 The AC Heating Power of LEDs*

To have a better understanding of the nature of the real AC heating power of LEDs, let us consider the model of LEDs' I–V characteristics in which we separate the forward current component responsible for light output and heat loss. As discussed in Chap. 2, light output is associated to the so-called radiative recombination processes and heat dissipation is due to the so-called nonradiative recombination processes, as illustrated by Fig. 6.34 of Sect. 6.5.2.2 in Chap. 6. With this in mind, we can write

$$\begin{aligned} I_F = I_{dis}(V_F) + I_{rad}(V_F) = I_{0_dis} \cdot [\exp(V_F/mV_T) - 1] \\ + I_{0_rad} \cdot [\exp(V_F/nV_T) - 1] \end{aligned} \quad (4.52)$$

where $I_{0_dis}$ and $I_{0_rad}$ are the current constants of the different current components associated with the nonradiative and radiative recombination processes; $m$ and $n$ are the corresponding ideality factors (introduced in Sect. 2.1.3.2 of Chap. 2).

Equation (4.52) is true for the forward characteristics of the LED only. However, most AC LEDs utilize both halves of the sine wave with appropriate circuitry. This way Eq. (4.52) can be used for AC voltage, although during the two different half-waves $I_F$ may flow in different elementary diodes of an AC-driven LED chain.

With $V_{AC} = V_{MAX} \cdot \sin(\omega t)$ voltage change the current of the LED can be described as:

$$I_F(t) = I_{0_dis} \cdot [\exp(V_{MAX} \cdot \sin(\omega t)/mV_T) - 1] + I_{rad}(V_{MAX} \cdot \sin(\omega t)) \quad (4.53)$$

The AC generator voltage is also substituted into the $I_{rad}(V)$ function representing the light emission. The dissipated AC power of the LED is determined by the AC voltage drop across the LED (the AC generator voltage) and the current *not* associated with light generation:

$$P_{dissAC}(t) = I_{0_dis}[\exp(V_{MAX} \cdot \sin(\omega t)/mV_T) - 1] \cdot V_{MAX} \cdot \sin(\omega t) \quad (4.54)$$

Figure 4.75 shows $P_{dissAC}(t)$, the time function and the relative amplitudes of its first eight harmonic components.

For internal use by Mentor Graphics marketing only

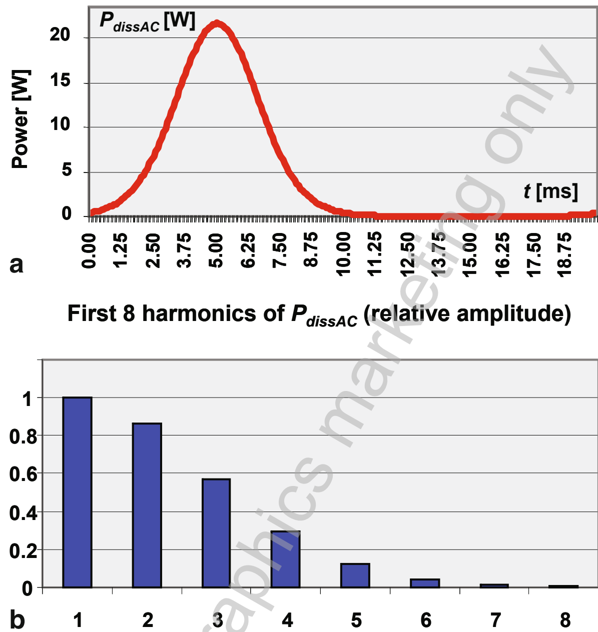


**Fig. 4.75** **a** AC dissipation waveform (1 period) for a purely AC voltage generator-driven LED as per Eq. (4.54) and **b** the relative amplitudes of its first eight harmonics—see Eq. (4.50). (Source: [26] © IEEE, with permission)

Substituting the $\exp(V_{MAX} \cdot \sin(\omega t)/mV_T)$ term with the Taylor-series approximation of the exp() function and performing the multiplication with $V_{MAX} \cdot \sin(\omega t)$ in Eq. (4.54), we obtain:

$$\begin{aligned} P_{dissAC}(t) = V_{MAX}^2 \cdot \frac{I_0}{mV_T} \cdot \frac{1}{1!}\sin^2(\omega t) + \\ + V_{MAX}^3 \cdot \frac{I_0}{(mV_T)^2} \cdot \frac{1}{2!}\sin^3(\omega t) + \\ + V_{MAX}^4 \cdot \frac{I_0}{(mV_T)^3} \cdot \frac{1}{3!}\sin^4(\omega t) + \ldots \end{aligned} \tag{4.55}$$

We can see that due to the nonlinearity of the LEDs' I–V characteristics, higher harmonics of the base frequency of the AC voltage generator will appear in the dissipation. The even harmonics add to the DC level of the dissipated power, since $\sin^2(\alpha) = [1 - \cos(2\alpha)]/2$, $\sin^4(\alpha) = [3 - 4 \cdot \cos(2\alpha) + \cos(4\alpha)]/2$, etc.

The first harmonic represents a ½, the fourth $a^3/_8 \times$ ½ part of the DC level and so on. Since $\sin^3(\alpha) = [3 \cdot \sin(\alpha) - \sin(3\alpha)]/4$, the odd harmonics cause the base harmonics to appear in the power change but at a lower factor only.

Another extreme case is the AC current driven situation when a sinusoidal AC current is forced through the AC LED. The resulting voltage waveform and the amplitudes of the harmonic components the $P_{dissAC}$ can also be analytically expressed for this situation—for details of this calculation, refer to [55].

In Fig. 4.76, measured waveforms of an AC voltage-driven LED + ballast resistor configuration are shown together with the harmonics of its AC dissipation.

For internal use by Mentor Graphics marketing only

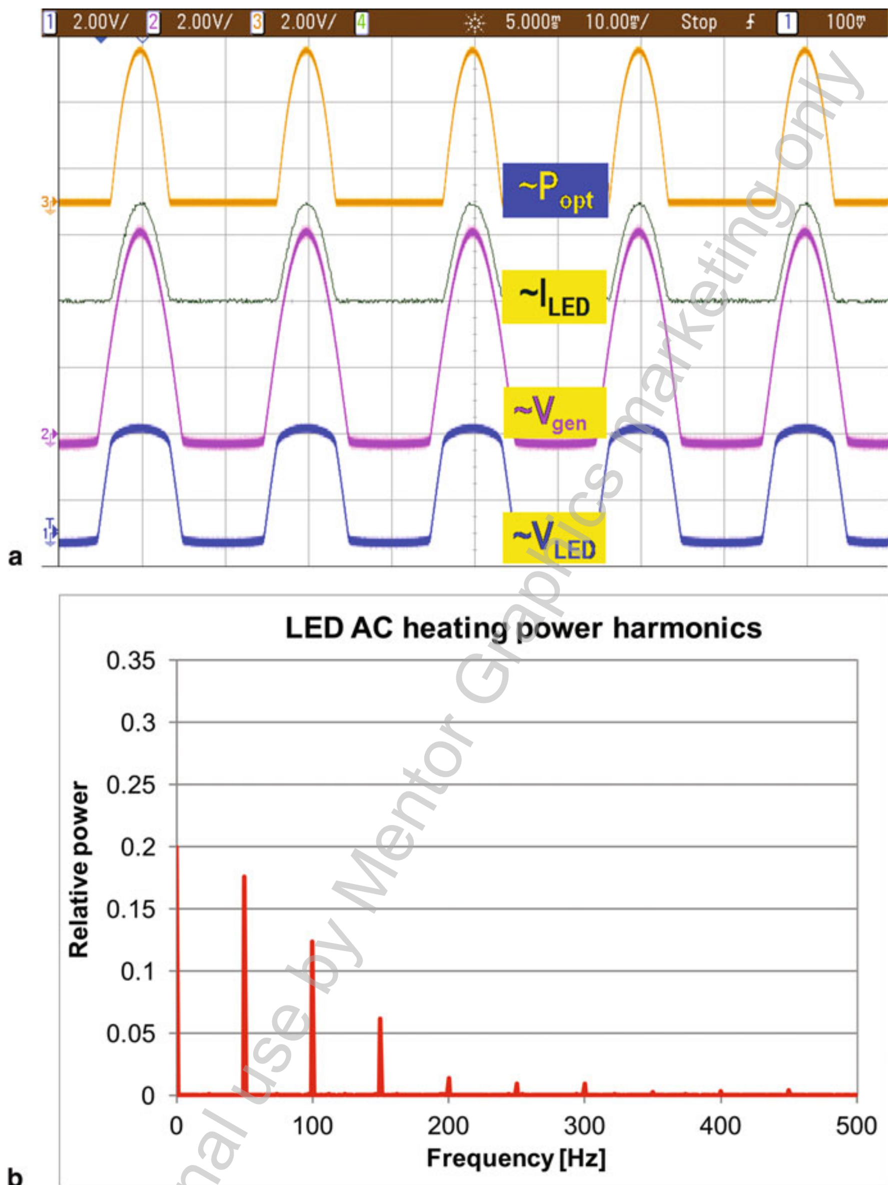


**Fig. 4.76** **a** Different measured AC waveforms of power LED + ballast resistor, driven by an AC voltage generator **b** the relative amplitudes of its AC heating power

For internal use by Mentor Graphics marketing only

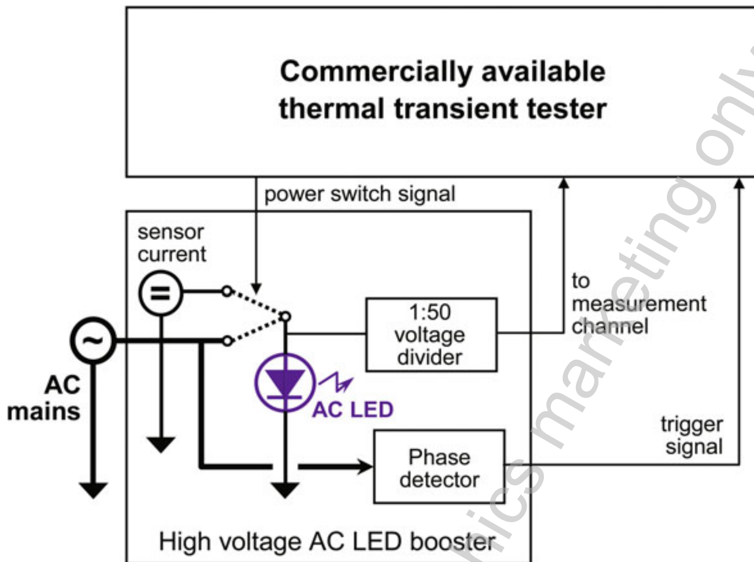


**Fig. 4.77** Schematic diagram of a possible thermal test setup for the measurement of the AC thermal impedance of mains-driven AC LEDs. (Source: [53] © EDA Publishing)

For internal use by Mentor Graphics marketing only

## *4.7.4 Possible Test Methods and Definitions of the Thermal Impedance of AC LEDs*

### 4.7.4.1 Direct Measurement

Direct measurement of the real AC thermal impedance of LEDs should be performed with care. Depending on the mains frequency different values are expected: the thermal impedance at 50 Hz is always larger than that at 60 Hz. The period of the mains voltage (20 ms/16.66 ms) is much longer than the smallest thermal time constants of usual LEDs—about 20 % of the thermal change of an LED occurs in this time interval.

Adapting the principles of the JEDEC JESD51-1 standard-compliant thermal transient measurements, the AC LED under test must be heated by the AC mains power source. Once reaching stationary current/voltage waveforms of a constant shape, the AC power can be cut off and the junction temperature drop can be measured by the usual electrical test method. The schematic of a possible test setup is shown in Fig. 4.77.

To assure repeatability, the power has to be switched down at a well-defined phase of the AC signal, since the measured impedance curves strongly depend on this phase. Figure 4.78 illustrates this for a low AC voltage-driven single LED + ballast resistor arrangement. Besides the dependence on the phase, another difficulty of such a measurement approach is the realization of the sharp switching between a 120 or 230 V AC power source (with no harmonic distortion) and a DC measurement current.

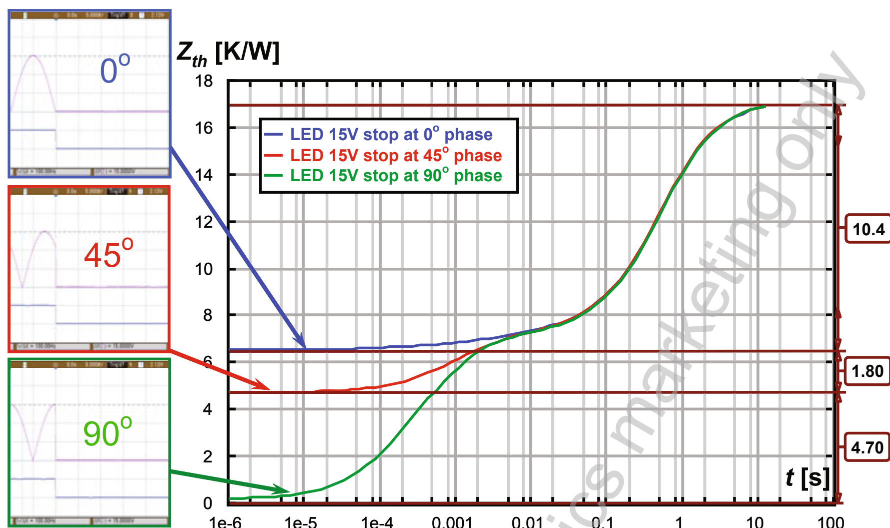


**Fig. 4.78** Measurement results obtained by a low voltage version of the test setup outlined in Fig. 4.77

For internal use by Mentor Graphics marketing only

### 4.7.4.2 JESD51-1-Compliant Thermal Tests and Calculus

The most straightforward way is using the junction-to-ambient *thermal impedance*, which is a *unique property* of a semiconductor package. There are several ways of representing it, with well-defined transformation methods among the different representations as summarized in Sect. 4.1.8.

Powering an AC LED by appropriately high DC voltage (up to 150..280 V), one can measure the $Z_{th}$ thermal impedance as defined in the JEDEC JESD51-51 electrical test method for LEDs. As recommended by the JESD51-52 standard, the measurement of the total radiant flux should also be performed. Such measurements can be performed with usual, commercially available test equipment.

The measured time domain thermal impedance curve can be transformed into frequency domain—this way one can obtain the $Z_{th}(\omega)$ function. At this point, we have the frequency domain model of the LED suitable for being driven by arbitrary waveforms.

As a next step, the AC voltage needed (120 V / 60 Hz or 230 V / 50 Hz) has to be applied. Once the AC LED has reached its stationary state, the waveforms of its AC voltage, current, and its periodic radiant flux can be measured (see, e.g., Fig. 4.76a in Sect. 4.7.3). From these waveforms, the actual $P_{dissAC}(t)$ heating power can be calculated. With Fourier analysis, the $P_n$ harmonic components of the LED's heating power can be calculated.

Taking the values of the $Z_{th}(\omega)$ at the harmonic frequencies of the dissipation, the waveform of the AC junction temperature can be calculated with the help of Eq. (4.54).

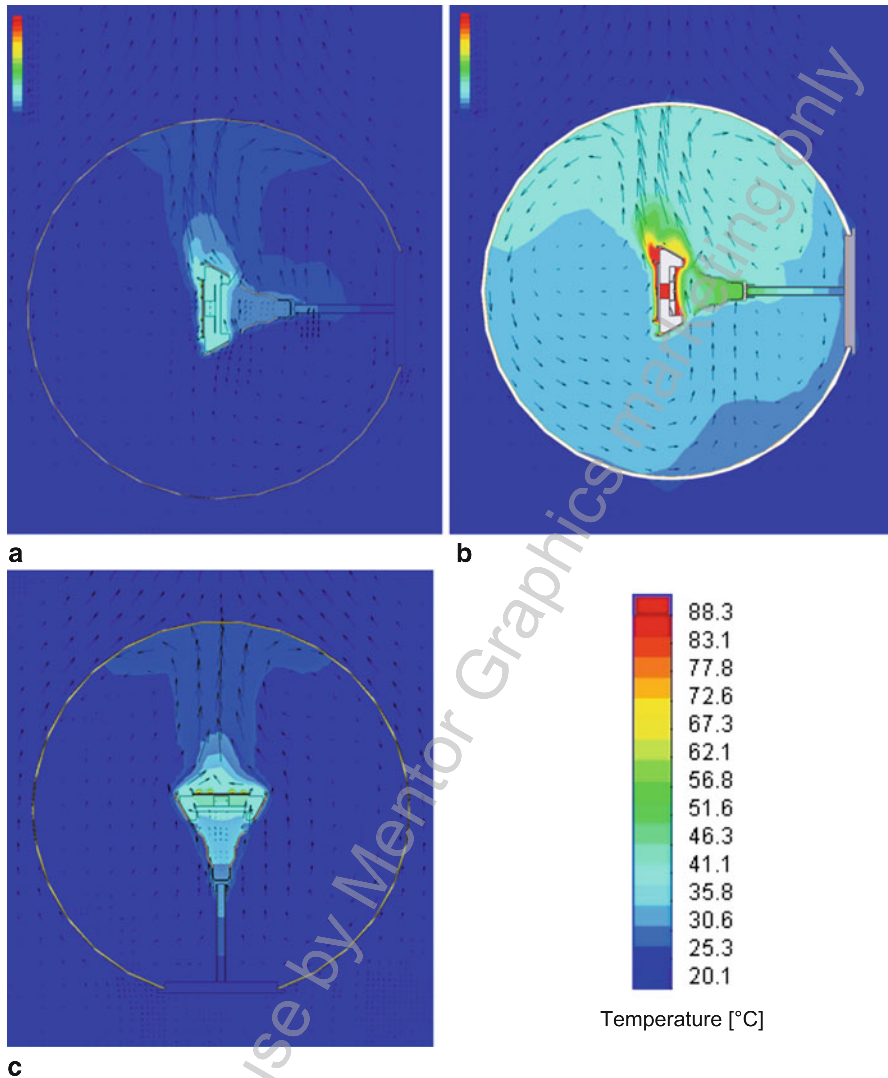


**Fig. 4.79** An integrating sphere as thermal test environment for an LED lamp. Sphere properties (size, material) and lamp orientation influence the maximal junction temperature

For internal use by Mentor Graphics marketing only

Once the $T_{JAC}(t)$ and $P_{dissAC}(t)$ functions are known, the *effective AC thermal impedance* as a *thermal metric* can be derived. There are several possibilities to define such a thermal metric, such as the ratio of (some proper) mean values. Equation (4.56) and (4.57) provide two different examples for a possible calculation of such a value

$$Z_{thAC} - Z_{thAC_mean} = T_{JAC} - Z_{thAC_mean}/P_{dissAC_RMS} \tag{4.56}$$

$$Z_{thAC} - Z_{thAC_mean} = T_{JAC} - Z_{thAC_mean}/P_{dissAC-RMS} \tag{4.57}$$

where in both cases, e.g., $P_{dissAC_RMS}$ is the RMS value of the periodic heating power. In the first case also the RMS value, in the second case the maximal value of the junction temperature waveform is used.

### *4.7.5 Test Environments*

For component-level testing LEDs, the JESD51-50 series of standards recommend a temperature-controlled cold plate as thermal test environment. This would be the natural choice for MCPCB assembled AC-driven LEDs such as the Acriche series from SSC.

For AC-driven retrofit LED lamps, however, *natural convection* is the usual operational environment, therefore, it seems that a standardized natural convection test environment would be required and another thermal metric, some sort of junction-to-ambient AC thermal impedance would make sense. As we are interested in the real heating power, the total radiant flux of AC-driven LEDs is also to be measured, typically in an integrating sphere.

Actually, the integrating sphere can also serve as a thermal test environment, providing hopefully repeatable test conditions. Again, care has to be paid, since the lamp orientation in the sphere, the sphere size, the thermal conductivity of the sphere wall, and even the thermal conditions of the testing laboratory may have significant influence on the ultimate stationary junction temperature response. This can be easily revealed by CFD simulation. In Fig. 4.79, an integrating sphere serves as a natural convection thermal test environment for a retrofit LED lamp. The sphere properties (size, material) and the lamp orientation influence the maximal junction temperature (CFD analysis results obtained by the FloEFD tool from Mentor Graphics).

## References

1. Lasance C J M, den Hertog D., Stehouwer P. (1999) Creation and evaluation of compact models for thermal characterisation using dedicated optimisation software. In: Proceedings of the 15th IEEE Semiconductor Thermal Meas-urement and Management Symposium (SEMI-THERM'99), San Diego, USA, 9-11 March , pp 189-200
2. Farkas G, Poppe A, Kollár E, Stehouwer P (2003) Dynamic Compact Models of Cooling Mounts for Fast Board Level Design. In: Proceedings of the 19th IEEE Semiconductor Thermal Measurement and Management Symposium (SEMI-THERM'03). San Jose, 11-13 March 2003. pp. 255-262.
3. Szabó P, Poppe A, Rencz M Studies on the possibilities of in-line die at-tach characterization of semiconductor devices. In: Proceedings of the 9th Electronics Packaging Technology Conference (EPTC'07), 10-12 December 2007, Singapore, pp. 779-784 (ISBN: 978-1-4244-1324-9)
4. Szabó P, Rencz M, Farkas G, Poppe A. Short time die attach characteri-zation of LEDs for in-line testing application. In: Proceedings of the 8th Electronics Packaging Technology Conference (EPTC'06): Volume One. Singapore, 6-8 December 2008, pp. 360-366 (ISBN: 1-4244-0664-1)

For internal use by Mentor Graphics marketing only

5. JEDEC Standard JESD51-1. Integrated Circuits Thermal Measurement Method - Electrical Test Method (Single Semiconductor Device). www.jedec.org/sites/default/files/docs/jesd51-1.pdf (December 1995)
6. JEDEC Standard JESD51-51 Implementation of the Electrical Test Method for the Measurement of the Real Thermal Resistance and Impedance of Light-emitting Diodes with Exposed Cooling Surface. www.jedec.org/sites/default/files/docs/JESD51-51.pdf. (April 2012)
7. Siegal B. An_Introduction_to_Diode_Thermal_Measurements, www.thermengr.net/An_Introduction_to_Diode_Thermal_Measurements6.pdf
8. Siegal B (1978) Measuring thermal resistance is the key to a cool semiconductor. Electronics 51:121-126
9. Sofia J W (1995) Analysis of thermal transient data with synthesized dynamic models for semi-conductor devices. IEEE Trans Comp Pack Manuf 18(1):39-47
10. JEDEC Standard JESD51. Methodology for the Thermal Measurement of Component Packages (Single Semiconductor Devices). This is the overview document for the JESD51- series of specifications. www.jedec.org/sites/default/files/docs/Jesd51.pdf. (December 1995)
11. Guenin B Update on Thermal Standards Work by JC15.1. www.ewh.ieee.org/soc/cpmt/presentations/cpmt0303a.pdf
12. Guenin B Update on JEDEC Thermal Standards. Electronics Cooling Vol.18. www.electronics-cooling.com/2012/09/update-on-jedec-thermal-standards. 17 September 2012
13. JEDEC Standard JESD51-14 Transient Dual Interface Test Method for the Measurement of Thermal Resistance Junction-to-Case of Semiconductor De-vices with Heat Flow through a Single Path. www.jedec.org/download/search/jesd51-14.pdf. (November 2010)
14. JEDEC Standard JESD51-50 Overview of Methodologies for the Thermal Measurement of Single- and Multi-Chip, Single- and Multi-PN Junction Light-Emitting Diodes (LEDs). www.jedec.org/sites/default/files/docs/jesd51-50.pdf. (April 2012)
15. Farkas G, van Voorst Vader Q, Poppe A, Bognár Gy (2005) Thermal Investigation of High Power Optical Devices by Transient Testing. IEEE Trans Comp Pack Techn 28(1):45-50
16. Farkas G et al Electric and Thermal Transient Effects in High Power Optical Devices" Proceedings of the 20th IEEE Semiconductor Thermal Measurement and Management Symposium (SEMI-THERM'04). San Jose, March 2004, pp. 168-176.
17. Rencz M, Székely V (2004) Studies on the nonlinearity effects in dynamic compact model generation of packages. IEEE Trans Comp Pack Techn 27(1):124-130
18. Poppe A, Molnár G, Temesvölgyi T Temperature dependent thermal re-sistance in power LED assemblies and a way to cope with it. In: Proceedings of the 26th IEEE Semiconductor Thermal Measurement and Management Symposium (SEMI-THERM'10), 21-25 February 2010, Santa Clara, USA, pp. 283-288. (ISBN: 978-1-4244-6458-1)
19. Székely V (1991) On the representation of infinite-length distributed RC one-ports. IEEE Trans Circuit Sys 38(7):711-719
20. Székely V, Rencz M (2000) Thermal Dynamics and the Time Constant Domain. IEEE Trans Comp and Pack Techn 23(3):687-594
21. Székely V, Bien T V (1988) Fine structure of heat flow path in semiconductor devices: a measurement and identification method. Solid-State Electronics 31(9):1363-1368
22. Protonotarios E N, Wing O (1967) Theory of nonuniform RC Lines, part I: analytic properties and realizability conditions in the frequency domain. IEEE Trans Circuit Theory 14(1):2-12
23. Székely V (1998) Identification of RC Networks by deconvolution: Chances and Limits. IEEE Trans Circuits and Sys I - Fundamental Theory and App 45(3):244-258
24. Székely V, Rencz M, Poppe A, Courtois B (2001) THERMODEL: a tool for thermal model generation, and application for MEMS. Analog Integrat Circuit Signal Process 29(1-2): 49-59
25. Rencz M, Poppe A, Kollár E, Ress S, Székely V (2005) Increasing the Accuracy of Structure Function Based Thermal Material Parameter Measurements. IEEE Trans Comp and Pack Techn 28(1):51-57
26. Poppe A, Siegal B, Farkas G Issues of Thermal Testing of AC LEDs. Proceedings of the 27th IEEE Semiconductor Thermal Measurement and Management Symposium (SEMI-THERM'11), San Jose, USA, 20-24 March 2011, pp 297-304


For internal use by Mentor Graphics marketing only

27. Vermeersch B (2009) Thermal AC modelling, simulation and experimental analysis of microelectronic structures including nanoscale and high-speed effects. PhD Tesis, D/2009/10.500/24, University of Ghent, Ghent, Bel-gium. http://lib.ugent.be/fulltxt/RUG01/001/330/941/RUG01-001330941_2010_0001_AC.pdf
28. Poppe A, Molnár G, Csuti P, Szabó F, Schanda J Ageing of LEDs: A Comprehensive Study Based on the LM80 Standard and Thermal Transient Measurements. In: CIE 27th Session-Proceedings, CIE 197:2011: (Volume1, Part 1-2). 10-15 July 2011, Sun City, South Africa, Vienna: CIE, pp. 467-477
29. Rencz M, Székely V, Morelli A, Villa C (March 2002) Determining Partial Thermal Resistances with Transient Measurements, and Using the Method to Detect Die Attach Discontinuities. In: Proceedings of the 18th IEEE Semiconductor Thermal Measurement and Management Symposium (SEMI-THERM'02), March 12-14, 2002, San Jose, USA, pp. 15-20
30. Steffens O, Szabó P, Lenz M, Farkas G (March 2005) Thermal transient characterization methodology for single-chip and stacked structures. In: Proceedings of the 21st IEEE Semiconductor Thermal Measurement and Management Sym-posium (SEMI-THERM'05), 15-17 March 2005, San Jose, USA, pp 313-321
31. Schweitzer D, Pape H, Chen L, Kutscherauer R, Walder M (March 2011) Transient dual interface measurement-A new JEDEC standard for the measurement of the junction-to-case thermal resistance. In: Proceedings of the 27th IEEE Semiconductor Thermal Measurement and Management Symposium (SEMI-THERM'11), 20-24 March 2011, San Jose, USA, pp 222-229
32. Pape H, Schweitzer D, Chen L, Kutscherauer R, Walder M (2011) Development of a standard for transient measurement of junction-to-case thermal re-sistance. In: Proceedings of the 12th International Conference on Thermal, Mechanical and Multi-Physics Simulation and Experiments in Microelec-tronics and Microsystems (EuroSimE'11), 2011, pp 1/8- 8/8
33. Schweitzer D, Pape H, Chen L (2008) Transient Measurement of the Junction-to-Case thermal resistance using structure functions: chances and limits. In: Proceedings of the 24th IEEE Semiconductor Thermal Measurement and Management Symposium (SEMI-THERM'08), 16-20 March 2008, San Jose, USA, pp 193-199
34. Schweitzer D (2008) Transient dual interface measurement of the Rth-JC of power packages. In: Proceedings of the 14th International Workshop on THERMal INvestigation of ICs and Systems (THERMINIC'08), 24-26 September 2008, Rome, Italy, pp 14-19
35. Schweitzer D, Pape H, Kutscherauer R, Walder M (2009) How to evaluate transient dual interface measurements of the Rth-JC of power packages. In: Proceedings of the 25th IEEE Semiconductor Thermal Measurement and Management Symposium (SEMI-THERM'09), 15-19 March 2009, San Jose, USA, pp 172-179
36. Müller S, Zahner T, Singer F, Schrag G, Wachutka G (2011) Evaluation of thermal transient characterization methodologies for HighüPower LED applications. In: Proceedings of the 17th International Workshop on THERMal INvestigations of ICs and Systems (THERMINIC'11), 27-29 September 2011, Paris, France, pp 104-109
37. ASTM Standard D 5470, 2012, Standard Test Method for Thermal Trans-mission Properties of Thin Thermally Conductive Solid Electrical Insulation Materials. ASTM International, West Conshohocken PA USA, 2012, DOI: 10.1520/D5470-12; www.astm.org
38. Mentor Graphics' DynTIM tester webpage: www.mentor.com/products/mechanical/products/dyntim
39. Mentor Graphics' T3Ster thermal transient tester webpage: www.mentor.com/products/mechanical/products/t3ster
40. Vass-Várnai A, Székely V, Sárkány Z, Rencz M (2011) New level of accuracy in TIM measurements. In: Proceedings of the 27th IEEE Semiconductor Thermal Measurement and Management Symposium (SEMI-THERM'11), 20-24 March 2011, San Jose, USA, pp 317-324
41. Vass-Várnai A, Sárkány Z, Rencz M (2012) Characterization method for thermal interface materials imitating an in-situ environment. Microelectronics J 43(9):661-668
42. ANSI/IESNA IES-LM-80-08 Standard (2009) Approved Method for Measuring Lumen Maintenance of LED Light Sources. ISBN 978-0-87995-227-3
43. Hu J, Yang L, Shin M W (2005) Mechanism and Thermal Effect of Delamination in Light Emitting Diode Packages. In: Proceedings of the 11th International Workshop on THERMal

For internal use by Mentor Graphics marketing only